University of Southampton

Faculty of Engineering and Physical Sciences

Institute of Sound and Vibration Research

MODELLING ELECTROCOCHLEAR RESPONSES

by

Dominika Behounek

Thesis for the degree of Doctor of Philosophy

July 2022

University of Southampton

Abstract

Faculty of Engineering and Physical Sciences

Institute of Sound and Vibration Research

Thesis for Degree of Doctor of Philosophy

MODELLING ELECTROCOCHLEAR RESPONSES

by

Dominika Behounek

The cochlea is a central part of the inner ear handling the task of transforming acoustical waves into electrical impulses that are then carried by the sensory nerves further into the brain. Despite being one of the smallest organs in the human body its functionality is highly complex and even after long years of research a lot of its mechanics is not well understood. The current knowledge of the electro-mechanical functionality of the cochlea is mostly based on crude 2-dimensional model approximations and, while the clinical manifestation of certain mechanisms have been a subject of numerous scientific publications, the exact link between those two remains largely unexplored.

Auditory potentials have elements thought to include components due to the receptor potentials of both inner- and outer hair cells. However, there is a deficiency of experimental and analytical research of these components and in particular their non-linear properties. If a reliable model that is able to simulate these components is produced, it may provide a tool for exploring how different pathologies are expected to show up in measurements of the cochlear microphonic and the new insight may lead to improved stimulus paradigms for extracting information about processes taking place in the cochlea.

In this doctoral thesis, the current state of the cochlear modelling field is discussed and explored further to understand the non-linear processes taking place within the cochlea using numerical models with a focus on the auditory evoked potential – cochlear microphonic. A novel protocol for two-tone suppression in cochlear microphonic measurements in normal-hearing patients is also introduced in an effort to correlate the model predictions with the experimental data.

The comparative analysis of the collected data set with the cochlear model simulation revealed that even though the model can successfully replicate *in vivo* measurements collected at a single point along the cochlea, at its present formulation, it cannot be used to reliably predict the cochlear microphonic recorded at the round window. This conclusion comes after the analysis of the experimental data indicated that the cochlear microphonic recorded by an extratymphanic electrode contains contributions from multiple locations along the cochlea, and not just from its basal segment, as it has been suggested in the past.

TABLE OF CONTENTS

LIST OF FIGURES

LIST OF TABLES

DECLARATION OF AUTHORSHIP

Print name: Dominika Behounek

Title of thesis: Modelling Electrocochlear Responses

I declare that this thesis and the work presented in it are my own and has been generated by me as the result of my own original research.

I confirm that:

1. This work was done wholly or mainly while in candidature for a research degree at this University;
2. Where any part of this thesis has previously been submitted for a degree or any other qualification at this University or any other institution, this has been clearly stated;
3. Where I have consulted the published work of others, this is always clearly attributed;
4. Where I have quoted from the work of others, the source is always given. With the exception of such quotations, this thesis is entirely my own work;
5. I have acknowledged all main sources of help;
6. Where the thesis is based on work done by myself jointly with others, I have made clear exactly what was done by others and what I have contributed myself;
7. None of this work has been published before submission.

Signature:……. Date:…..13/07/2022……

ACKNOWLEDGEMENTS

I would like to thank my supervisory team: Ben Lineton and Carl Verschuur for their guidance, expertise and patience. I learned a great deal in every single meeting and I cannot be more grateful for the wisdom they shared with me.

I would like to acknowledge Steve Elliott and Steve Bell for helping me to move forward with my research when I felt like I did not know what my next step is going to be. Also, thank you to Paul Teal for sharing the cochlear model code that this thesis was largely based on and for all of the helpful comments and feedback.

To all of the wonderful people I met at the University of Southampton – I could not have hoped for a better bunch to share my ups and downs with.

Thank you to my beloved family, for their constant support, words of motivation and the much-needed distractions. A special mention to my grandparents that always held me accountable when I could not do it myself and did so in the kindest way possible. It would not have been possible without you.

Last but not least, I extend my thanks to this project's supporters - Action on Hearing Loss who work tirelessly to provide high-quality support for people who are deaf, have hearing loss or tinnitus. Thank you for being advocates for everyone with hearing impairment and fighting for a better tomorrow.

ABBREVIATIONS

2D	2-dimensional
2TS	Two-tone suppression
3D	3-dimensional
ABR	Auditory brainstem response
ANSD	Auditory neuropathy spectrum disorder
AP	Action potential
B&K	Brüel & Kjær
BM	Basilar membrane
CAP	Compound action potential
CM	Cochlear microphonic
CP	Characteristic place
dB	Decibel
ECochG	Electrocochleography
EEG	Electroencephalogram
EMT	Electromechanical transduction
EP	Evoked potential
FFR	Frequency-following response
FFT	Fast Fourier transform
GUI	Graphical user interface
HB	Hair bundle
HL	Hearing level
I/O	Input/output

IHC	Inner hair cell
IQR	Interquartile range
MATLAB	Matrix Laboratory
MET	Mechanoelectrical transduction
ms	Millisecond
OAEs	Otoacoustic emissions
OC	Organ of Corti
ODE	Ordinary differential equation
OHC	Outer hair cell
OW	Oval window
PTA	Pure-tone audiometry
RW	Round window
SGC	Spiral ganglion cell
SNHL	Sensorineural hearing loss
SNR	Signal-to-noise ratio
SM	Scala media
SP	Summating potential
SPSS	Statistical Package for the Social Sciences (IBM software)
ST	Scala tympani
SV	Scala vestibuli
SPL	Sound pressure level
TM	Tectorial membrane

1. Introduction

The cochlea is the central part of the inner ear handling the task of transforming the acoustical waves into the electrical impulses that are then carried by the sensory nerves further into the brain. Despite being one of the smallest organs in the human body its functionality is highly complex and even after long years of research much of its mechanics is not well understood. The current knowledge of the electro-mechanical functionality of the cochlea is mostly based on crude 2-dimensional model approximations and while guidelines associating clinical manifestation of certain mechanisms with the cochlear physiology do exist, the exact link in between those two remains largely unexplored.

The primary objective of this thesis is to discuss the current state of the cochlear modelling research and explore further the understanding of non-linear processes taking place within the cochlea using numerical models with a focus on auditory evoked potentials – namely the cochlear microphonic. This specific component was selected in an effort to shed some light on how the cochlear microphonic can aid in recognising the factors causing Auditory Neuropathy Spectrum Disorder and its underlying mechanisms. There are several presumed aetiologies underlying ANSD which is currently diagnosed by the presence of normal or near-normal otoacoustic emissions (OAEs), present cochlear microphonic (CM) responses and absent or abnormal auditory brainstem responses (ABRs). These potentials have elements thought to include components from the receptor potentials of both inner- and outer hair cells. However, there is a deficiency of experimental and analytical research of these components, and in particular their nonlinear properties. If a reliable model that is able to simulate these components is produced, it may provide a tool for exploring how different pathologies are expected to show up in the measurements of the cochlear microphonic and that new insight may lead to improved stimulus paradigms for extracting information that can accurately differentiate the dysfunction.

However, at this point the models are not proven to be able to predict those electrical potentials even in normal hearing subjects, therefore this study attempts to explore the cochlear modelling results and compare those findings against a set of novel non-invasive cochlear microphonic measurements obtained in normal hearing subjects.

1.1. Outer and middle ear

Sound is transmitted from the ear canal through the middle ear via the tympanic membrane and ossicles into the cochlea. The cochlea acts as a converter from an acoustic stimulus into neural electrical signals which are then transmitted to the brain through the auditory nerve. This section describes the anatomy of the ear and explains its main mechanisms.

1.1.1. Outer ear

The external ear gathers sound energy and focuses it on the tympanic membrane. It consists of three main parts (Pickles, 1988):

- Pinna - the first part of the ear that interacts with the incoming sound and is responsible for gathering the sound waves and directing them towards the ear canal thanks to its special helical shape (Alberti, 2001),
- Auditory canal – about 2.5cm long tube leading from pinna to eardrum,
- Eardrum – a cone-shaped membrane that vibrates in response to stimuli and couples the sounds pressure waves propagated through the air to the ossicles of the middle ear.

1.1.2. Middle Ear

The tympanic cavity has a volume of about $2cm^3$ and is connected to the nasopharynx through the Eustachian tube, having a length of 35-38mm. This duct is normally closed but opens during yawning and partially during swallowing (Yule, 1873).

Closing the tympanic cavity permanently would cause disproportion between atmospherical pressure, interacting with the tympanic membrane through the outer ear and the pressure in the closed cavity. In extreme situations, it would put the tympanic membrane at risk of rupturing. Having the difference in pressure around 1kPa (around 1% of atmospheric pressure), severe hearing problems can occur, being the consequence of deflection of the eardrum in one direction, which causes non-linear changes and amplitude reduction of membrane vibrations.

The middle ear couples the sound energy propagated via air to the cochlea. Its transformer action is responsible for matching the impedance of the auditory meatus to that of the cochlear fluids, which is much higher (Purves *et al.*, 2001).

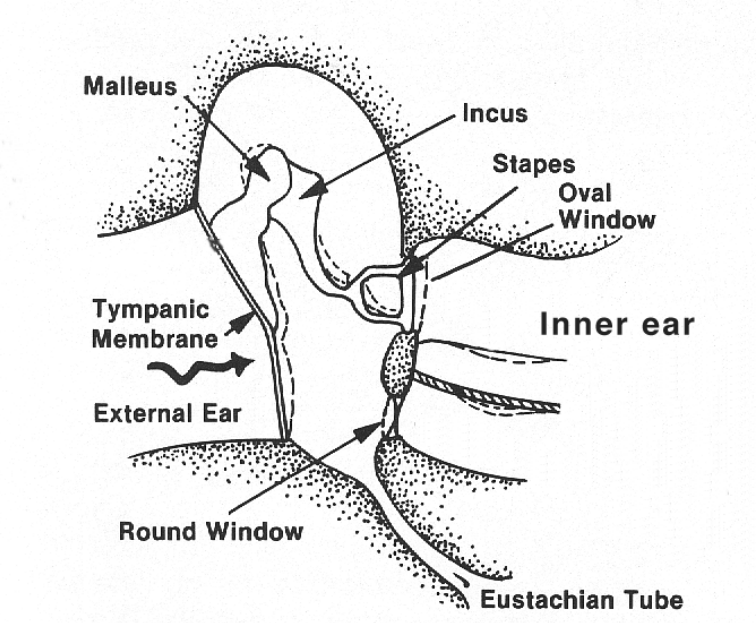

Figure 1.1: Illustration of the middle ear cross-section along with adjacent elements. Source: Scubamed, www.scubamed.com [14.07.2015]

To ensure the impedance matching, the acoustic stimuli are transmitted to the cochlea by three small bones: malleus, incus and stapes, together called ossicles (Figure 1). Middle ear bones are held

in place by several ligaments and two striated muscles:

- tensor tympani – attached to the malleus, close to the tympanic membrane, innervated by the 5th (trigeminal) cranial nerve,
- stapedius muscle – attached to the stapes, innervated by the 7th (facial) cranial nerve.

Contractions of the muscles increase the stiffness of the ossicular chain. It affects mostly responses below 1-2kHz (since they are stiffness controlled (Greger and Windhorst, 2013)). Striated muscles also play a role in protecting the hearing by contracting in response to loud sounds in order to decrease sound transmission to the cochlea. This protection mechanism known as 'acoustic reflex' can be activated by sound stimuli of approximately 85dB HL, vocalization, tactile stimulation or general bodily movement (Møller, 2006).

The ossicles chain is designed in a way so that the vibrations transmitted through the air and recorded at the tympanic membrane get 'translated' into the vibrations in the fluid. The eardrum vibrates in a specific way and has areas of higher deflection. Manubrium of the malleus is attached to the medial surface of the tympanic membrane at the places, where the peaks of the vibrations are not present. This reduces the amplitude of vibrating manubrium

but also doubles the force carried by it. Malleus and incus ensure the lever action ratio of 1.3 : 1 (Young and Ng, 2020). Lastly, the actively vibrating area of the eardrum for high SPL levels is assumed to be around 55mm^2 (2/3 of the entire eardrum area), while the footplate of stapes is assumed to be approximately 3.2mm^2. The proportion between these areas causes the pressure on the stapes footplate to be 17 times higher than on the eardrum. Summing up, the middle ear causes amplification of the signal by $2 * 1.3 * 17 \approx 44$ which is equal to 33dB (Keifer, 2016) for frequencies close to 2.5kHz (because in this frequency region the impedance of the middle ear has resistive characteristics, while for lower and higher frequencies it is reactance dependent and the efficiency of the transformator is lowered).

The transfer function of the middle ear can be described as having bandpass characteristics:

- low frequency attenuation due to elasticity of the tympanic membrane, ligaments of ossicles and compression and expansion of the ear in the middle ear cavity,
- greatest transmission in the range about 1 – 2kHz,
- 4kHz – irregularities due to resonances in the middle air cavity,
- high frequencies are attenuated.

1.2. The inner ear

In the inner ear, the two basic hearing mechanisms occur: mechanical frequency filtering and the transformation of a mechanical vibration into the afferent electrical impulses in receptor cells. It consists of three main parts: the semicircular canals, the vestibule and the cochlea. The vestibular system is physiologically an integral part of the inner ear, however, it does not contribute to the hearing process – it is a system required for maintenance of balance or equilibrium.

The semicircular canals consist of three main parts: the horizontal, posterior, and superior canals. Each of those provides a separate sense of directional balance. The superior canal detects side-to-side movement, like tilting the head toward the shoulders. The posterior canal detects forward and backward movement, like sit-ups. The horizontal canal senses movement on a vertical basis, as the head rotates up and down on the neck. The vestibular system is the inner ear region when semicircular canals converge. It contains sensory cells for linear acceleration.

Overall, the cochlea stands about 1cm to 5mm wide going from the base to the apical part and contains a coiled basilar membrane being about 35mm long in humans. It is estimated that cochlea is formed in about 2 and 5/8 twists (Yost, 2007).

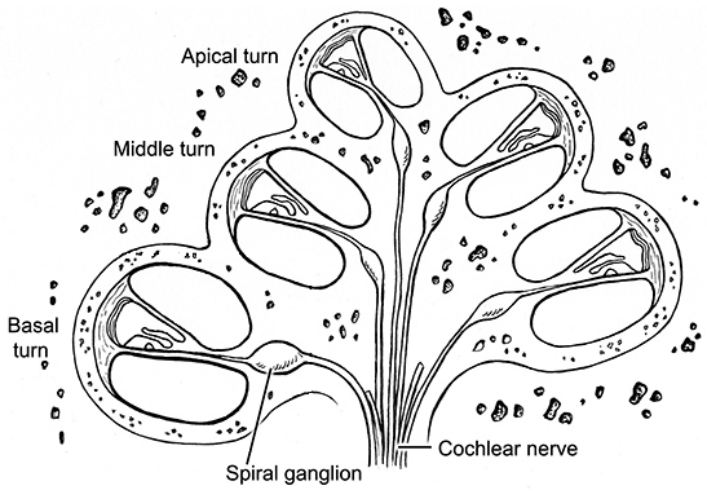

Figure 1.2: Illustration of the section through the cochlea. Source: http://www.wsiat.on.ca/ [28.01.2016]

1.2.1. Cochlear Structure

The cochlea is divided into three separate ducts: the scala vestibule, the scala media and the scala tympani. The scala vestibule is separated from the scala media by the Reissner's membrane which is very thin (merely two cells (Gelfand, 2009)) and flaccid, whereas the scala tympani is isolated from the scala media by the basilar membrane. The outer scalae: scala vestibule and scala tympani are directly connected to each other at the apex of the basilar membrane, through an opening called helicotrema. Thanks to the helicotrema both outer scalae are filled with the same fluid – the endolymph, while the scala media is filled with a different fluid – the perilymph.

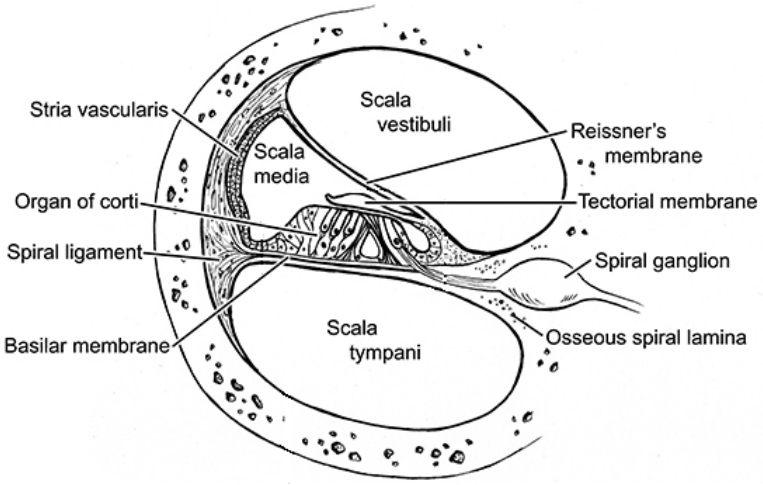

Figure 1.3: Illustration of the section through one turn of the cochlea. Source: http://www.wsiat.on.ca/ [28.01.2016]

Perilymph is similar to the extracellular fluid considering its ionic composition and has a potential of the surrounding bone, while the endolymph is similar to the intracellular fluid (having high K^+ and low Na^+ concentration). The stria vascularis is believed to be the source of the electrocochlear potential. Several experiments have been conducted to back up this theory. These included destroying Reissner's membrane to mix perilymph and endolymph to show that positive potentials were still observed near the stria vascularis, or using ototoxic agents influencing the stria vascularis which led to an observed reduction in the endocochlear potential (Tasaki and Spyropoulos, 1959).

In the bone surrounding the cochlea, there are two openings. First of them is the oval window, to which one of the middle ear ossicles, the stapes, is attached. The second one is the round window, connecting the cavity of the middle ear to the scala tympani.

1.2.2. Basilar Membrane and Tectorial Membrane

The basilar membrane is a rigid surface that extends across the length of the cochlea. Its width at the base is merely 0.04mm and gradually increases, reaching around 0.52mm at the apex. It is made of 20,000 to 30,000 reed-like fibres that are short and stiff near the oval window, getting longer and limber towards the apical part of the basilar membrane, where its pliancy is approximately 100 times higher than at the base (Brugge and Howard, 2002).

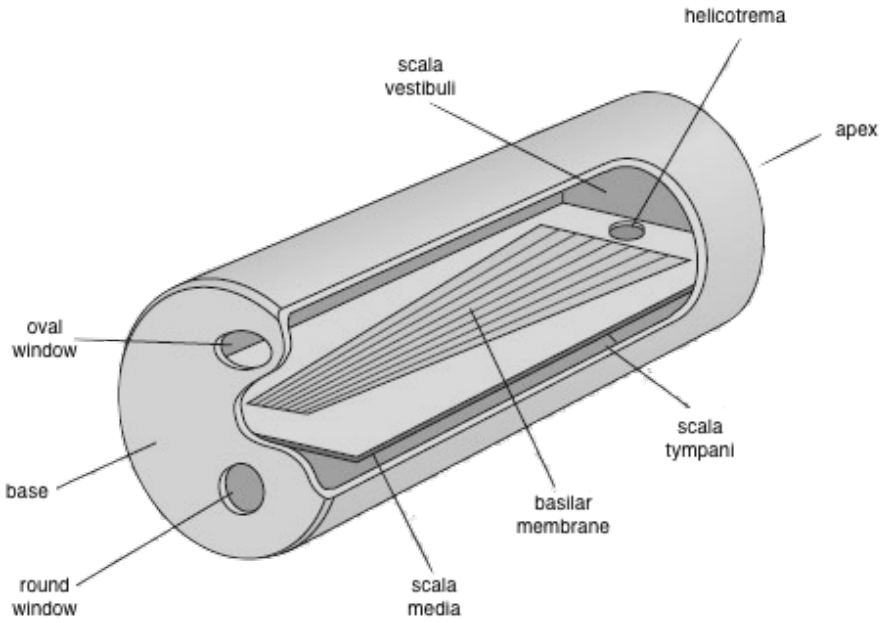

Figure 1.4: Schematic representation of uncoiled cochlea and its key structures. Source: www.open.edu.pl [15.07.2015]

When the stapes pushes the oval window, the liquid in the scala vestibule is displaced. It gives rise to a travelling wave. Each region of the basilar membrane is excited for different stimuli frequencies (high frequencies cause the base of the basilar membrane to vibrate, and low frequencies peak at the apical part). For a stimulus of a particular frequency, the vibration of the basilar membrane grows in amplitude as the wave travels towards the apical part and, after a certain point, it fades away rapidly. The farther from the base, the slower the wave travels. For low stimulus intensities, the response of the basilar membrane is sharply tuned, while for higher intensities, it is more broadly tuned.

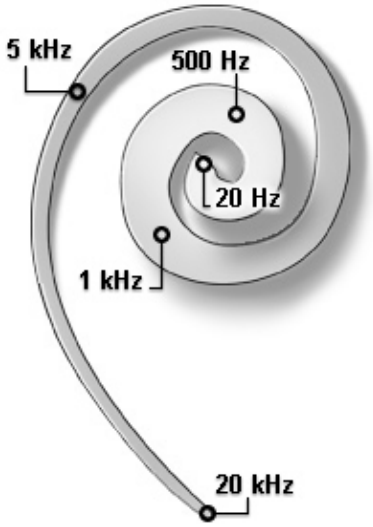

Figure 1.5: Tonotopic organisation of basilar membrane. Source: www.lipscomb.umn.edu [16.07.2015]

1.2.3. Organ of Corti and Sensory Hair Cells

The organ of Corti is a receptor organ of hearing, spiralling along the basilar membrane, given its rigidity by an arch of rods and pillar cells along its length. The upper ends of the rods are lined-up with the reticular lamina which separates fluids from scala media and scala tympani. It contains the sensory cells responsible for transducing mechanical motion into electrical activity and nerve fibres that transmit the electrical activity into the brain where it is perceived as an auditory signal.

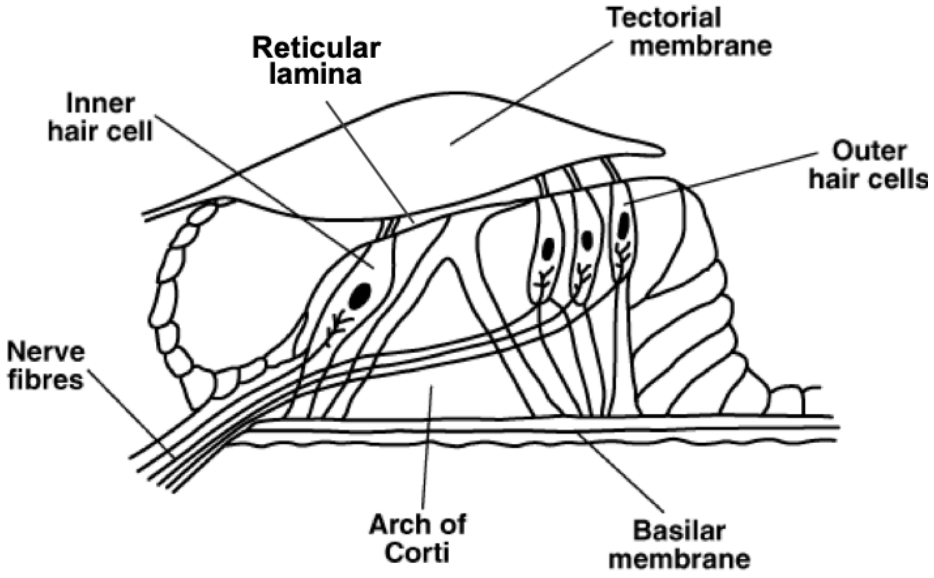

Figure 1.6: Schematic diagram of Organ of Corti. Source: www.blog.daum.net [28.01.2016}

There are two types of hair cells located within the Organ of Corti. Their length varies between 25 and 40 μm, with a width of 4 to 10 μm. In the human cochlea, there are 3,500 inner hair cells, forming one row, and about 12,000 outer hair cells, forming three rows at the basal part and up to five rows near the apex (Pujol, 2014).

Outer hair cells act as motor units that amplify the movement of the basilar membrane in response to a stimulus. The bottom of these cells is held by a cup-like depression supported by Deiters' cells (Encyclopedia Britannica, 2016) and their stereocilia are in contact with the tectorial membrane. They are stimulated by relative motion between those two. The enhanced motion of the basilar membrane is achieved through the somatic motility of the OHCs. With every sound wave, the cells shorten and elongate. This movement causes OHCs to push against the tectorial membrane and selectively amplify vibrations of the basilar membrane. This mechanism is responsible for allowing the perception of very quiet sounds (Hudspeth *et al.*, 2000). The hair cells are the shortest at the base of the cochlea and become progressively taller towards the apex (their stereocilia also follow this rule).

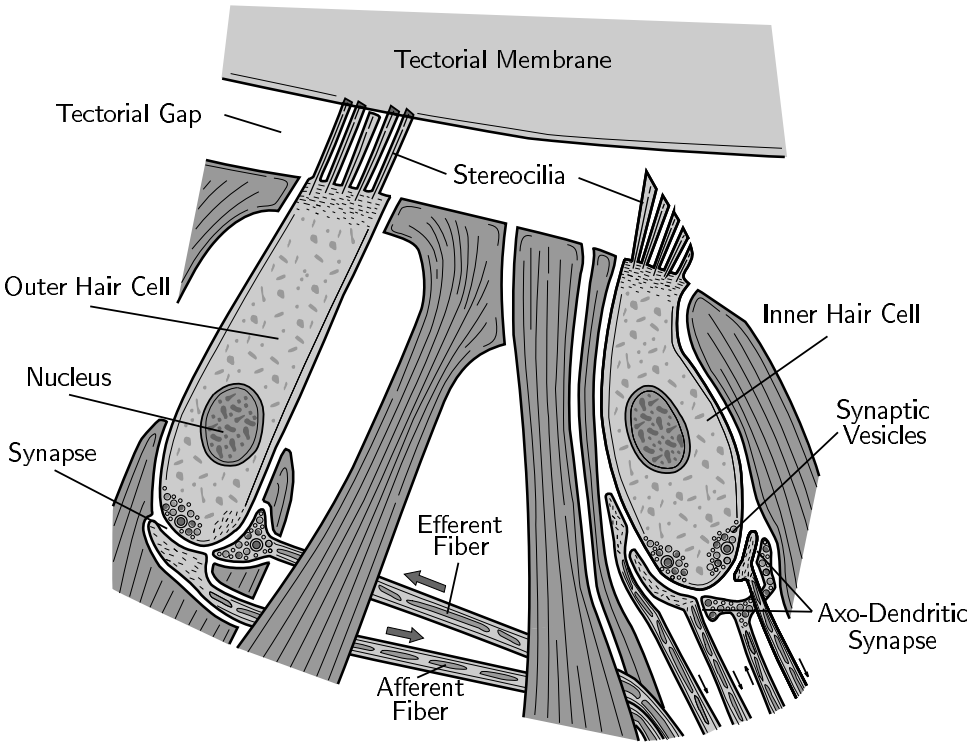

Figure 1.7: Detailed drawing of inner and outer hair cell. Source: Watts, L., 'Cochlear Mechanics: Analysis and Analog VLSI' (1993)

Inner Hair Cells (IHCs) are responsible for signal transduction. The detailed mechanism of their functionality will be introduced in one of the following sections.

1.3. Cochlear mechanics

The input signal is fed into the cochlea by the vibrating stapes. The stapes motion follows the exact waveform of the sound pressure waves transmitted through the air. The movement of the oval window driven by the stapes causes waves to propagate in the cochlear fluid and the membrane structure of the cochlea. The wave is not being transmitted solely by compression of the fluid since the cochlear fluid is assumed to be incompressible. It is rather propagated by the combined movement of the cochlear fluid and basilar membrane. The mechanism of the travelling wave within the cochlea will be described in this section.

1.3.1. Travelling wave

The geometry and mechanical properties of the basilar membrane are crucial to understanding how the pressure waves travel through the cochlea. At the basal end of the cochlea, the basilar membrane is narrow and stiff, and the waves causing its displacement propagate with high velocity and small amplitude. As the wave travels further towards the apex of the cochlea, the stiffness of the basilar membrane decreases and the waves slow down while increasing in amplitude (Lyon and Mead, 1998). At some point, called the characteristic place for the given input frequency, the membrane will vibrate with maximum amplitude (Dallos, Popper and Fay, 1996). The location of the characteristic place is dependent on the stimulus frequency. One of the ways to describe this relationship is with a Greenwood function that is defined for several mammalian species based on approximation derived from a series of experiments (Greenwood, 1996):

$$f_x(x) = C_0(10^{a_0\left(1-\frac{x}{L}\right)} - K_0) \qquad (1.1)$$

where: L – length of the cochlea, and C_0, a_0, K_0 – constant values dependent on the species given in Table 1.1.

Table 1.1: Parameters for Greenwood's function for selected species (LePage, 2003)

	C_0 [Hz]	a_0	K_0	L [mm]
Mouse	7130	0.99	1	6.8
Gerbil	38	2.2	0.631	12.1
Chinchilla	163.5	2.1	0.85	18.4
Guinea pig	350	2.1	0.85	18.5
Domestic cat	456	2.1	0.8	25
Macaque	360	2.1	0.85	25.6
Human	165.4	2.1	1	35
Cow	52.6	2.1	1	38.3
Elephant	81	1.8	1	60

Beyond the characteristic place, the basilar membrane becomes too flexible, and the vibration is too damped to facilitate further wave propagation for a given stimulus frequency. As a result, the displacement amplitude decreases rapidly as the wave enters the cut-off region.

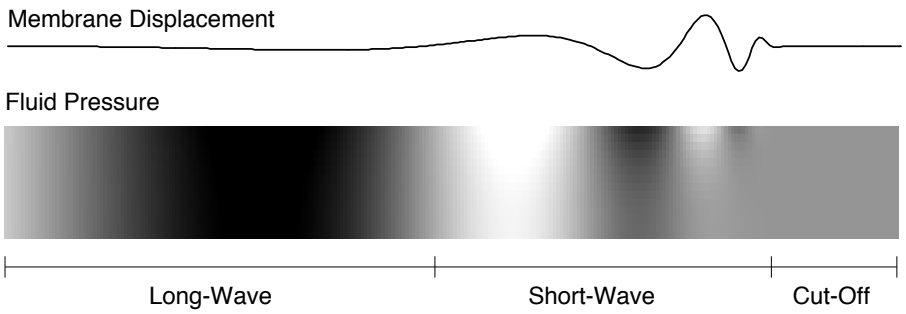

Figure 1.8: Wave propagation within the cochlea, showing the membrane displacement and fluid pressure
Source: www.lloydwatts.com [21.09.2019].

The schematics of the membrane displacement and fluid pressure in the lower chamber are illustrated in Figure 1.8. The wave propagating through the cochlea can be divided into three regions. The wave is said to be in a long-wave region when its wavelength is long compared to the height of the cochlear duct. In this region, the fluid motion is longitudinal, moving back and forth, and the propagation velocity is independent of the wavelength and is nondispersive. That means that for a complex stimulus all components travel together and the wave 'packet' keeps its original shape. When the wavelength becomes short compared to the height of the cochlear duct, the wave is in the short-wave region, and the propagation becomes dispersive. This indicates that for a complex acoustic signal its frequency components do not travel at the same speed. This mechanism causes the pressure across the scala to become less and less uniform, with the biggest pressure concentration near the cochlear partition. The consequence is for the wave to become more dispersive. Every propagation successively slows down, building up the energy in a very narrow region - the characteristic place. Finally, the wave dies out rapidly in the highly damped cut-out region (Shera, 2008).

1.3.2. The role of Organ of Corti elements in cochlear mechanics

The interactions between the elements of the Organ of Corti are far from understood, and a thorough and comprehensive analysis of its key elements is needed to grasp the complicated nature of the electro-mechanics of the inner ear.

Historically, the basilar membrane has often been a primary focus of the studies regarding cochlear mechanics, and its functionality was the main topic of interest when analysing the frequency decoding properties of the inner ear (Allen, 1998). Because of the difficulty in obtaining non-invasive measurements in a living cochlea, the Laser Doppler Vibrometer analysis of the basilar membrane motion was often the only way of gaining insight into the Organ of Corti (Nuttall, Dolan and Avinash, 1991). As a result, it was often hypothesised that the BM displacement was the central mechanism of the cochlear mechanics, and the main function of the cochlear amplifier driven by the electromotility of the outer hair cells was to provide a driving force to enhance the BM vibration. For that mechanism to be as effective as possible, the reticular lamina should act as a firm anchor for the hair cells, which consequently would implicate it is not sensitive to the outer hair cells' motility. That, in turn, would compromise the modes of excitation of the inner hair cells that are believed to be dependent on the drag of the fluid in the subtectorial space (a space between the reticular lamina and the tectorial membrane - a gel-like sheet running parallel

to the basilar membrane along the entire length of the cochlea that overlays the tips of the hair bundles of the outer and inner hair cells) (Steele and Puria, 2005).

More recent studies are starting to utilise modern technology for imaging and data collection leading to the improved understanding of the Organ of Corti elements and their interactions. One of the most notable developments was a study using a heterodyne low-coherence interferometer to accurately measure BM and RL motions in living a mouse cochlea (Ren, He and Kemp, 2016). In the study, it was observed that the reticular lamina motion is considerably larger than that of a basilar membrane both at the best frequency as well as the low frequencies confirming the findings from several other experiments (Chen *et al.*, 2011; Ramamoorthy *et al.*, 2014). Those findings suggest that the force generated by electromotility of the outer hair cells is meant to enhance the reticular lamina vibration more than that of the basilar membrane and should be accounted for in future cochlear models.

1.4. Electrical signals in the cochlea

Potentials arising from the inner ear and the auditory nerve provide a valuable tool for a wide range of clinical applications. Recording these electrical signals offers an insight into the peripheral auditory system. The following sections describe methods used to obtain those recordings, as well as introduce the potentials evoked in the cochlea and the auditory nerve.

1.4.1. Auditory Brainstem Response and Electrocochleography

Auditory Brainstem Response is an objective test allowing assessment of the hearing pathway and identifying neurological abnormalities of the auditory nerve along the auditory pathway up through the brainstem. This test can be run with all patients having difficulty with conventional behavioural methods of hearing screening (including newborn screening) and is also recommended for any person with clinical manifestations suggesting that their type of hearing loss might stem from an abnormality in the brain or the brain pathway.

The ABR is extracted from the signal recorded via electrodes placed on the scalp, using earphones placed into the ear canal, delivering clicks or tone bursts stimuli. The acquired signal is a series of vertex positive waves, five of which are evaluated during the hearing screening process.

They occur within the first 10ms after the start an auditory stimulus and are being generated by (Herdman, 2007):

- wave I – 8th cranial nerve (distal end),
- wave II – cochlear nucleus (or proximal end of 8th nerve),
- wave III – superior olivary complex,
- wave IV – lateral lemniscus,
- wave V – inferior colliculus.

Recorded electrical responses contain a waveform with a series of peaks present. They provide information about how long it takes for the various structures of the auditory pathway to respond to the stimulus. Delays in these peaks can aid in identifying the presence of acoustic neuromas along the central hearing pathways.

In electrocochleography measurements, the recording electrode is placed as close to the cochlea as possible, in the ear canal or on the tympanic membrane. In some cases, the recording electrode may be a transtympanic needle electrode guided through the tympanic membrane into the round-window niche to provide a stronger signal than extratympanic recordings. The electrocochleography is mostly used to determine if the inner ear has an excessive amount of fluid pressure associated with Meniere's Disease (MD), which can cause symptoms such as hearing loss, dizziness or tinnitus (Vassiliou *et al.*, 2011). It is also used as a way of diagnosing ANSD.

The waveform recorded during the test consists of three components: the summating potential (SP), the action potential (AP) and the cochlear microphonic, all of which are described in the following sections. Additionally, a $\frac{SP}{AP}$ ratio can act as an additional diagnostic tool in patients with excessive fluid pressure in the cochlea as its value is found to be elevated in about 60% of the population diagnosed with MD (Ferraro and Tibbils, 1999).

1.4.2. Receptor Potential, Action Potential and Phase Locking

Stereocilia are the core mechanism responsible for the transformation of sound vibration into a neural signal that can be interpreted by the brain.

Both types of hair cells have a similar electro-mechanical transduction mechanism. The auditory nerve fibre potential varies from -70mV to -55mV, and the endolymph surrounding them is characterised by an endocochlear potential of +80mV. This results in a potential difference being as high as 135-150 mV. The deflection of the stereocilia causes ion channels to open, and a massive

influx of potassium and calcium ions from the endolymph to the hair cell occurs, causing its depolarisation (Hudspeth *et al.*, 2000). This leads to a release of a transmitter and subsequent auditory nerve fibre activation (Faris, 2011). The level of hair cell depolarisation depends on the force with which the stereocilia bend. After exceeding a certain level, an action potential occurs. The threshold potential of a nerve cell is around 15mV higher than its resting potential, so for auditory nerves, its value will vary between -55mV and -40mV. In the peak moment of the cycle, the cell potential raises up to +40 mV. During the refractory period, the nerve cell is insensitive and cannot fire again until its polarisation comes back to the resting potential (Gelfand, 2009).

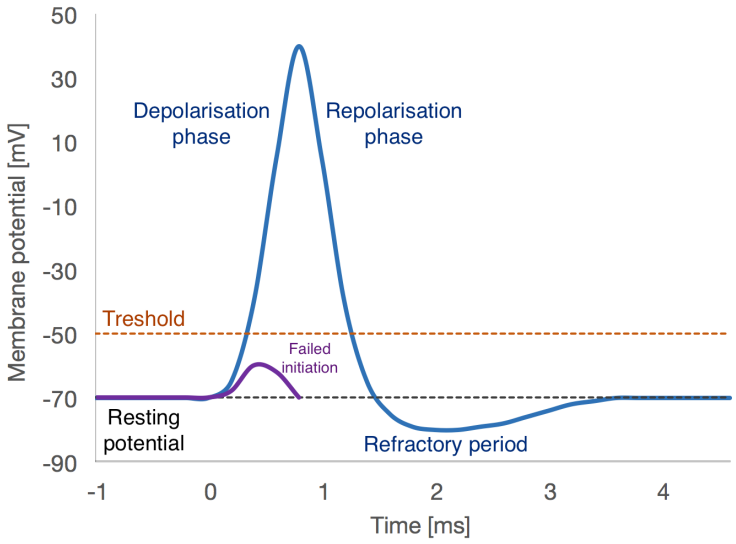

Figure 1.9: Schematic representation of the transmission of a nerve impulse. The graph shows the depolarisation and repolarisation phase of the action potential together with the refractory period. If the membrane potential does not reach the threshold value the potential returns to a resting potential of -70mV after a failed initiation.

Depolarisation occurs only in one direction of stereocilia bending. In another direction, the cell is unable to produce action potential but a spontaneous firing can be present – firing occurs without stimulation at a random rate, varying between 0 up to over 100 spikes per second (Yost, 2007). Since the action potential does not depend on how much the stereocilia are being bent (hence, the basilar membrane vibration amplitude) the information about the loudness of the sound is perceived through the number of nerve firings in time. Figure 1.10 shows responses of single nerve fibre for different levels of stimulus.

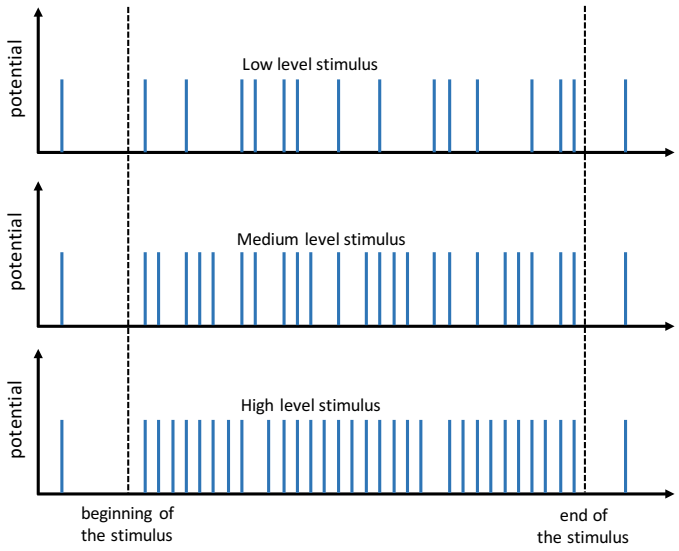

Figure 1.10: Nerve spikes plotted against time in a single neuron fibre for low, medium and high stimulus levels. The amount of nerve firings is shown to increase as the stimulus intensity becomes higher. Additionally, several spontaneous nerve firings are depicted outside of the period where stimulus was present.

In theory, the maximum frequency of the nerve firing can be estimated assuming that each firing occurs right after the refractory period. For a single neuron fibre of the auditory nerve, the time required to go back to resting potential is around 1.3ms, which would give the frequency of 770Hz.

For a simple, pure tone stimulus, the nerves fire around a set point of the sine wave cycle in a process that is referred to as phase locking. The refractory period of each auditory nerve fibre might render them unable to fire every consecutive cycle, but when the AP does occur, it happens around a constant phase angle of the stimulus (Palmer and Russell, 1986). However, phase-locking cannot be observed for all of the frequencies within the hearing range. It starts getting less significant around 1 – 2 kHz and disappears completely around 4 – 5 kHz (Reichenbach and Hudspeth, 2014).

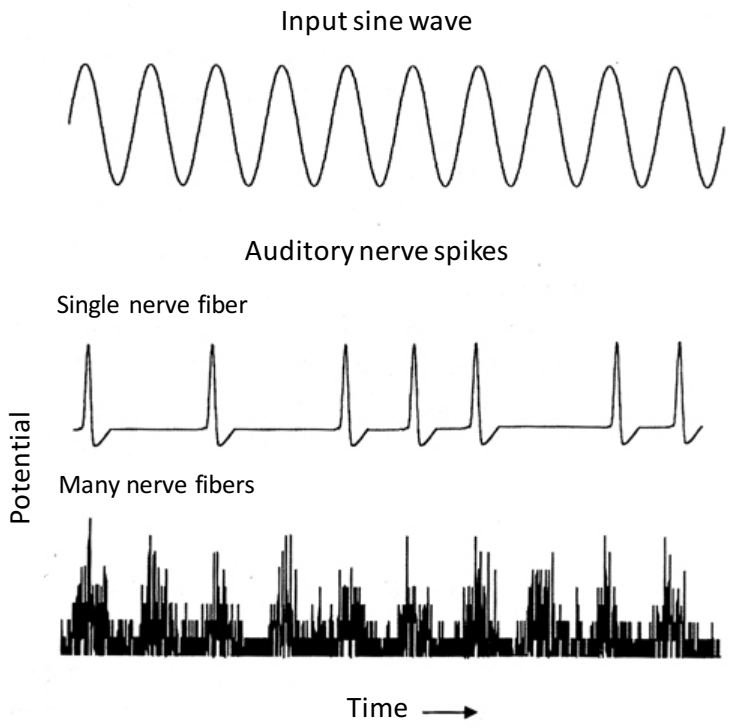

Figure 1.11: Illustration of phase-locking mechanism for pure tone stimulus. The plot illustrates the firing of single and multiple auditory nerve fibres in response to a pure tone stimulus. Source: www.acousticlab.org [11.07.2019].

1.4.3. Cochlear microphonic

The cochlear microphonic (CM) is derived predominantly from the currents flowing through the hair cells. The site of its generation is the border of the endolymphatic space, namely the reticular lamina. It is proposed that the vector sum of the extra-cellular components of receptor potentials arising from OHCs is the key contributor to the generation of the CM (Charaziak, Shera and Siegel, 2017a) because they outnumber IHCs by over three-fold (Jahan *et al.*, 2013). The CM is also speculated to arise mainly from the basal part of the basilar membrane, while the contributions from the apical section are negligible (Withnell, 2001). This stems from the way the recording electrode sums up the potentials produced by hair cells situated at different points on the travelling wave. At the basal part of the travelling wave, almost all of the basilar membrane deflections occur with the same phase, whereas moving to the apical part, the phase changes at a greater rate with distance. A proportion of the hair cells will then make the scala media go positive, and others - negative. The potentials will then cancel each other out and will not be recorded on the remote electrode. Figure 1.12 illustrates this principle.

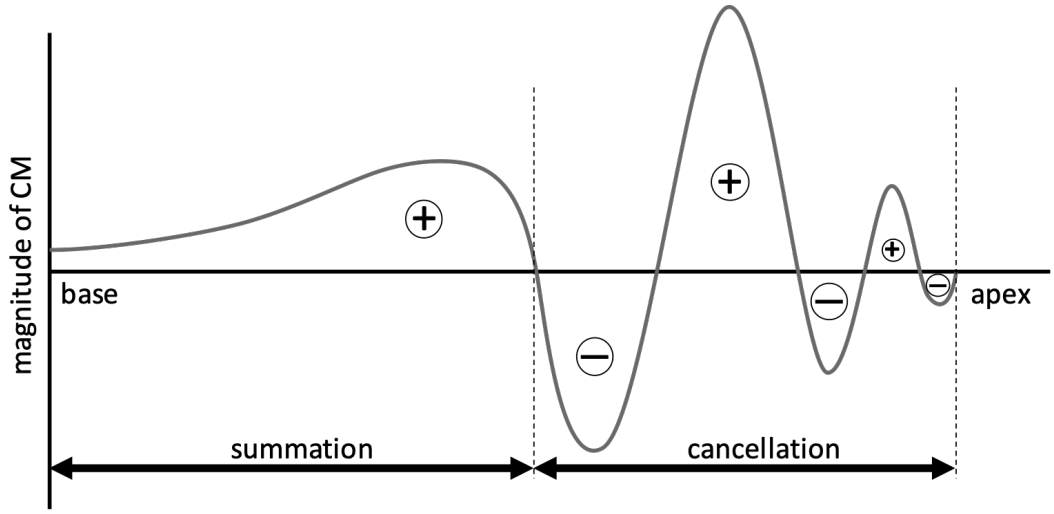

Figure 1.12: The influence of the current spread on the recording of cochlear microphonic. The basal part of the cochlear microphonic response is marked as the summation region when the signal polarity stays positive, while the apical part shows a cancellation region due to alternating polarity of the cochlear microphonic

When the hair cells' transducer channels open, the ion influx inside the cell causes them to go more positive. The current is drained from the scala media rendering it less positive. When the ion channels close again, the current flow reduces, and the polarisation of the scala media moves back more positive. Therefore, the potential changes in scala media have the opposite phase to the potential changes in the hair cells and scala tympani. The alternating current (AC) response recorded during electrocochleography (ECochG) approximately follows the shape of the acoustic stimulus waveform. CM's spatial localisation for low-intensity stimuli mimics the travelling wave – for low frequencies the response is going to be visible near the apex, and for high frequencies near the base. The peak of the response compares well with the localisation of the peak of the travelling wave envelope. However, along with stimulus intensity growth, the CM peak shifts towards the base of the cochlea and tends to be situated basally to the travelling wave envelope peak (Dong and Olson, 2013).

1.4.4. Summating potential

The summating potential is a direct current (DC) feedback that appears to follow the time-displacement pattern on the cochlear partition in response to the acoustic stimulus envelope. It is believed to be derived directly from the stimulus-evoked potentials in hair cells of the Organ of Corti. It is mainly a distortion product of a sound stimulation caused by the basilar membrane not being deflected the same amount in both directions (Pickles, 1988).

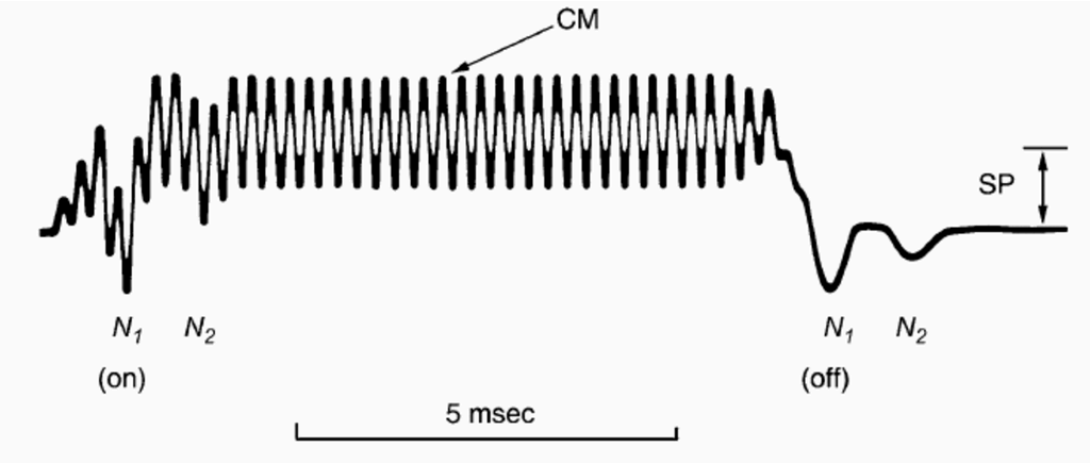

Figure 1.13: Response recorded with gross electrodes, showing N1 and N2 potentials onset, followed by the cochlear microphonic response. The graph marks the DC offset as the summating potential (Pickles, 1988)

Some of the components of SP are believed to represent a sum of various nonlinearities associated with transduction processes in the cochlea. Therefore, the magnitude of the summating potential reflects the amount of distortion introduced by these processes. It is recorded as a unidirectional shift in the cochlear microphonic baseline. The direction of this shift is either positive or negative and depends on a complex interaction between stimulus parameters and the location of the recording electrodes.

1.4.5. Gross neural potential (compound action potential)

The gross neural potential is interpreted as the summed effect of all action potentials travelling down the auditory nerve. It consists of two components: the N1 and N2 potentials that can be recorded with gross electrodes in response to stimulus onset (Pickles, 1988). The responses are evoked by clicks or by tone pips (Dallos, Popper and Fay, 1996). Measurements performed in rodents indicated that the N2 potential, as well as the positive potential between the N1 and N2, was generated by secondary auditory neurons situated in the cochlear nucleus (Møller, 1983), and they correspond to wave I and wave II in electrical responses recorded during ABR testing. While recording the CAP, the first component (N1) appears about 1ms, and the second one (N2) 2ms after a presentation of a moderate- to high-level stimulus, although both the latency and the amplitude of CAP peaks are dependent on the stimulus intensity: the amplitude increases while the latency decreases with higher-level stimuli (Celesia, 2013). Fibres of characteristic

frequencies of 4kHz and higher seem to contribute the most to recorded responses (Antoli-Candela and Kiang, 1978).

IHC damage has a predictable effect on CAP, resulting in a reduction of the CAP amplitude while only slightly affecting the threshold for excitation of auditory nerve fibres (typically 10-20dB SPL stimulus). OHC damage, on the other hand, causes a shift in the CAP threshold while maintaining the amplitude of the potentials (Özdamar and Dallos, 1976).

1.4.6. Latencies of auditory evoked potentials

A different type of auditory evoked potential arises as the signal moves down the auditory path. The expected latencies are a helpful tool to differentiate between the origins of each of the responses. A summary of expected latencies and corresponding auditory evoked potentials is collected in Table 1.2.

Table 1.2: Latencies of auditory evoked potentials. Adapted from (Terence W. Picton, 2010)

Latency	Transient response	Steady-state response	Sustained response
0-5 ms	Cochlear Nerve Compound Action Potential (CAP: N1, N2)	Cochlear Microphonic	Summating Potential
1-15ms	Auditory Brainstem Response (ABR: I-VII)	Frequency Following Response; Fast (>70Hz) Auditory Steady-State Responses	Slow wave component of the frequency following response
10-50ms	Middle-latency Response (MLR: Na, Pa, Nb)	40Hz Potential	N/A
30-500ms	Vertex Potential (P1, N1, P2, N2)	Slow (<30Hz) Auditory Steady-State Responses	Cortical Sustained Potential

1.4.7. Artifacts in cochlear evoked potentials measurements

Gathering measurement data from scalp-placed electrodes is prone to contamination caused by different phenomena that are not generated by the auditory nervous system. Those responses are classified as artefacts and can be differentiated based on their origin:

- physiologic – originating from the subject,
- physical – originating from the environment.

The secondary classification categorizes them into artefacts that are stimulus-related and stimulus-independent. The table below provides an overview of the different origins of artefacts that can affect the auditory evoked potentials recordings and the mitigation strategies.

Table 1.3: Physiological and physical sources of artefacts in evoked potentials measurements. Adapted from (Terence W. Picton, 2010)

Classification	Source	Spectral content	Origin	Control strategy
Physiologic	**Skin**	0.1 - 2Hz	Activation of skin and sweat glands	Cool ambient temperature in the test rom
	Blood Vessels	0.1 - 20Hz	Potentials related to the blood flow	Averaging
	Tongue	0.1 - 20Hz	Movement of the tounge in the oral cavity	Instructing the subject, artifact rejection
	Eye Blinks	1 - 5Hz	Eyelid moving over the cornea	Instructing the subject to voluntarily fixate the eyes, artifact rejection
	Eye movement	0 - 50Hz	Rotation of the eyeball	Instructing the subject to voluntarily fixate the eyes, artifact rejection
	Electrocardiogram	1 - 50Hz	Depolarization of the cardiac muscle	Averaging
	Scalp Muscle Reflexes	20 - 50Hz	Scalp microreflexes	Relaxation, comfortable position, sleep
	Muscles	10 - 500Hz	Spontaneous muscle activity	Relaxation, comfortable position, sleep

Physical	**Power cables and transformers**	In the UK: 50Hz + harmonics	Spectral content generated at the frequency of the power source	Magnetic shielding, braided electrode wires, lowering the interelectrode impedance
	Electrodes	All of the frequencies in the amplifier band-pass	Noise generated due to the changing electrode impedance	Lowering the interelectrode impedance, use of common-mode rejection amplifier, "right-leg" reference electrode
	Transducer	At stimulus frequency	Electromagnetic field generated by the voice coil	Alternating stimulus polarity, magnetic shielding of the transducer, placing transducer and distant from the subject as possible
	Movement	0-100Hz	Movement of electrodes through static magnetic fields	Artifact rejection protocol

1.5. Auditory neuropathy spectrum disorder

Auditory Neuropathy Spectrum Disorder (ANSD) or Auditory Neuropathy (AN) is not a particularly common type of hearing disorder and accounts for approximately 10% of permanent hearing loss cases (Uus and Bamford, 2006). In ANSD, the outer hair cell activity is preserved but the neural activity in the auditory nerve is disrupted (Lindsey, 2014). Consequently, people with ANSD might well be able to hear/react to environmental sounds but still have difficulties in understanding speech and/or interpreting sounds (Uus, Young and Day, 2011) to the greater extent than would be indicated by the degree of hearing loss that is appearing during the pure-tone audiometry. Since these symptoms might also apply to other types of hearing disorders, the correct diagnosis of the AN can be rather challenging. However, the development of auditory brainstem response measurements (ABR) in the ‘70s (Starr, 1978) provided, for the first time, a helpful measure to evaluate the auditory brainstem function objectively. In a healthy person without AN, a typical result for ABR would show five distinct waves (Wave I - V) generated by different parts of the auditory nerve occurring within 10ms after exposure to the stimulus signal (Jewett and Williston, 1971). To determine dysfunction of the auditory nerve, the relative amplitudes of these waves have to be evaluated with respect to a “normal” response (Starr and Achor, 1975; Rance and Starr, 2015). This, in conjunction with objective measures of the hair cell activity using otoacoustic emissions (OAEs) and cochlear microphonic (CM),

have become the standard tools to diagnose auditory neuropathy in patients and help to distinguish AN from impairments due to loss of sensory receptors (SNHL) caused by old age, exposure to high-intensity noise, ototoxic drugs, certain infectious diseases, head injuries or benign tumours on the auditory nerve. Meanwhile, auditory neuropathy is believed to arise from three possible sources: damage to the inner hair cell, a faulty connection between the IHC and the auditory nerve or damage to the auditory nerve itself.

The usual clinical findings that define auditory neuropathy are: the presence of outer hair cell integrity in evoked otoacoustic emission (OAE) or cochlear microphonic (CM) and the absence of synchronised neural activity at the level of the 8th nerve and brainstem (Kumar and Jayaram, 2005). To differentiate ANSD from 'typical' sensorineural hearing loss a classification can be made, as described in Table 1.4 (Feirn *et al.*, 2013):

Table 1.4: Classification of hearing loss and the implied diagnosis depending on the clinical evaluation

Clinical findings	**Implied diagnosis**
• ABR absent/severely abnormal • CM or OAE present	ANSD
• ABR absent/severely abnormal • CM or OAE not recordable	SNHL
• ABR present but elevated	SNHL

Usually, the absence of both CM and OAE strongly suggests that a patient has 'conventional' hearing loss (SNHL). However, the typical presence of otoacoustic emissions in ANSD makes it difficult to put a correct diagnosis. Furthermore, it is not uncommon that the presence of OAE and CM varies over time, sometimes even from one day to another (Uus, Young and Day, 2011), which can complicate the diagnosis even more.

To understand the term 'neuropathy' we can look at the definition used by neurologists to describe pathologies of peripheral nerves (pathologies of their neuronal cell bodies of origin are not a part of this category and are rather referred to as neuronopathy or ganglionopathy (Waddell *et al.*, 2013)). Neuropathy can be divided into three main categories (Rapin and Gravel, 2003):

- myelinopathies – affected are Schwann cells wrapped around axons in the form of myelin sheaths; it slows down or blocks nerve conduction,
- axonopathy – the axon itself is damaged; it causes the most distal section of the peripheral nerves to die, eventually leading to degeneration and death of the whole axon,
- mixed neuropathies – a combination of myelinopathies and axonopathy.

Considering those definitions, even looking at the name of this type of hearing impairment, we encounter an indication of many misunderstandings surrounding AN, as strictly speaking the term 'neuropathy' would point only to the damage of the auditory nerve, which is not necessarily accurate.

In approximately 40% of the cases, AN is caused by genetic factors (Manchaiah *et al.*, 2011), and it is estimated that 1 in 7000 neonates is born with AN which makes it responsible for around 10% of permanent hearing loss in children (Rance, 2005). Previous studies have linked AN to infants with low birth weight who experienced a severe deficit of oxygen supply before, during or after birth and who were born with hyperbilirubinemia (Simmons and Beauchaine, 2000).

One of the other causes for 8th nerve dysfunction is hereditary motor and sensory neuropathies (HMSN). This term refers mostly to Charcot-Marie-Tooth disease (CMT) characterized by progressive loss of muscle tissue and touch sensation across various parts of the body due to demyelination of nerves in the peripheral nervous system and breakdown of axons and neural cell bodies. Nonetheless, previous research has shown that 52% of patients experiencing the 8th nerve dysfunction had no identified risk factors whatsoever (Sininger and Starr, 2001).

Depending on the exact aetiology of the hearing impairment, different root causes are expected to manifest differently in tests.

Let's consider IHC pathology first - the compound action potential (CAP) represents a summed response of all of the spiral ganglion cells (auditory neurons) and the magnitude of that signal is believed to represent the IHC output. The condition that has to be met to have a recordable CAP is for the neural fibres to fire in synchrony. Thus, performing CAP and ABR click tests would result in no visible response if the IHCs were no longer functioning. However, if the 8th nerve was directly stimulated, the CAP and ABR should both be present pointing at the IHC damage as a source of AN

(El-Badry and McFadden, 2009). Those individuals would also not show OAE suppression due to malfunctioning afferent-efferent reflex arc.

If both OHCs and IHCs were preserved the pathology could be limited to damaged spiral ganglion cells (SGC). SCG pathology would result in CAP and ABR being absent for both acoustical and electrical stimulation (Rapin and Gravel, 2003).

Demyelinating neuropathy of the 8th nerve can also be a cause of AN. In that case, we can expect to observe delayed wave I and II in ABR and increased I – III interval together with prolongation of wave III – V or even their absence (Rance and Chisari, 2016).

If ABR recording shows preserved waves I – III but waves III – V absent or atypical, it implies that the hair cells, SGC and auditory nerve are functioning, and the pathology of the central auditory pathway in the brainstem might be the source of the impairment. However, this might not always affect the hearing if the brainstem pathology is not extensive (Rapin and Gravel, 2003).

1.6. Aims and thesis structure

The initial aim of this doctoral research was to use the existing model of the cochlear electro-mechanics (Ayat, Teal and McGuinness, 2014) and introduce modifications allowing for the accommodation of different input stimuli, extraction of additional mechanical and electrical cochlear responses and integration of inner hair cell model prediction that would reflect the current research findings more accurately, as well as use the adjusted models to make novel predictions about the non-linear processes taking place in the cochlea with a primary focus on the two-tone suppression phenomenon and how it is expected to show up in mechanical and electrical responses of the model.

To further investigate the auditory evoked potentials and their non-linear behaviour, a series of experiments were designed and performed on normal hearing participants using non-invasive, extratympanic measurement techniques utilising three different types of electrodes. Findings from those assessments were discussed in the context of existing cochlear models and their feasibility to make predictions about in-vivo measurements. The purpose of this evaluation was to gain more insight into the auditory evoked potentials, specifically the cochlear microphonic. Currently, CM is used as a tool that aids in the diagnosis of the auditory neuropathy spectrum disorder but its evaluation is mainly based on observing whether it is present or not during the test. Meanwhile, because of the difficulties in recording the CM in conventional clinical settings, any other CM components potentially carrying important information

about the processes taking place in the cochlea remain rather unexplored. With that in mind, the study intended to advance what is known about the CM by evaluating the responses in normal-hearing subjects.

Chapters 2 and 3 are dedicated to the current formulations of the cochlear models from "idealistic" frequency domain formulation, through the state space time domain formulation to a full lumped parameter electromechanical model and are based wholly on the existing literature to guide the reader through the bases of the cochlear modelling. The chapters include multiple validation tests performed on the model and describe minor modifications of the formulation and parameters.

Chapter 4 documents an addition of an inner hair cell model to the existing formulation and presents novel predictions of the complete model obtained using a combination of two tones as the input stimulus.

Chapter 5 describes three novel experiments built around the cochlear microphonic potential and measured in normal hearing subjects. It also reviews the findings in detail and discusses the implications for cochlear modelling.

Chapter 6 summarises the findings from both the cochlear model and the experimental data, discusses the results in the context of relevant published research and debates whether the numerical model can be used to predict the measured cochlear microphonic responses. It also proposes further steps that should be taken to deepen our understanding of the cochlear electro-mechanics and improve the theoretical and experimental work.

1.7. Contributions to knowledge

The primary contributions of this work are as follows:

- In-depth analysis of the current cochlear models
- Implementation of the inner hair cell model formulation and obtaining its outputs along multiple locations of the cochlea
- Simulation of the two-tone interaction and analysis of the two-tone suppression patterns in mechanical responses of the basilar membrane and reticular lamina, and in electrical responses of the outer hair cells, inner hair cells and the scala media (cochlear microphonic)
- Experimental work on normal hearing subjects
  - in-depth comparison of non-invasive measurement techniques for the auditory evoked potentials
  - obtaining input-output functions from cochlear microphonic
  - obtaining two-tone suppression measurements in cochlear microphonic potential
- A comprehensive evaluation of the *in vivo* measurement in the context of the cochlear modelling results and commentary on the origin of the cochlear microphonic based on up-to-date knowledge about the physiology of the inner ear.

2. The bases of modelling cochlear mechanics

The rectangular-box model of the cochlea is shown in Figure 2.1. The cochlear fluid is defined as inviscid and incompressible, with density ρ. On the top, bottom and right side the model is surrounded by rigid walls. The basilar membrane is located in the centre of the model. It is assumed that its stiffness, damping and mass vary with position along the cochlea. The system is driven by the motion of the stapes. Because of the characteristics of the cochlear fluid, the inward movement of the oval window must result in equal onward movement of the round window. Therefore, the fluid on both sides of the basilar membrane moves in the opposite direction and the pressure in corresponding points in upper and lower chambers has the same value but opposite sign.

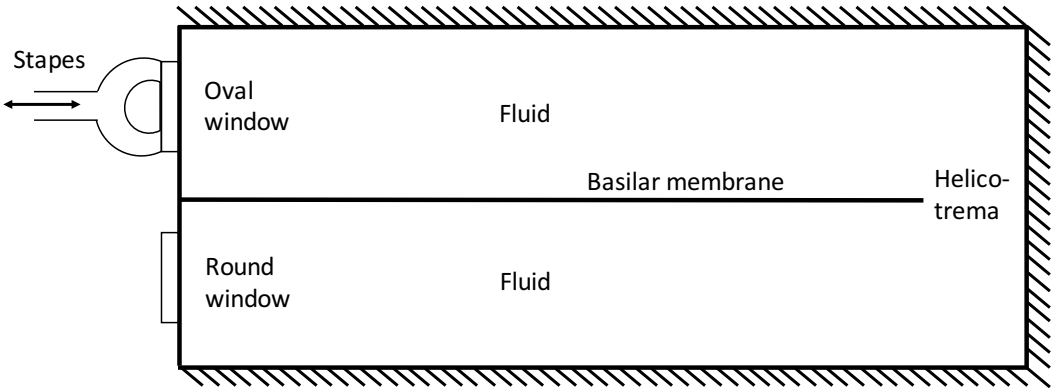

Figure 2.1: A simple physical two-dimensional model of an uncoiled cochlea depicting stapes driving the oval window, the round window and the fluid chambers separated by the basilar membrane with the opening at the helicotrema

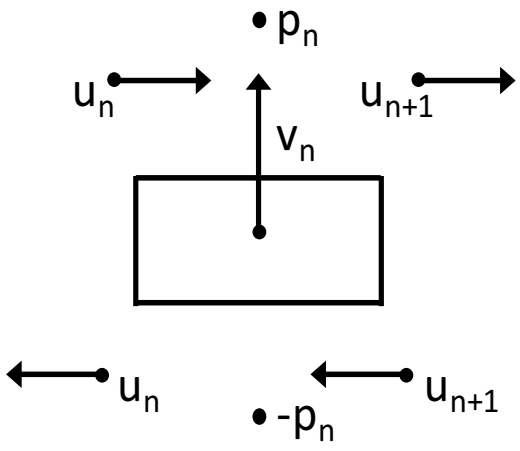

Figure 2.2: Model of a single CP and parameters of the fluid adjacent to it; u_n – fluid velocity uniform across height, p_n – pressure in the chamber, v_n – basilar membrane velocity upwards

When considering a general model, the cochlea is assumed to be longitudinally decoupled. That means that membranes can be divided into a finite number of segments and that the equation of motion for every single cochlear partition is independent of the equations that describe the motion of other sections along its length. Even though a single cochlear partition is assumed to be structurally independent, the motion of the nearby elements is coupled to one another through the cochlear fluid. Each cochlear 'slice' can be described with parameters detailed in Figure 2.2.

2.1. Frequency domain formulation

Frequency-domain formulation of cochlear mechanics allows fast analysis of, for example, basilar membrane motion or frequency response for selected cochlear partition. The results obtained from frequency domain models are a steady state response of the system – they describe a system that does not change its behaviour over time and does not consider the transient part of the response (Kleppner and Kolenkow, 2010). Those types of models work well assuming the cochlea is linear even though, in reality, the system is nonlinear (Dallos, Popper and Fay, 1996). Nonetheless, they are a good starting point to develop a more realistic time-domain simulation, and they provide a practical baseline to compare the time-domain models to. The following sections introduce a frequency domain formulation based fully on cited literature and contain results obtained from a single frequency excitation for the model implemented in MATLAB.

2.1.1. Neely & Kim model

The Neely & Kim model (Neely and Kim, 1986) is a frequency-domain formulation of a cat cochlea. It is based on a lumped-element representation that includes an active element in the inner ear micromechanics that enhances the amplitude of a travelling wave and provides a sharp response in the BM displacement at the characteristic place for the stimulus frequency. It is based on physical principles, anatomical properties and *in vivo* measurements of the mammalian cochlea. N&K model assumes that the motions of the basilar membrane and tectorial membrane are perfectly linear, and the cochlear partitions along the length of the cochlea are lumped two degrees of freedom systems with local masses, stiffness and damping characterising their physical properties. Figure 2.3 shows a model of a single cochlear partition: *m*, *k*, *c* denote mass, stiffness and damping respectively, ξ_t – TM displacement, ξ_b – max. displacement of the BM over its width, *g* – BM to IHC lever gain, P_d – pressure difference across the BM, P_a – pressure source in the OHC.

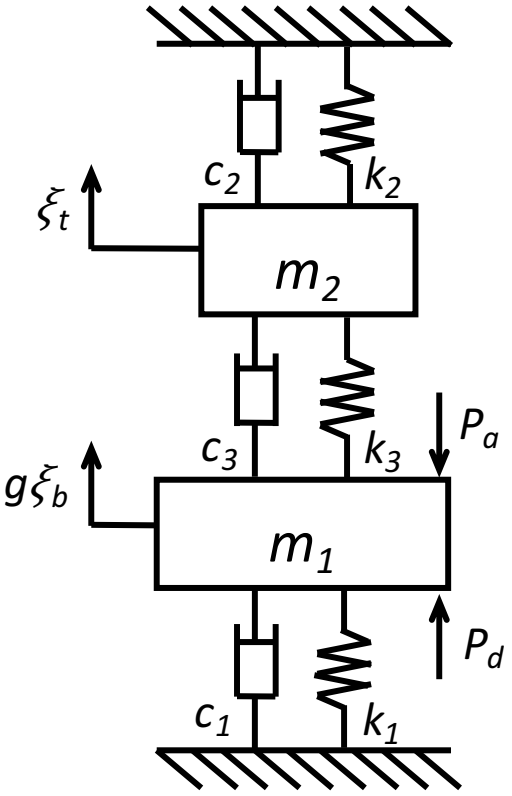

Figure 2.3: Schematic drawing of a single cochlear partition, adapted from N&K depicting BM (*m1*) and TM (*m2*) and their interactions

The model incorporates active elements, which are implemented as pressure sources located within the outer hair cells. They are controlled by the basilar membrane motion and feed the mechanical energy into the cochlea at an expense of the electrochemical energy. Characteristics of those pressure sources can be described as dampers with negative damping values for certain frequencies.

The physical parameters of the modelled cochlea are presented in Table 2.1 and are based on the cat cochlea.

Table 2.1: Physical parameters of the modelled cat cochlea

Parameter	**Value**
L (length)	$25\ [mm]$
H (height)	$2\ [mm]$
W (width)	$1\ [mm]$
ρ (cochlear fluid density)	$1000\ [kg \cdot m^{-3}]$

2.1.1.1. Macromechanics

The basic macromechanical equation arises from consideration of conservation of mass and conservation of momentum in the x-direction. A one-dimensional approximation of cochlear fluid mechanics is considered (Reichenbach and Hudspeth, 2014):

$$\frac{d^2}{dx^2} P_d(x) = \frac{2\rho}{H} \ddot{\xi}_p(x). \qquad (2.1)$$

The boundary conditions for the cochlea are defined as follows:

$$\frac{d}{dx} P_d(0) = 2\rho \ddot{\xi}_s, \qquad (2.2)$$

$$\frac{d}{dx} P_d(L) = 2\rho \ddot{\xi}_h, \qquad (2.3)$$

where ξ_p – displacement of the cochlear partition averaged over its width, ξ_s – inward displacement of the stapes footplate, ξ_h – displacement of fluid from scala vestibule to scala tympani through the helicotrema.

In a frequency-domain formulation, assuming the linearity, the displacement variables can be expressed as:

$$\ddot{\xi}_p(x) = \frac{i\omega P_d(x)}{Z_p(x)} \qquad (2.4)$$

where $Z_p(x)$ – the corresponding mechanical impedance dependent of the local mass, stiffness and damping parameters of the basilar membrane.

2.1.1.2. Micromechanics

In order to solve the macromechanical equations (2.1) - (2.3), the micromechanics of the system can be described in terms of the mechanical impedances of each cochlear partition component, as pictured in Figure 2.3. Mechanical impedance defines the relationship between the input force and the resulting motion of a mechanical system and is frequency-dependent. In the equations (2.5) – (2.8) the stimulus $s=i\omega$ where ω is the radial frequency of the stimulus. The driving-point impedance of the cochlear partition $Z_p(x)$ varies along the basilar membrane length and is dependent on:

- g – BM to IHCs lever gain,
- b - the ratio of $\frac{avg\ CP\ displacement}{max\ CP\ displacement}$,
- γ - OHCs force-generation gain,
- Z_1 – mechanical impedance of the Organ of Corti (on Figure 2.3 marked as ξ_b – maximum displacement of the basilar membrane over its width)

$$Z_1 = \frac{k_1}{i\omega} + c_1 + i\omega m_1, \qquad (2.5)$$

where *k1* is the compliance of the OC, *c1* is the damping of the OC and *m1* is the mass of the OC,

- Z_2 – the mechanical impedance of the tectorial membrane (on Figure 2.3 marked as ξ_t – the TM contribution to the shear displacement between TM and RL that defines the displacement of both OHCs and IHCs (ξ_c))

$$Z_2 = \frac{k_2}{i\omega} + c_2 + i\omega m_2, \qquad (2.6)$$

where *k2* is the compliance of the TM, *c2* is the damping of the TM and *m2* is the mass of the TM.

For clarity, the hair cell displacement ξ_c is defined as:

$$\xi_c(x) = g(x)\xi_b(x) - \xi_t(x), \qquad (2.7)$$

- Z_3 – the coupling between the Organ of Corti and the tectorial membrane (associated with the hair cell displacement ξ_c)

$$Z_3 = \frac{k_3}{i\omega} + c_3, \qquad (2.8)$$

where *k3* is the compliance linked to the coupling between the OC and the TM and *c3* is the damping linked to the coupling between the OC and the TM,

- Z_4 – the frequency-dependent phase shift between the active pressure output (P_a on Figure 2.3) and the hair cells displacement ξ_c

$$Z_4 = \frac{k_4}{i\omega} + c_4. \qquad (2.9)$$

where *k4* is the compliance linked to the motion of the hair bundle ξ_c and *c4* is the damping linked to the motion of the hair cells ξ_c.

The parameters needed for calculations are gathered in Table 2.2.

Table 2.2: Parameters for Neely & Kim model *(Neely and Kim, 1986)*

Parameter	Value	Units
g	1	—
b	0.4	—
γ	1	—
k1	$11 \cdot 10^9 e^{-400x}$	$N \cdot m^{-3}$
k2	$70 \cdot 106 e^{-440x}$	$N \cdot m^{-3}$
k3	$10^8 e^{-400x}$	$N \cdot m^{-3}$
k4	$61.5 \cdot 108 e^{-440x}$	$N \cdot m^{-3}$
c1	$200 + 15000 e^{-200x}$	$N \cdot s \cdot m^{-3}$
c2	$100 e^{-220x}$	$N \cdot s \cdot m^{-3}$
c3	$20 e^{-80x}$	$N \cdot s \cdot m^{-3}$
c4	$10400 e^{-200x}$	$N \cdot s \cdot m^{-3}$
m1	$30 \cdot 10^{-3}$	$kg \cdot m^{-2}$
m2	$5 \cdot 10^{-3}$	$kg \cdot m^{-2}$

The cochlear partition impedance derived from the coupling of all of the elements together has a form of:

$$Z_p = \frac{g}{b}\left[\frac{Z_1 + Z_2(Z_3 - \gamma Z_4)}{Z_2 + Z_3}\right]. \qquad (2.10)$$

2.1.1.3. Model responses

The gain parameter γ of the active elements is set to agree with the published responses. Decreasing the gain results in loss of tuning in the model, while larger gain values can cause spontaneous oscillations and generate SOAEs that can be studied using time domain models. Figure 2.4 shows the effects of different gain settings on the basilar membrane motion along with its phase plots.

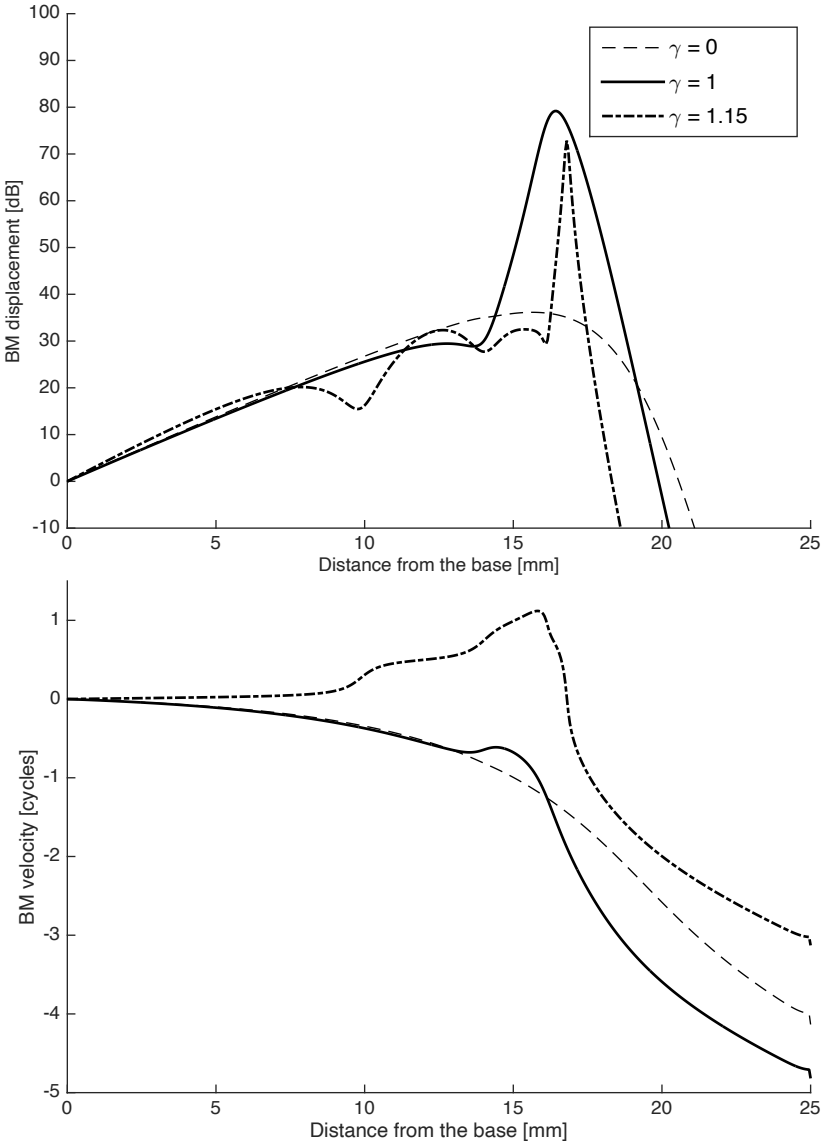

Figure 2.4: Basilar membrane velocity and phase with relation to different gain (γ) values

It should be noted that looking at the solution for γ = 1.15 the phase curve has a positive slope. In further model stabilities studies conducted in the time domain it was shown that for high gain values the system is unstable, which makes the frequency domain results invalid (Ku, 2008).

From the phase response characteristics, it can be observed the cochlea is emitting sound (the travelling wave propagates outwards from the stapes, not along the cochlear length).

In the model, the active elements within the cochlea do not provide the same amount of amplification for all of the frequencies at their characteristic place. Figure 2.5 compares the magnitudes of the basilar membrane velocity for two selected frequencies and demonstrates that the difference between the passive (γ = 0, dashed line) and active (γ = 1, solid line) case is 60dB for a 6.4kHz pure tone stimulus while for a 700Hz tone the amplitude gain of the cochlear amplifier is only 30dB. This example shows that a cochlear amplifier has a considerable impact on high frequencies while low frequencies are much less influenced by it. However, it should be noted that this amount of amplification caused by active elements is reasonable only for low-intensity inputs, near the hearing threshold, and, for higher intensities, the active force has to be significantly lower to account for the compressively non-linear growth of the OHC forces.

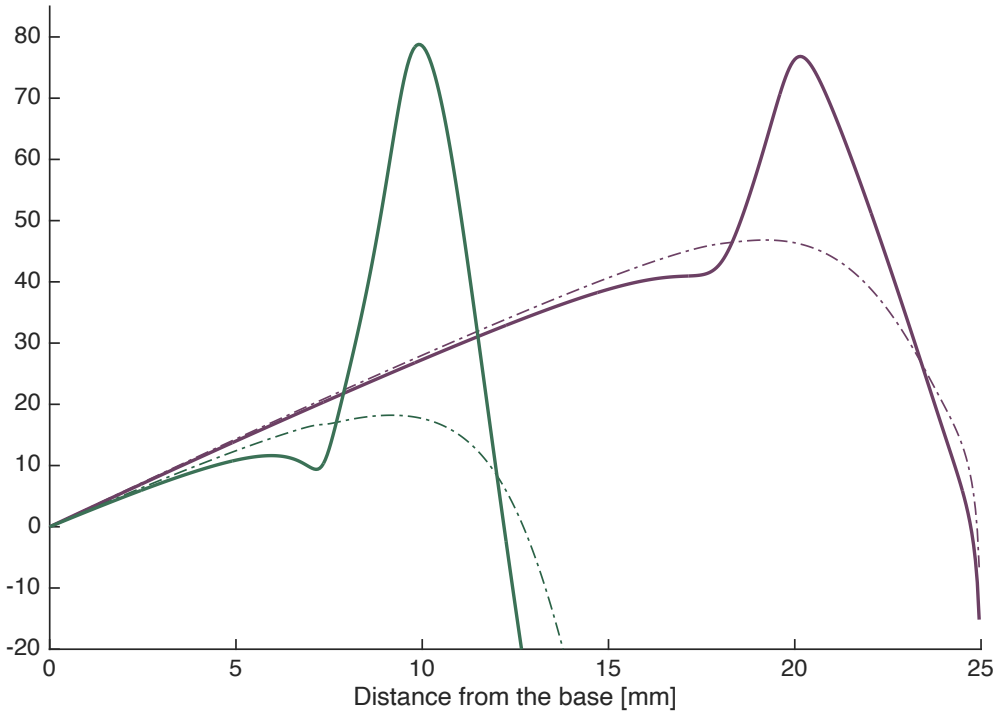

Figure 2.5: Differences in the magnitude of basilar membrane velocity for 'passive' and 'active' (γ = 0 and γ = 1) cochlea for 700Hz and 6.4kHz stimulus

2.2. Time domain formulation

Time domain simulations are the key to gaining more insight into the mechanical responses of the cochlea. It facilitates using more sophisticated stimuli and enables nonlinearities to be incorporated into the system. The following section explains the process of implementing a time domain cochlear model in state space formulation to guide the reader through the principles of the time-domain formulation and presents the results of the simulations. The implementation of the model is based on the mechanics described in Neely & Kim model but translated onto the equivalent Kanis & de Boer quasilinear approach to save computational resources. This method approximates the nonlinear model behaviour of the cochlea by applying a limiting, saturating function onto the OHC pressure output in the frequency domain to obtain a quasilinear cochlear partition impedance that is then fed back into the micromechanical model until the subsequent predictions of the CP velocity converge (Young, 2011). The primary aim of those modifications is to obtain a steady-state part of the response without the need for running a simulation that can take hours to complete. The Kanis & de Boer model formulation and parameters are described in Appendix A. The simulation was run in MATLAB, using the ode45 solver for differential equations.

2.2.1. State space representation

The model is implemented in a state space formulation (Elliott, Ku and Lineton, 2007). This allows for the dynamics to be described in a time domain as a set of coupled first-order differential equations. Following the Neely & Kim description of fluid mechanics, equations (2.1) - (2.3) expressed in the time domain are being used as a starting point. One-dimensional wave propagation in the cochlea is described as:

$$\frac{\partial^2 p(t)}{\partial x^2} - \frac{2\rho}{H}\ddot{\xi}_p(t) = 0, \qquad (2.11)$$

Equation (2.2) has to be rewritten to take under consideration the two superposing components of $\ddot{\xi}_s(t)$, namely $\ddot{\xi}_{SO}(t)$ - the acceleration due to an external stimulus, and $\ddot{\xi}_{SR}(t)$ - the acceleration due to the loading by the internal pressure response in the cochlea at *x = 0*. Therefore, the basal boundary condition can be written as:

$$\left.\frac{\partial p(t)}{\partial x}\right|_{x=0} - 2\rho\ddot{\xi}_{SR}(t) = 2\rho\ddot{\xi}_{SO}(t). \qquad (2.12)$$

To add a small damping at the helicotrema the apical boundary condition is defined as:

$$\left.\frac{\partial p(t)}{\partial x}\right|_{x=L} = 2\rho\ddot{\xi}'_N + \frac{1}{H}p_N \qquad (2.13)$$

Using the concept of the discretised cochlea proposed by Neely (1981), the cochlea can be divided into a number of discreet sections and be defined as discretised spatial derivatives. The full details of that formulation are available in Appendix B.

Following the derivation proposed by Elliot et al. (2007), the coupled cochlea with distributed micromechanics and dynamic boundary conditions can be represented in general state space form:

$$\dot{\mathbf{x}}(t) = \mathbf{A}\mathbf{x}(t) + \mathbf{B}\mathbf{u}(t), \qquad (2.14)$$

2.2.2. Model responses - comparison with frequency domain

Simulations in the time domain require much more complicated algorithms to be implemented in MATLAB. In order to verify if the linear time domain model is giving correct results,

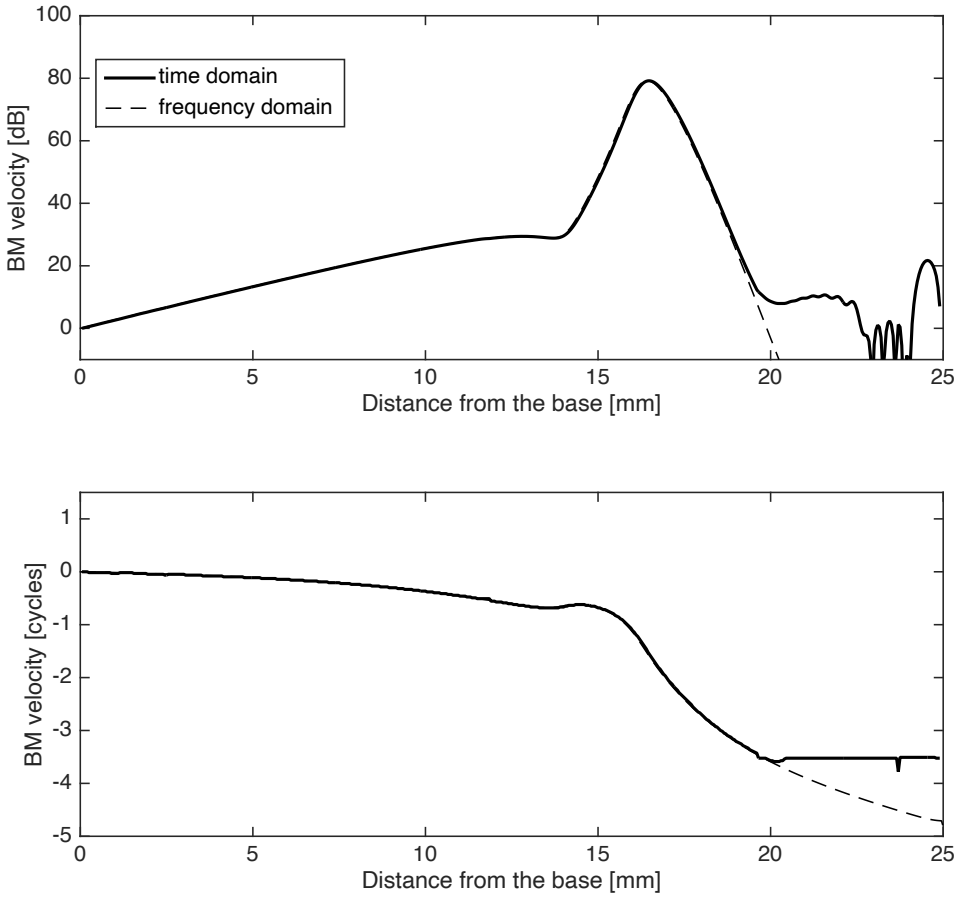

Figure 2.6: Comparison between frequency domain model and time domain model. The agreement of the two is clearly illustrated, with exception of the remainder of the transient response that can be visible at the apical part of the simulated cochlea

the comparison of the pure tone stimulus response in the time domain against the frequency domain was made and is illustrated in Figure 2.6.

The ripples that can be observed in time domain response are a reminiscence of the transient response of the system. To get rid of those artefacts the time of the simulation has to be significantly longer to allow for the transient responses to die down but the outputs of the frequency domain and time domain models are in good agreement.

2.2.3. Model responses - nonlinearity

In linear active models the active pressure is obtained from the model as follows:

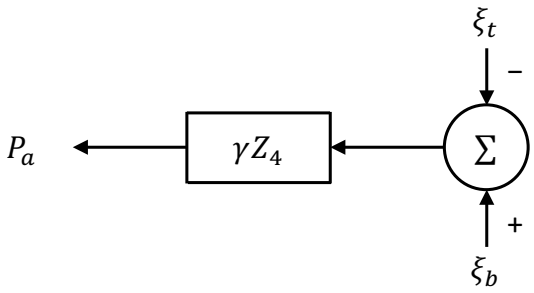

Figure 2.7: Active pressure in linear cochlea

$$P_a(t) = k_4\xi_d(t) + c_4\dot{\xi}_d(t) \quad (2.15)$$

The nonlinearity introduced to the system can have two types:

- Electromechanical transduction (EMT)

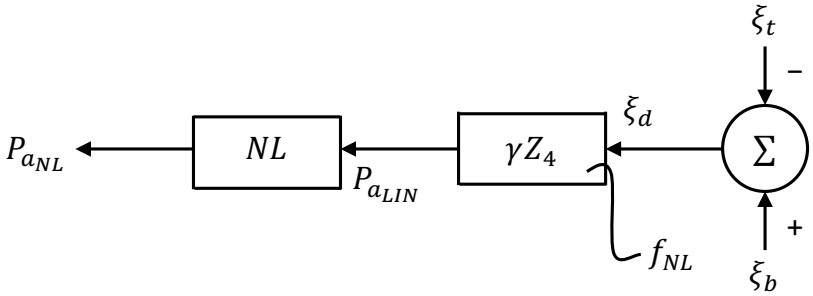

Figure 2.8: Active pressure in cochlea with EMT nonlinearity

where

$$P_{a_{NL}}(t) = P_{a_{max}} tanh\left[\frac{P_{a_{LIN}}(t)}{P_{a_{max}}}\right] \quad (2.16)$$

- Mechanoelectrical transduction - MET

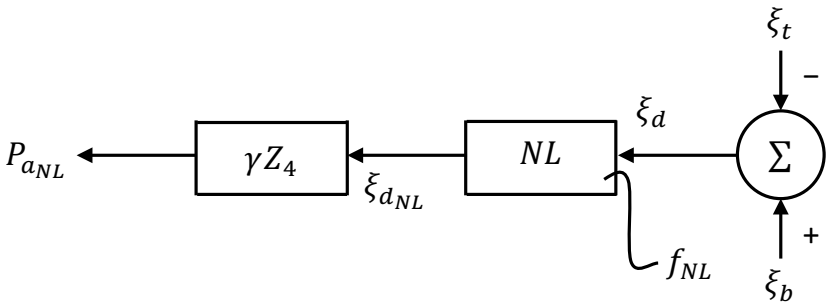

Figure 2.9: Active pressure in cochlea with MET nonlinearity

where

$$\xi_{NL}(t) = \xi_{max} tanh\left[\frac{\xi_d(t)}{\xi_{max}}\right] \quad (2.17)$$

$$P_{a_{NL}}(t) = k_4 \xi_{NL}(t) + c_4 \dot{\xi}_{NL}(t) \quad (2.18)$$

The type of nonlinearity implemented in this model is the EMT nonlinearity, and the saturating function f_{NL} is a hyperbolic tangent.

A linear model assumes that the cochlear amplifier is working in the same way for stimuli of all levels. In reality, along with the stimulus intensity increase, the OHC feedback force begins to saturate (Kanis and de Boer, 1993). To control the gain fed into the system, a scaling function f_{NL} is applied to the OHC feedback force to control the contribution from cochlear the amplifier to the basilar membrane response.

Figure 2.10 illustrates the active cochlea behaviour obtained in response to 3 different stimulus levels with a frequency of 10kHz.

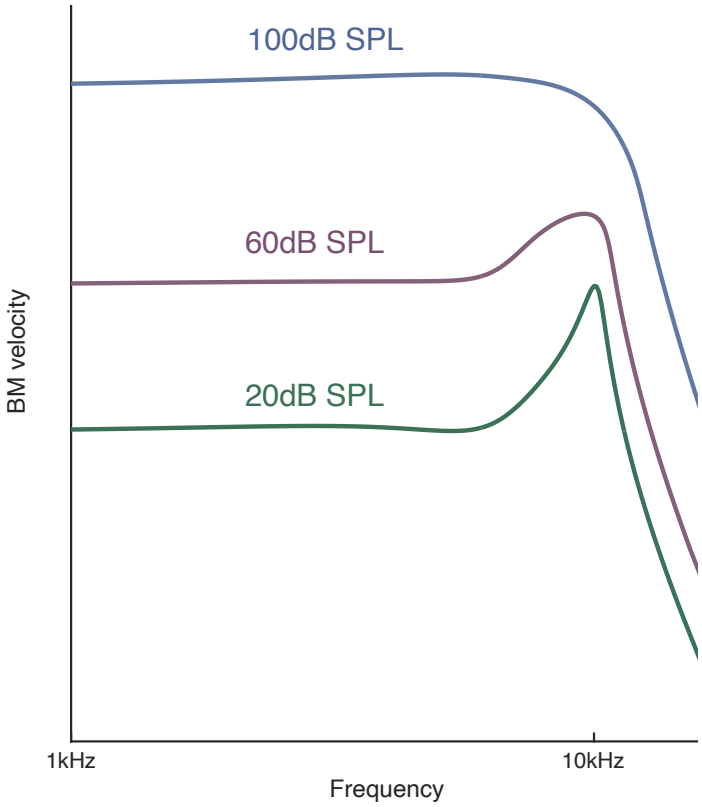

Figure 2.10: Basilar membrane velocity in response to stimuli of 20, 60 and 100dB SPL at 10kHz stimulus frequency

The relation between stimulus level and the basilar membrane displacement enables us to observe the way a nonlinear cochlea responds to different intensity sounds. For low stimulus levels, the contribution of the cochlear amplifier is significant, while for high intensities, the response characteristics begin to look more like those of a passive cochlea. Figure 2.11 obtained from the model shows this relation.

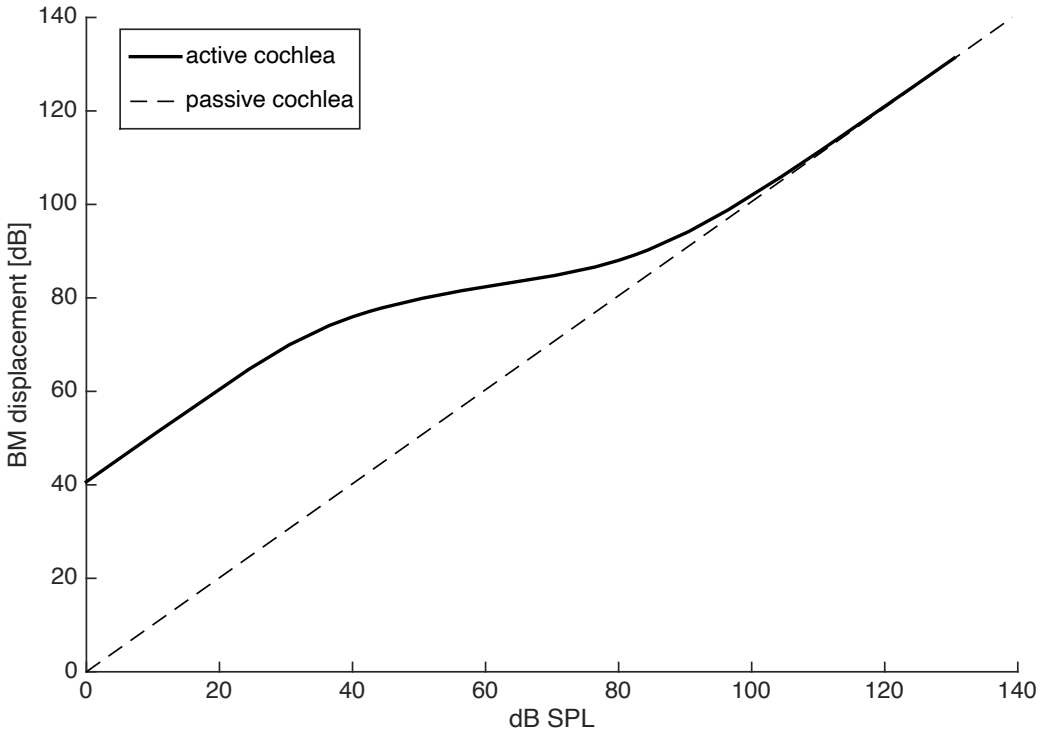

Figure 2.11: Nonlinear growth and the saturation of the BM response in the characteristic place for 1.6kHz stimulus normalised so that the displacement of 0dB for a passive cochlea corresponds to excitation with a stimulus at 0dB SPL level

To better illustrate the mechanism behind the saturation in the nonlinear cochlea, the active pressure from a single outer hair cell located at the characteristic place for 1.6kHz stimulus of 70dB SPL is plotted in Figure 2.12.

Comparing results from the linear formulation of the cochlea with nonlinear pressure responses, it can be observed that at the peak values the OHC feedback active pressure saturates.

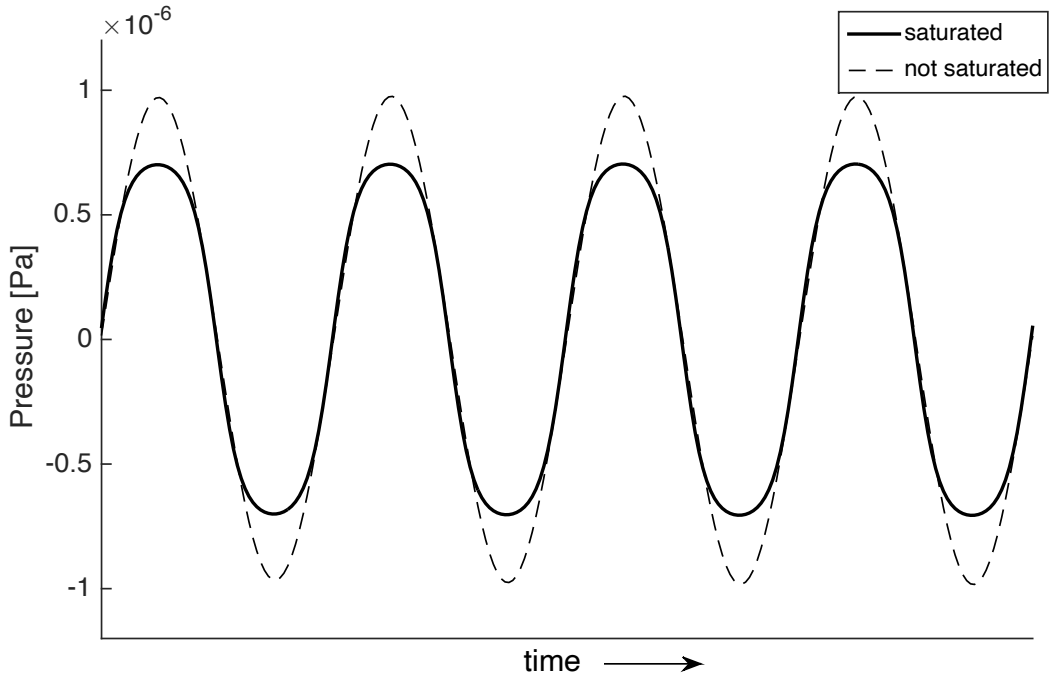

Figure 2.12: Saturated active pressure in a nonlinear model for a characteristic place for 1.6kHz in comparison to a non-saturated active pressure from linear model

If the pressures from Figure 2.12 are plotted as the input-output function, the shape of the scaling hyperbolic tangent can be obtained, which is shown in Figure 2.13.

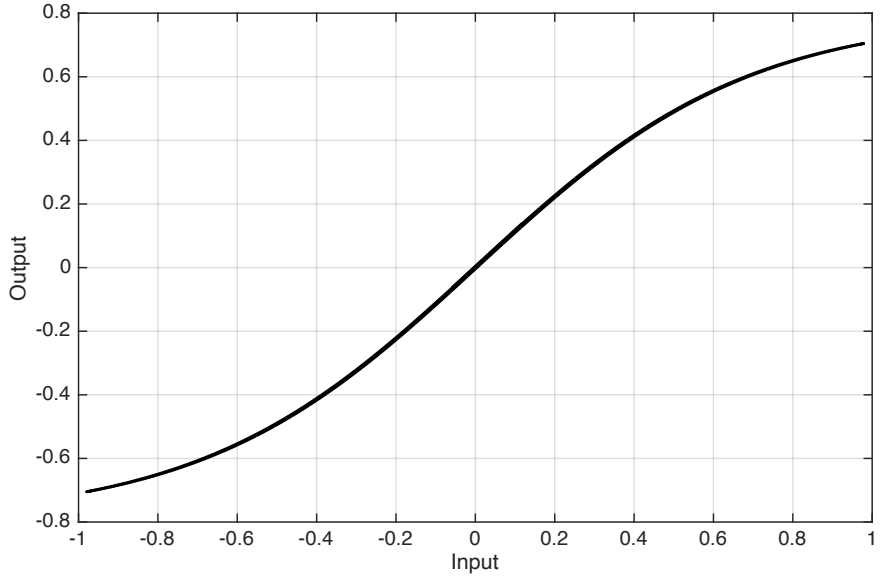

Figure 2.13: Input vs. output plot illustrating the curve of the hyperbolic tangent scaling function

3. Electromechanical model of the cochlea

The models presented in the previous chapter were based on a mechanical approximation of the cochlear function. OHC feedback was still incorporated, however, it was modelled as a force acting upon a basilar membrane rather than using a realistic OHC model. In reality, the cochlea is described far more accurately by an electromechanical model. The mechanical responses are believed to be coupled to the electrical properties making it necessary to simulate both in order to obtain valid responses from the model. Implementing electrical responses also allows observing potentials arising in the cochlea, which opens the possibility to gain insight into *in vivo* measurements. The following sections of this chapter explain the functionality of an integrated electromechanical model of the cochlea using existing published literature.

3.1. Piezoelectric model of the outer hair cell

Mammalian outer hair cells are believed to be responsible for cochlear amplification through electromechanical feedback. The term "electromotility" is used to describe a process in which a cell (in this case, an outer hair cell) changes its physical dimension when supplied with an external electrical potential (Ashmore, 2008). Properties like this are associated with piezoelectric materials, therefore a hair cell can be modelled as a tubular piezoelectric element (Mountain and Hubbard, 1993). The OHC length changes are believed to be associated with the cell membrane potential rather than the whole cell potential (Santos-Sacchi and Dilger, 1988). The elements responsible for OHCs electromotility are the motor molecules (prestin) present within the OHC lateral wall. Hyperpolarisation of the membrane leads to elongation of the cell and depolarisation results in cell contraction (Brownell *et al.*, 1985). If we assume that the OHC has a constant volume, we can describe the cell's movement as:

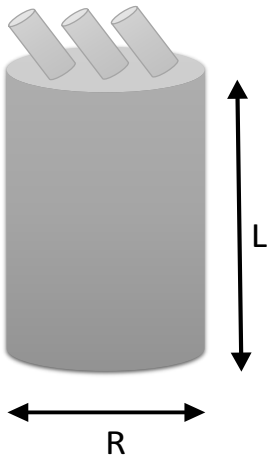

Figure 3.1: Schematic drawing of the outer hair cell

$$V_0 = 2\pi(R + \Delta R)^2(L + \Delta L) \qquad (3.1)$$

where ΔR and ΔL are the voltage-induced changes in the radius and length of the hair cell, respectively. Previous studies (Santos-Sacchi, 1991) have shown that in the characteristic place for the stimulus frequency, the length changes of an isolated OHC were approximately 20nm for every mV change of the membrane potential.

The simplified, one-dimensional linear model circuit is drawn in Figure 3.2 where G_A – apical tension-sensitive conductance, E_{SM} – endolymphatic potential in scala media, G_B - basolateral membrane conductance, E_B - equilibrium potential, C_M – linear part of the cell membrane capacitance, Z_{OHC} – electrical analogue of the OHC mechanical impedance, Z_{OC} - electrical analogue of the organ of Corti mechanical impedance.

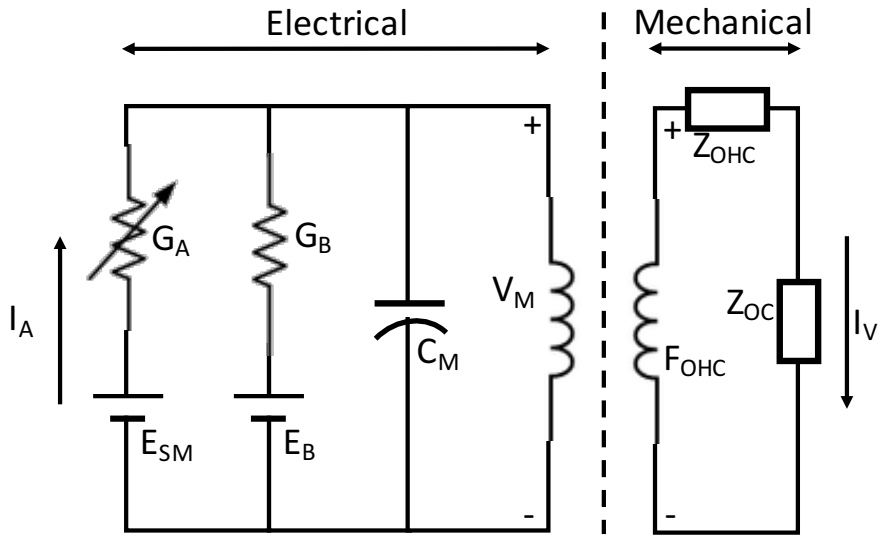

Figure 3.2: Electrical model of the outer hair cell (adapted from Mountain & Hubbard 1993)

This example is presented to demonstrate the general rules of outer hair cells electromotility. In reality, OHCs electromechanical feedback is significantly more complicated due to its non-linear properties and an attempt to model it more accurately will be described in the following section.

3.1.1. Nonlinear piezoelectric model

If we apply the nonlinearity to the piezoelectric model, the main principles of the formulation remain unchanged. The relation between the motility of the OHC and the membrane charge (*Q*) can be described as (Ayat et al. 2014):

$$\xi_o = TQ \qquad (3.2)$$

Where ξ_o is a displacement of the OHC and *T* is a piezoelectric constant defined as an electric polarization generated in a material per unit mechanical stress applied to it (Moheimani and Fleming, 2006). While this relation can be assumed linear, the nonlinearity is introduced by defining *Q* as a nonlinear function of:

$$\tilde{V} = V_{OHC} - T f_{OHC} \quad (3.3)$$

where f_{OHC} is a force induced by OHC electromotility. The membrane charge produces a current:

$$i_Q = \frac{\partial Q}{dt} = \frac{\dot{\xi}_o}{T} \quad (3.4)$$

Furthermore, we define gating capacitance (Hakizimana *et al.*, 2012) C_g that is assumed to be constant:

$$C_g = \frac{\partial Q}{\partial \tilde{V}} \cong \frac{Q}{\tilde{V}} \quad (3.5)$$

3.2. Electrical lumped model of the Organ of Corti

We are considering a slightly modified version of the Liu & Neely formulation (Liu and Neely, 2010). This model is designed in a way that allows the prediction of the cochlear potentials, including cochlear microphonic (Ayat et al. 2014). The definition of the model's macromechanics remains the same as defined in equations (2.1) - (2.3).

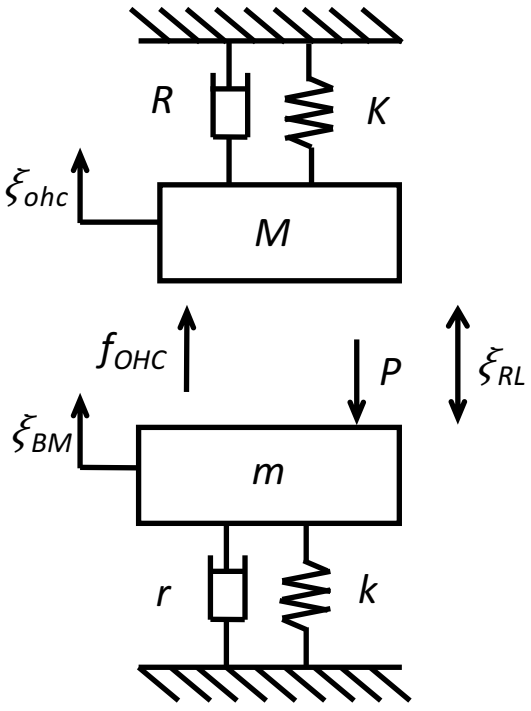

Figure 3.3: Organ of Corti micromechanical model *(adapted from Ayat et al. 2014)*

The micromechanical model looks very similar to the one presented in previous chapters (Figure 2.3 with the difference in the way of how the active process is modelled, in this case, being OHC internal tensile force f_{OHC} rather than the pressure acting upon the basilar membrane (see Figure 3.3).

The cochlea is divided into sections, with each of them consisting of two masses representing basilar membrane and outer hair cell load. The equations describing each section are defined as follows:

$$f_{OHC} = M\ddot{\xi}_o + R\dot{\xi}_o + K\xi_o \quad (3.6)$$

$$-P = m\ddot{\xi}_b + r\dot{\xi}_b + k\xi_b \quad (3.7)$$

To be able to couple the mechanical formulation with the electrical network model, we need to describe a relationship between MET current and the reticular lamina displacement ξ_r:

$$i_r = I(\alpha_v\dot{\xi}_r + \alpha_d\xi_r) \quad (3.8)$$

where α_v and α_d are gain coefficients describing the MET's sensitivity.

The antisymmetric function *I* is defined as:

$$I(\eta) = I_{max}\left(\frac{1}{1 + exp\left(\frac{-4\eta}{I_{max}}\right)} - \frac{1}{2}\right) = \frac{I_{max}}{2}tanh\frac{2\eta}{I_{max}} \quad (3.9)$$

$$\eta = \alpha_v\dot{\xi}_r + \alpha_d\xi_r \quad (3.10)$$

The Organ of Corti can be defined as N number of separate sections, where every section consists of a model of OHC and elements connecting consecutive elements to each other via cochlear fluid spaces. A circuit representing a single section is presented in Figure 3.4.

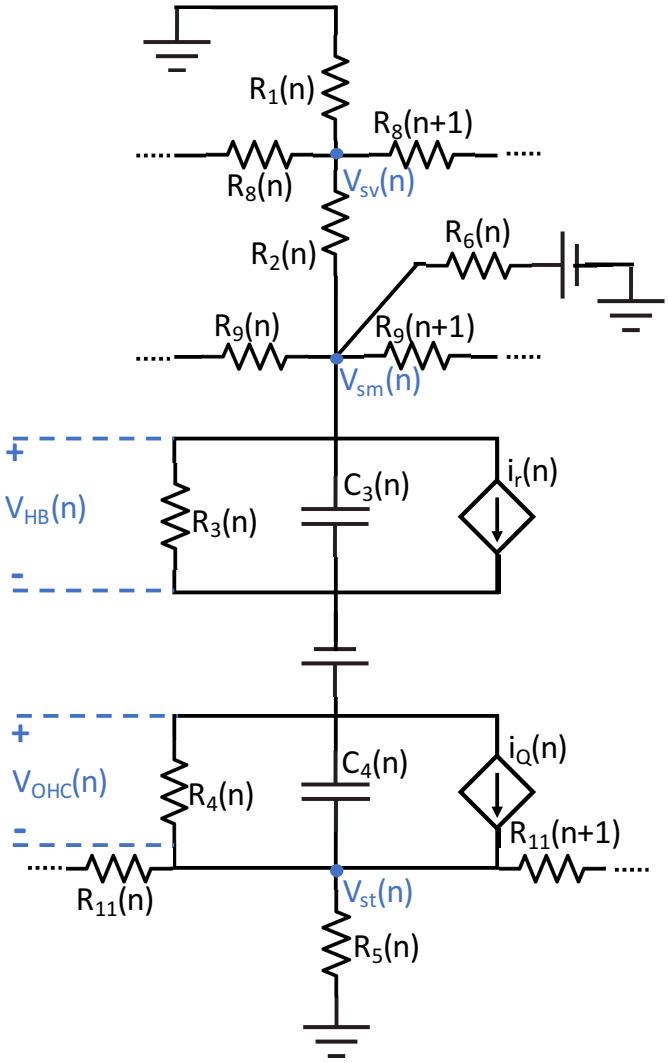

Figure 3.4: Circuit representing a cross-section of the cochlea including electrical coupling (adapted from Ayat et al. 2014)

Table 3.1 lists the parameters used during implementation of the circuit representing electrical coupling in the cochlea along with physical parameters used for modelling and provides short descriptions of those parameters.

Table 3.1: Set of parameters used for the simulation of a cochlear model with 700 sections (Liu & Neely 2010; Ayat et al. 2014)

Parameter	Value			Unit	Notes
	Base	Middle	Apex		
H_{scala}	$1.78 \cdot 10^{-3}$	$8.35 \cdot 10^{-4}$	$3.94 \cdot 10^{-4}$	$[m]$	height of scala
W_{scala}	$3.54 \cdot 10^{-3}$	$1.67 \cdot 10^{-3}$	$7.89 \cdot 10^{-4}$	$[m]$	width of scala
W_{BM}	$3.1 \cdot 10^{-4}$	$3.98 \cdot 10^{-4}$	$5.11 \cdot 10^{-4}$	$[m]$	width of BM
m	$1.24 \cdot 10^{-2}$	$7.14 \cdot 10^{-2}$	$4.1 \cdot 10^{-1}$	$[kg \cdot m^{-2}]$	BM mass per unit area
r	$4.8 \cdot 10^{2}$	$7.97 \cdot 10^{2}$	$1.69 \cdot 10^{3}$	$\left[\frac{kg}{s \cdot m^2}\right]$	BM resistance
k	$1.96 \cdot 10^{8}$	$1.0 \cdot 10^{7}$	$3.14 \cdot 10^{5}$	$\left[\frac{kg}{s^2 \cdot m^s}\right]$	BM stiffness
M	$2.8 \cdot 10^{-11}$	$5.0 \cdot 10^{-10}$	$2.8 \cdot 10^{-8}$	$[kg]$	OHC load mass
R	$9.4 \cdot 10^{-7}$	$9.23 \cdot 10^{-7}$	$1.85 \cdot 10^{-6}$	$[kg \cdot s^{-1}]$	OHC load resistance
K	$1.96 \cdot 10^{-1}$	$1.06 \cdot 10^{-2}$	$7.64 \cdot 10^{-4}$	$[kg \cdot s^{-2}]$	OHC load stiffness
α_d	$1.6 \cdot 10^{-3}$	$6.23 \cdot 10^{-4}$	$2.04 \cdot 10^{-4}$	$[A \cdot m^{-1}]$	current/RL displacement
α_v	$4.36 \cdot 10^{-6}$	$1.78 \cdot 10^{-6}$	$6.81 \cdot 10^{-7}$	$[C \cdot m^{-1}]$	current/RL velocity
T	$2.4 \cdot 10^{6}$	$2.4 \cdot 10^{6}$	$2.4 \cdot 10^{6}$	$[m \cdot C^{-1}]$	piezoelectric ratio
R_1	10	10	10	$[\Omega \cdot m]$	scala vestibuli to ground
R_2	25	25	25	$[\Omega \cdot m]$	scala vestibuli to scala media
R_3	1100	—	3300	$[\Omega \cdot m]$	hair bundle resistance
R_5	4	4	4	$[\Omega \cdot m]$	scala tympanii to ground
R_6	27	27	27	$[\Omega \cdot m]$	scala media to ground
R_8	0.5	1	3	$\left[\frac{M\Omega}{m}\right]$	scala vestibuli longitudinal resistance

R_9	10	2	4	$\left[\frac{M\Omega}{m}\right]$	scala media longitudinal resistance
R_{11}	0.3	1	2.5	$\left[\frac{M\Omega}{m}\right]$	scala tympani longitudinal resistance
C_g	$1.8 \cdot 10^{-11}$	$3.3 \cdot 10^{-11}$	$7.0 \cdot 10^{-11}$	$[F]$	gating capacitance
C_3	$5.6 \cdot 10^{-8}$	—	$3.2 \cdot 10^{-7}$	$\left[\frac{F}{m}\right]$	membrane basolateral capacitance
C_4	$2.8 \cdot 10^{-7}$	$6.46 \cdot 10^{-7}$	$1.6 \cdot 10^{-6}$	$\left[\frac{F}{m}\right]$	membrane apical capacitance
β	1			—	sigmoid function parameter

The constant electrical potential in the cochlea is provided by the stria vascularis $V_2(n)$ and the resting membrane potential of the OHC is denoted as $V_1(n)$. The potentials of the scala vestibuli, scala media and scala tympani are represented as V_{sv}, V_{sm} and V_{st} respectively, while the potential V_{sm} can be approximated as a sum of V_{OHC} and V_{HB}. V_{sm} is of significant interest for this study as it is speculated to be the main local component of the cochlear microphonic potential (with 180° degrees phase shift) (Ayat, Teal and McGuinness, 2014).

Applying Kirchoff's circuit law (sum of the currents out of each node must be equal to zero) to the model of a cochlear section the voltages and currents from Figure 3.4 diagram can be calculated.

$$\frac{v_{sv}(n)}{R_1(n)} + \frac{v_{sv}(n) - v_{sv}(n-1)}{R_8(n-1)} + \frac{v_{sv}(n) - v_{sv}(n+1)}{R_8(n)} + \frac{v_{sv}(n) - v_{sm}(n)}{R_2(n)} = 0 \qquad (3.11)$$

$$\frac{v_{sm}(n) - v_{sv}(n)}{R_2(n)} + \frac{v_{sm}(n) - V_2(n)}{R_6(n)} + \frac{v_{sm}(n) - v_{sm}(n-1)}{R_9(n-1)} + \frac{v_{sm}(n) - v_{sm}(n+1)}{R_9(n)} + \frac{v_{hb}(n)}{R_3(n)} + C_3(n)\dot{v}_{hb}(n) + i_3(n) = 0 \qquad (3.12)$$

$$\frac{v_{st}(n) - v_{st}(n-1)}{R_{11}(n-1)} + \frac{v_{st}(n) - v_{st}(n+1)}{R_{11}(n)} + \frac{v_{st}(n)}{R_5(n)} - \frac{v_{ohc}(n)}{R_4(n)} - C_4(n)\dot{v}_{ohc}(n) - i_4(n) = 0 \quad (3.13)$$

$$i_3(n) + \frac{v_{hb}(n)}{R_3(n)} + C_3(n)v_{hb(n)} = i_4(n) + \frac{v_{ohc}(n)}{R_4(n)} + C_4(n)v_{ohc(n)} \quad (3.14)$$

$$v_{sm}(n) = v_{st}(n) + v_{ohc}(n) - V_1(n) + v_{hb}(n) \quad (3.15)$$

The exact state space representation of this particular model is described in Appendix C and is largely based on Paul Teal's previous work and the unpublished documentation that was kindly made available to be used for the purpose of this research.

3.3. Model evaluation

The model was implemented in MATLAB. The core of the code was developed by Paul Teal and Mohammad Ayat and modified by the author of this work to reflect the most current information available on cochlear mechanics. It was previously reported by the authors of the model that the basilar membrane was more sharply tuned compared to the reticular lamina (Ayat, Teal and McGuinness, 2014). This appears to not necessarily be true if we consider the recent developments that were discussed in section 1.3.2, pointing out that the reticular lamina's vibration is larger in magnitude than that of a basilar membrane.

Therefore, we assume the reticular lamina to be more closely related to the neural excitation patterns with its sharper tuning than the basilar membrane.

In all simulations, HB capacitance was included ($C3(n) \neq 0$), and the sigmoid function parameter β was set to 1.

3.3.1. Mechanical responses

The first step to validate the simulation results was to generate responses for single tone stimuli for different levels.

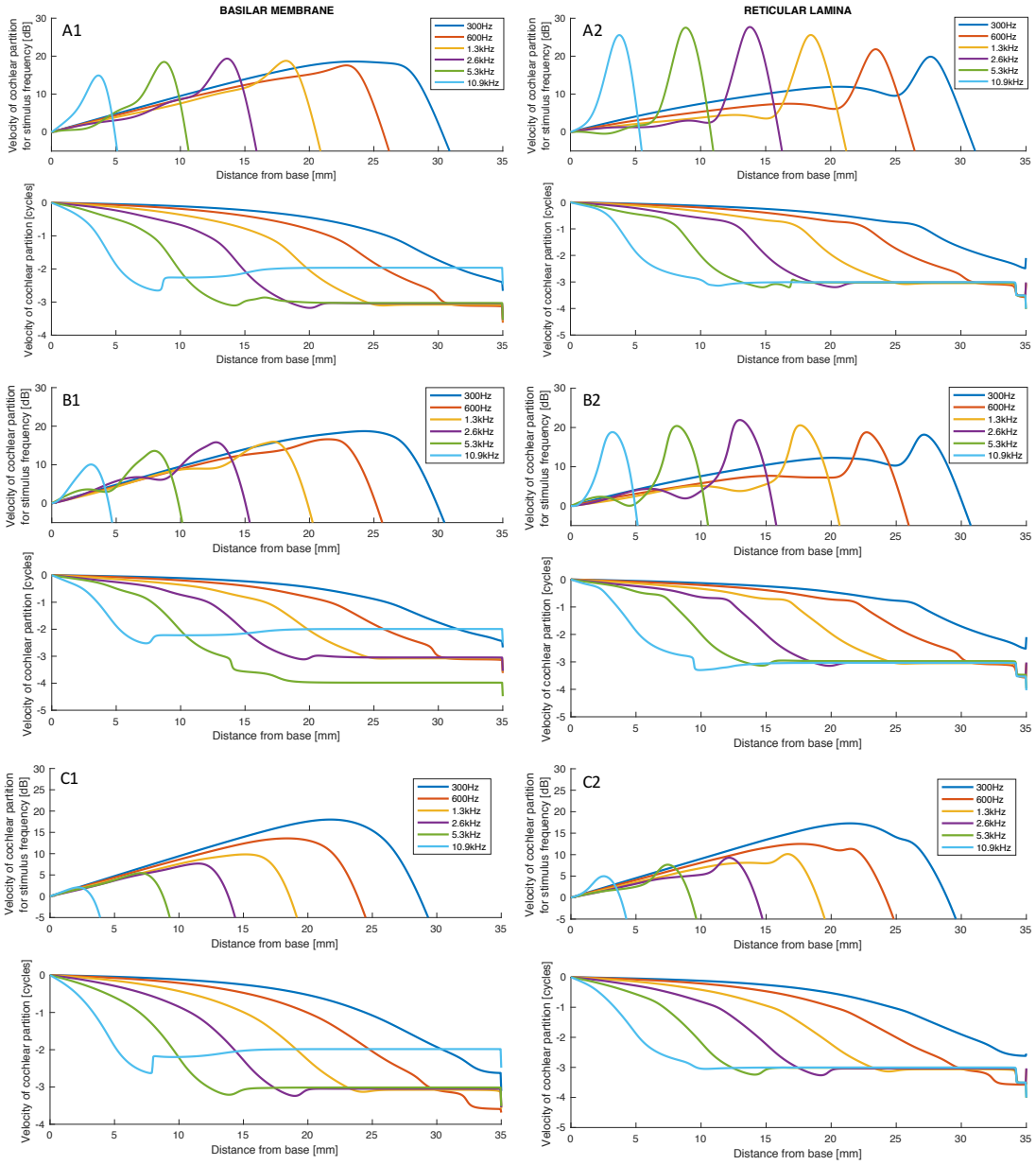

Figure 3.5: Model responses to stimuli of different frequencies and levels. Fig A1, A2 - responses to the stimulus of 20dB HL, B1, B2 - responses to the stimulus of 40dB HL, C1, C2 - responses to the stimulus of 60dB HL.

The stimulus level expressed in dB HL was determined from saturation curves obtained from this model, presented further in Figure 3.10 by comparing modelled responses with previously published findings regarding cochlear active processes saturation. From the responses acquired for the stimuli of different frequencies presented in Figure 3.5, it can be seen that the level of saturation for lower frequencies, for example, 300Hz, appears to be disproportionally big. Those "edge" cases tend to be problematic when it comes to the simulations as they require a lot of simulation time for the transient response, which will increase the lower the stimulus frequency is, to die down and should always be treated with caution.

From Figure 3.5, we can observe the saturation occurring within the model, but to better illustrate the phenomena responses for a stimulus of the same frequency but different levels are presented below in Figure 3.6. Results were obtained by running multiple simulations for different stimulus levels between 0dB and 80dB and tracking FFT responses at stimulus frequency for all the locations along the basilar membrane and reticular lamina.

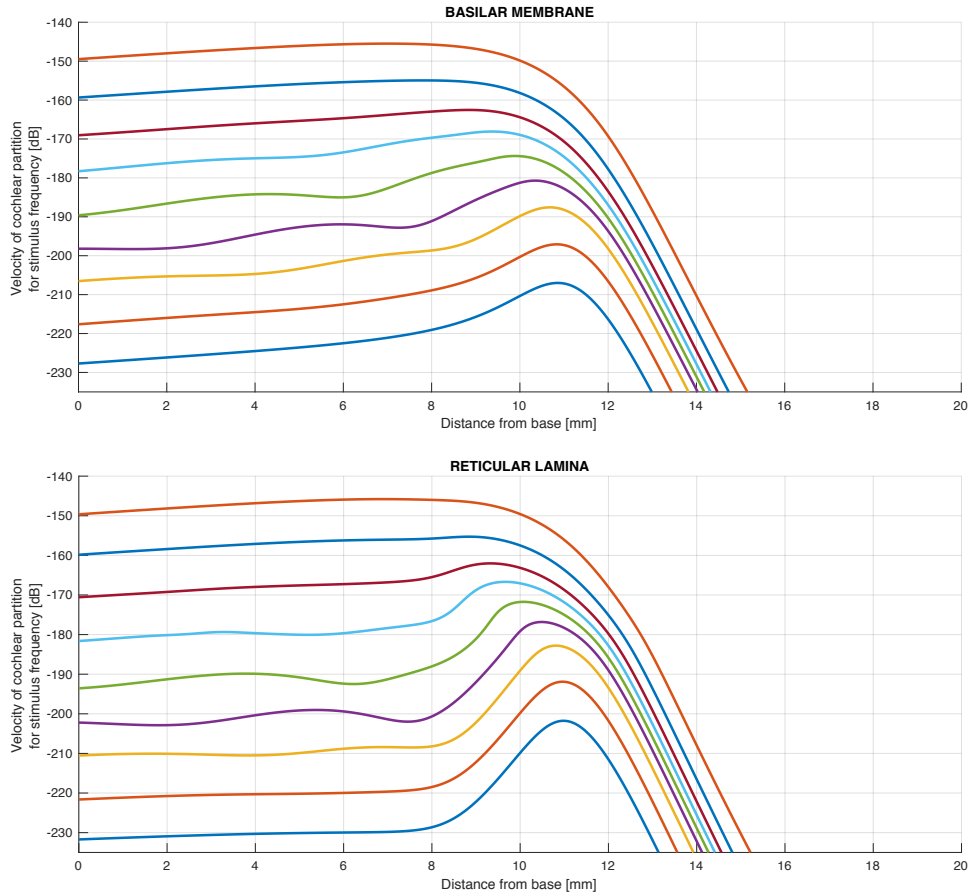

Figure 3.6: BM and RL responses to a different level of 4kHz stimulus; the level varies in between 0dB and 80dB with 10dB steps

The amount of amplification observed from the simulation appears to be ca. 30dB at low stimulus levels for RL responses, and ca. 15dB for BM responses. The obtained outputs appear to be in good agreement with the previously published findings (Liu and Neely, 2010).

To take a closer look at the place-frequency characteristics of the proposed model comparison between theoretical values for calculating characteristic places for frequencies within hearing range is being made (see equation (1.1)). To obtain these results 100 simulations were performed for frequencies within 20Hz – 20kHz range with 50Hz step for low-level stimulus (to ensure full activation of the cochlear amplifier) to track the peak location of BM displacement for every stimulus frequency.

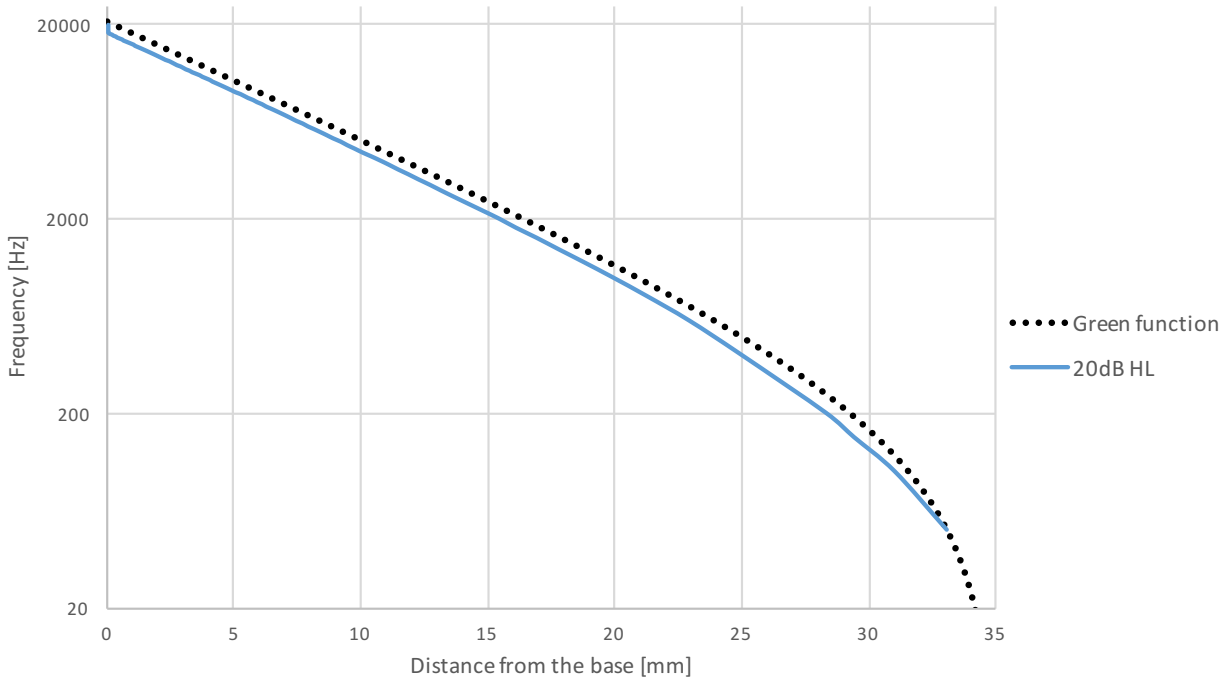

Figure 3.7: Place - frequency map for the basilar membrane in comparison to the predicted Greenwood distribution

The obtained curve appears to be in fairly good agreement with the proposed Greenwood curve, although the characteristic place location is slightly shifted from the theoretical values.

3.3.2. Defining nonlinearity

From the plots presented in the previous section we can clearly observe the nonlinear saturation occurring within the cochlea when stimulated with higher level inputs.

Nonlinearity in the model is defined by four parameters: I_{max} – the maximum range of OHC receptor current, β - Boltzmann sigmoid function parameter, α_d – current generated as a consequence of the RL displacement, and α_v - current generated as a consequence of the RL velocity.

The distribution of the maximum OHC receptor current along the cochlea is plotted in Figure 3.8, and both α parameters are shown in Figure 3.9.

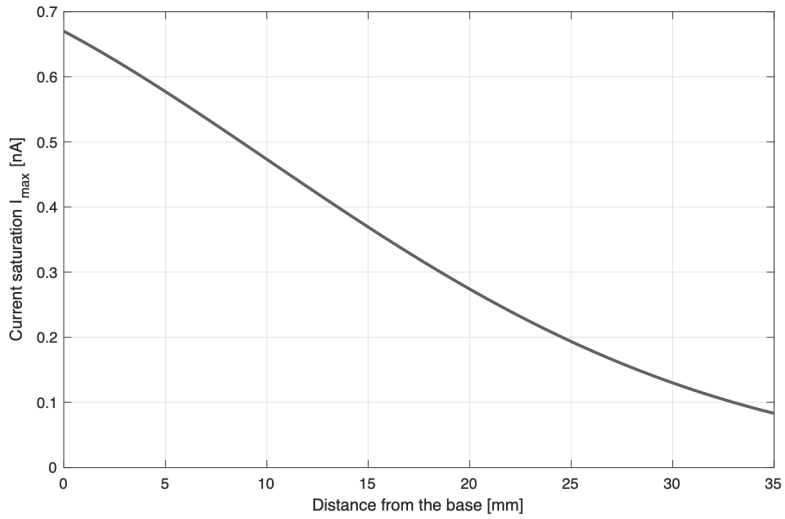

Figure 3.8: Maximum range of OHC receptor current

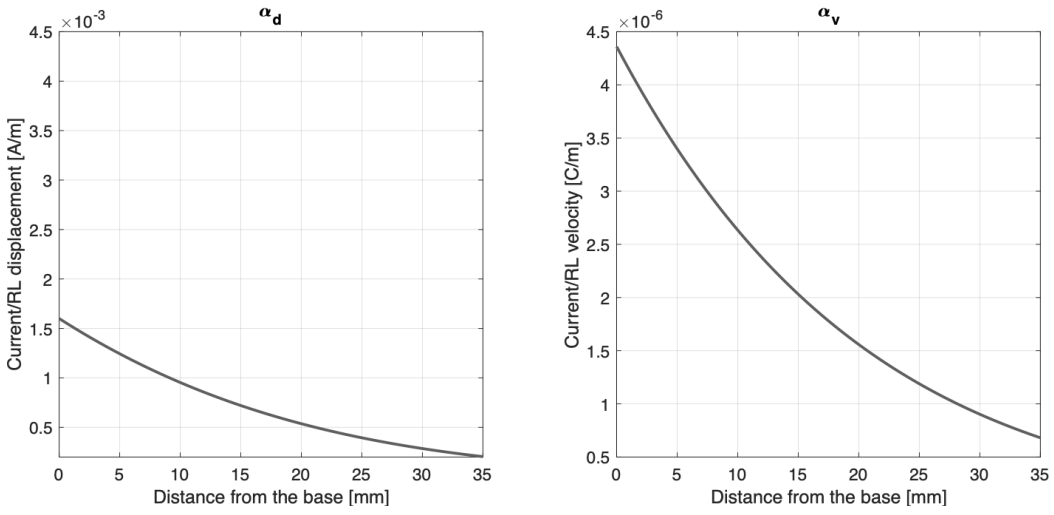

Figure 3.9: Generation of current in response to RL displacement and velocity

Stimulating the system with different level inputs, we can obtain the saturation curves for selected frequencies. They are presented in Figure 3.10. The values 'follow' the peak of the response (they are acquired from varying points on the RL depending on the peak location).

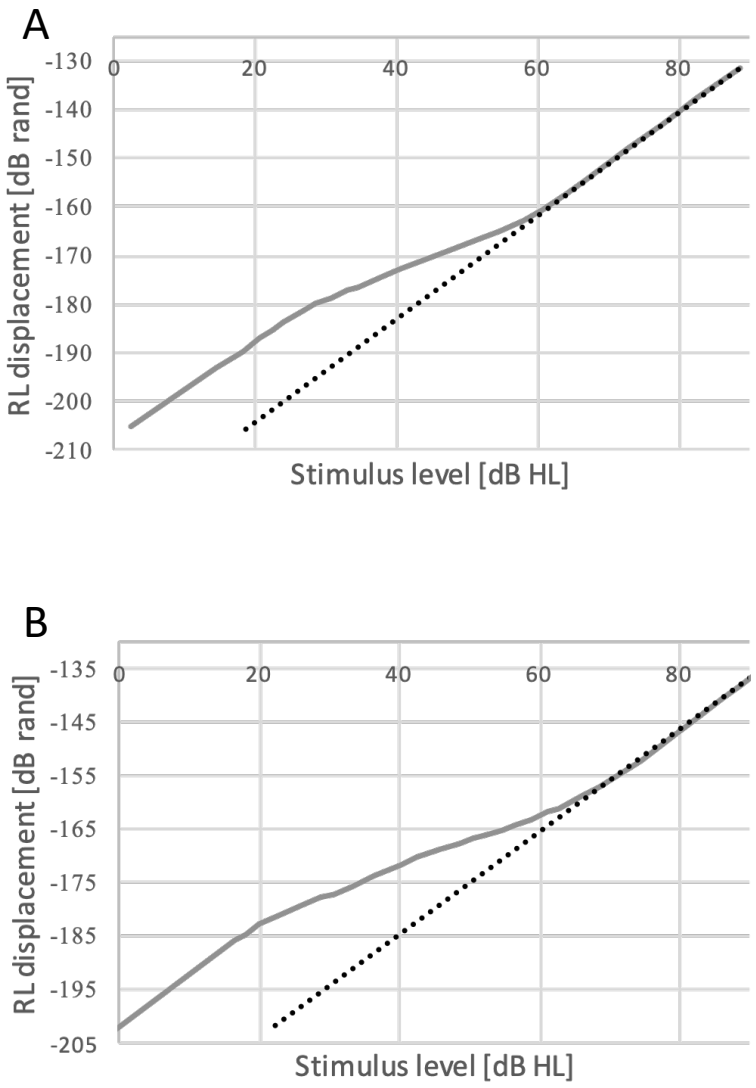

Figure 3.10: Saturation curves for reticular lamina for A: 1kHz and B: 5kHz stimulus frequency; dashed line shows linear characteristics for reference

Finally, the quality of the system was evaluated. To obtain the quality factor, 100 simulations were run for frequencies within the 20Hz – 20kHz range with 50Hz step for a low-level stimulus of 10dB HL ensuring full activation of the cochlear amplifier.

The frequency corresponding to the peak of the response was tracked along with its level in decibels. The next step was to find the two points on the reticular lamina (below and above this peak) where the response was 10dB lower than the peak corresponding to the stimulus frequency. Finally, the stimulus frequency was divided by this 10dB bandwidth below the peak. The results are presented in Figure 3.11.

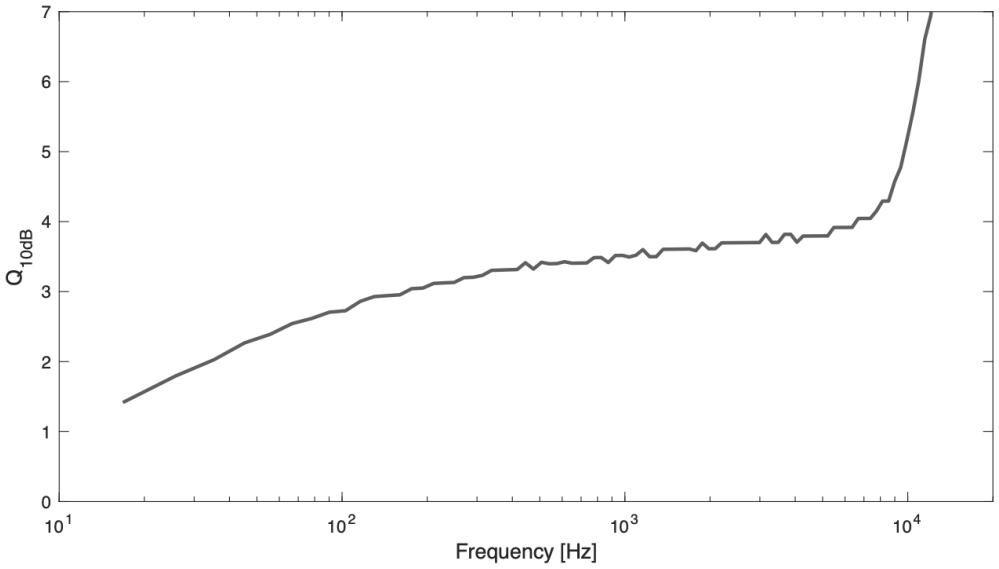

Figure 3.11: Tuning sharpness for the cochlear model (Q factor) obtained from the reticular lamina

The above results suggest a slightly sharper tuning with Q_{10dB} values between 2 and 4, while previous studies (Ruggero and Temchin, 2005) reported Q_{10dB} values between 2 and 5 for the frequencies that the data was available, namely 2kHz – 8kHz.

3.3.3. Electrical parameters of the model

The resistances used for implementing the electrical network representing the Organ of Corti were based on previously published findings (Strelioff, 1973). The values distribution along the cochlea is shown in Figure 3.12.

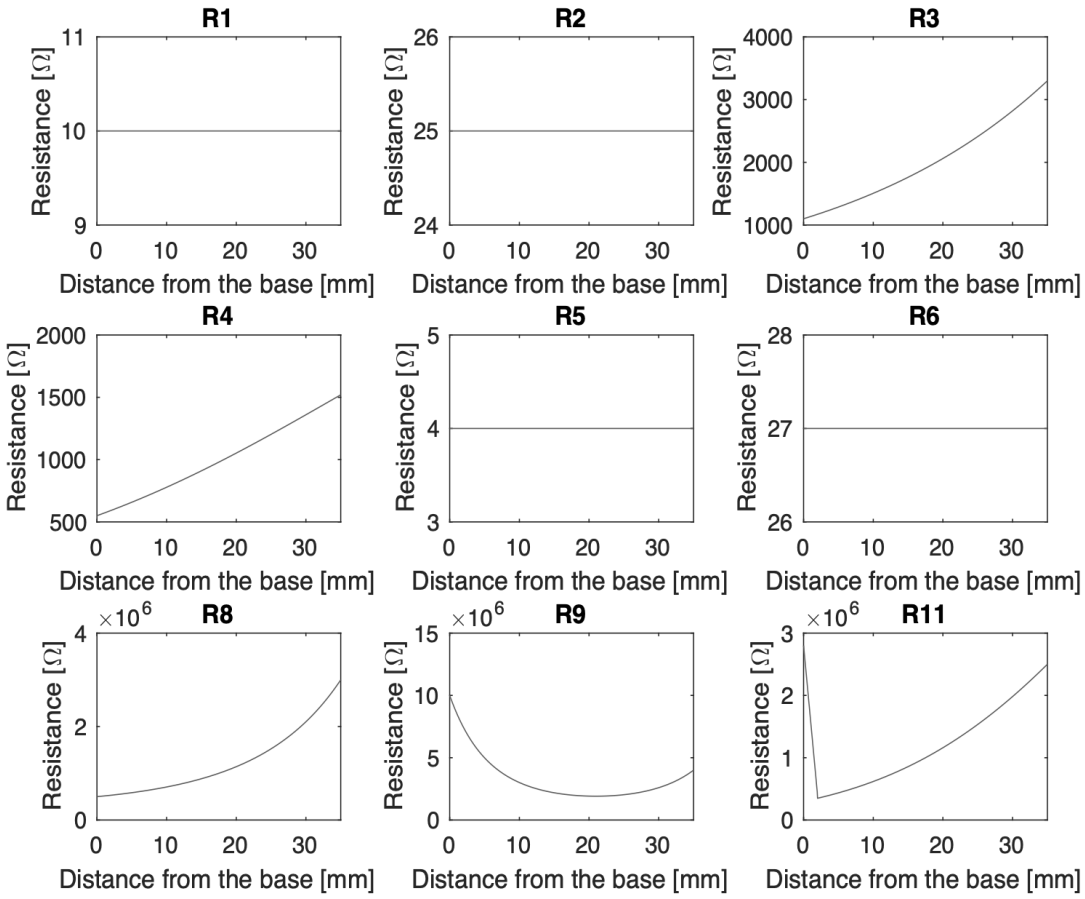

Figure 3.12: Longitudinal distribution of the network model resistors

The values describing the outer hair cells (R_3, R_4, C_3 and C_4) can be used to evaluate the OHC membrane time constant using the total membrane capacitance and conductance at resting potential. The RC time constant τ carries the information about the input – output delay in a circuit (the higher the τ, the longer the delay). Effectively, it describes the low-pass filtering properties of a system. That relationship can be defined as follows:

$$\tau_{tot}(n) = \frac{C_m(n)}{G_r(n)} = \frac{C_3(n) + C_4(n)}{\frac{1}{R_3(n)} + \frac{1}{R_4(n)}} \qquad (3.16)$$

The membrane time constant can be presented in relation to a place along the cochlea for its corresponding characteristic frequency as shown in Figure 3.13.

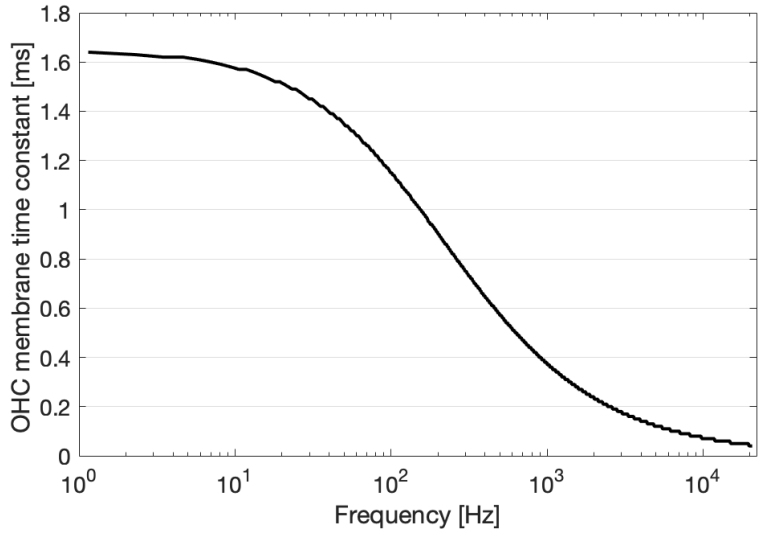

Figure 3.13: OHC membrane time constant

3.3.4. Electrical potentials

The primary potentials used to assess electrical responses of the system are the V_{OHC} and V_{HB}, and the scalae potentials can be calculated using these voltages. In Figure 3.14, amplitudes of the outer hair cell and the hair bundle potentials for different frequencies are illustrated. The sharp tuning similar to the RL responses can be observed both in V_{OHC} and V_{HB}. The amplitudes of both potentials match very closely, however, we can observe a phase difference of π radians between the two, which is believed to be the source of broader tuning curves of the CM, in comparison to the BM motion (Ayat *et al.*, 2015).

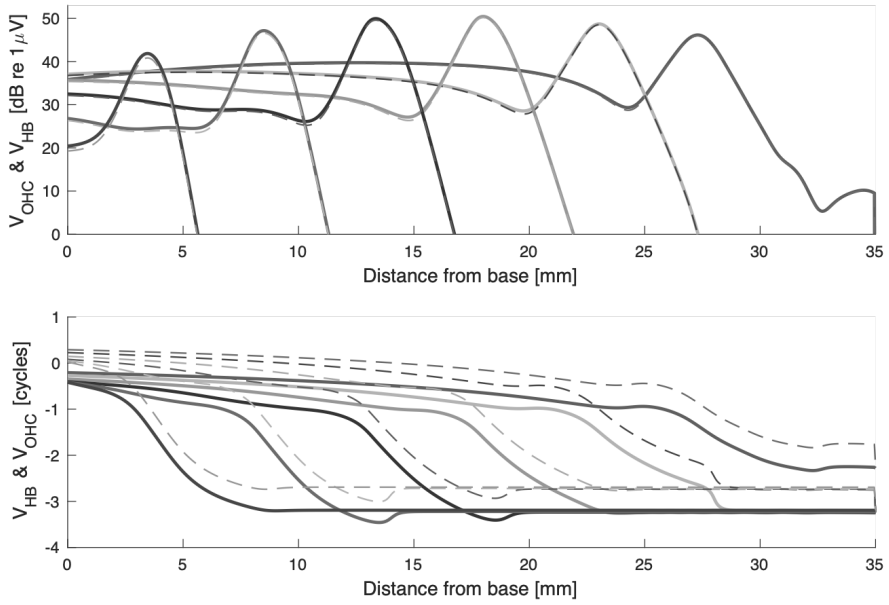

Figure 3.14: V_{OHC} and V_{HB} potentials for 300, 600, 1300, 2600, 5300 and 10900Hz; the solid line shows V_{OHC} and the dashed line V_{HB}

This half a cycle difference is even more apparent upon inspecting the time responses of the two potentials, as shown in Figure 3.15.

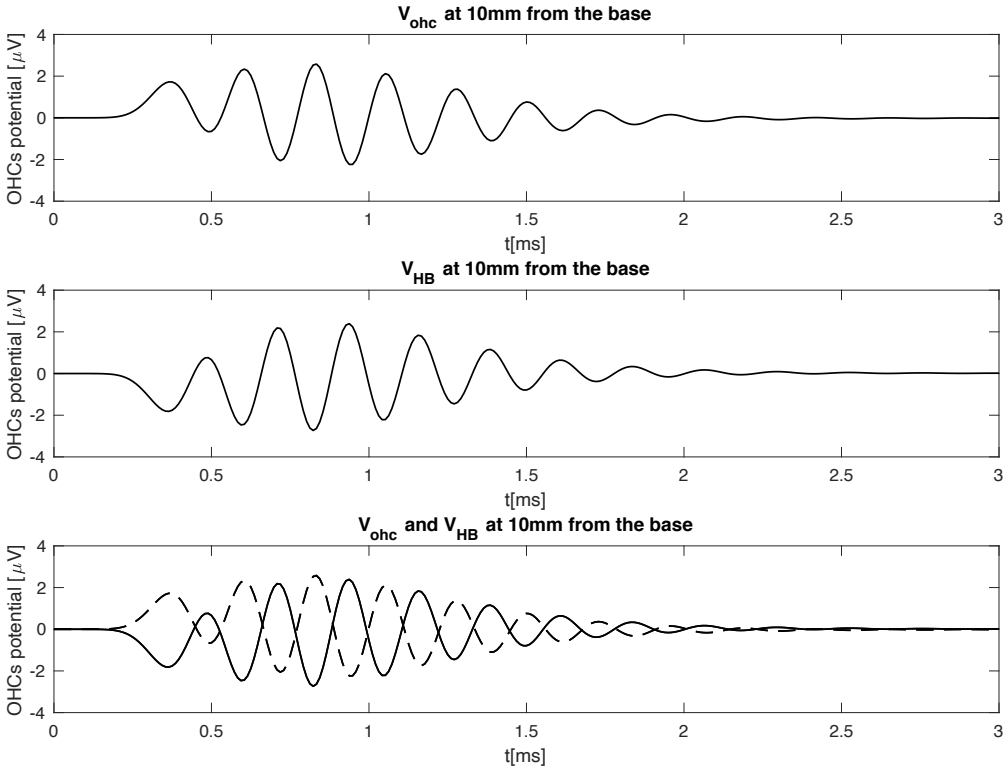

Figure 3.15: V_{OHC} and V_{HB} time responses at characteristic place for 2000Hz

The V_{sm} potential, in comparison to the V_{OHC}, is not as sharply tuned, which is what can be seen in previously reported measurements (Fridberger *et al.*, 2004) and in Figure 3.16. Furthermore, the adjustment of the resistances and capacitances of the model improved the V_{sm} responses to the lower frequency stimuli compared to the previously published results (Ayat, P D Teal and McGuinness, 2014) where the scala media voltages were dropping off sharply for the stimulus frequencies below 1kHz.

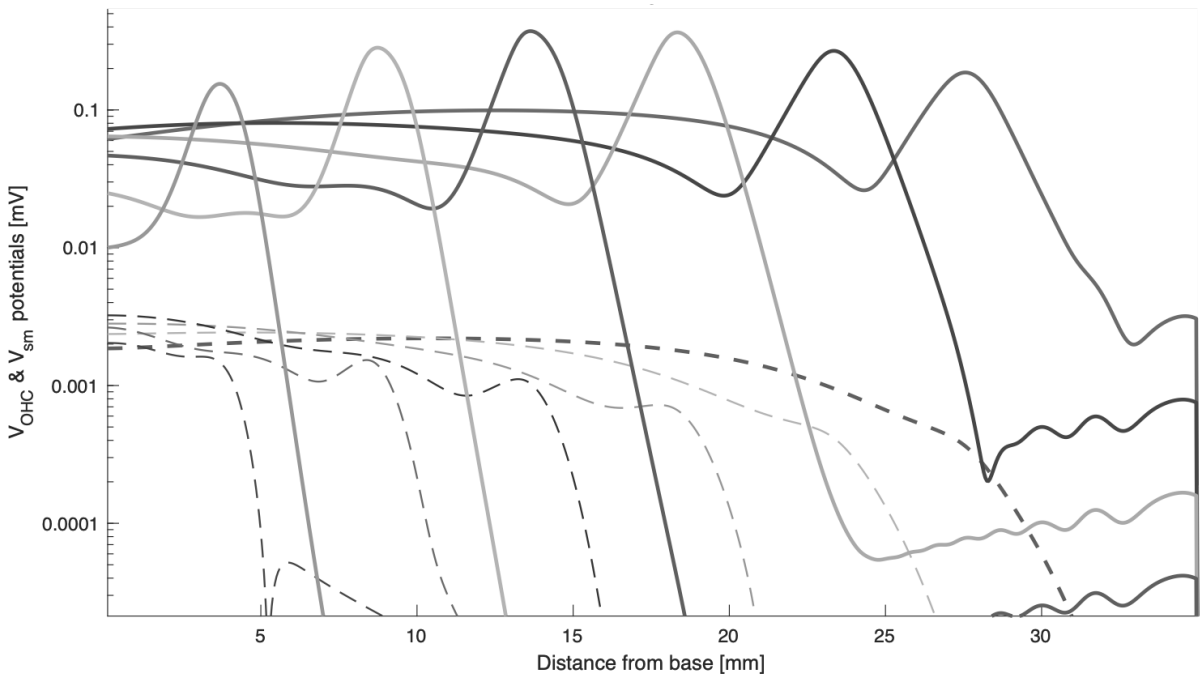

Figure 3.16: V_{OHC} and V_{sm} tuning curves for 300, 600, 1300, 2600, 5300 and 10900Hz; the solid line shows V_{OHC} and the dashed line V_{sm}

4. Model modifications and novel predictions

This chapter, and the subsequent ones, describes the original work carried out for the purpose of this thesis that, to the author's best knowledge, has not been previously reported. That includes adding the inner hair cell model into the MATLAB formulation of the cochlear model in section 4.1 and modifying the code to feature the possibility of using other stimuli in addition to the pure tone input, allowing for novel simulations of two-tone interactions between the model's components, shown in section 4.2 and 4.3.

4.1. Inner hair cell model

To obtain a more comprehensive picture of the electrical processes taking place in the cochlea, a model of the inner hair cell was implemented in MATLAB and added to the existing formulations. A model based on measurements in the inner hair cell of a live guinea pig was used (Mountain and Cody, 1999). It is based on the assumption that the sensory epithelium of the cochlea is excited by more than one source of vibration: the pressure waves and the forces generated by the outer hair cells. It has been suggested that there are multiple mechanisms responsible for the vibration of the organ of Corti, not only considering different frequencies but also different levels of the stimulus. This adds complexity to the already intricate mechanisms of the cochlea. However, Mountain and Cody suggest that it is the non-linear outer hair cell force that is the primary mechanical input into the inner hair cell for low and moderate stimulus levels below 85dB SPL. This assumption is based on a study suggesting that when the OHCs in the cochlea are damaged, the IHC component is no longer observable *in vivo* (Liberman and Kiang, 1984). For high-intensity stimulus, where the cochlear amplifier ceases to be active, the IHCs can retain their function even if the OHCs are severely damaged, however, for the purpose of the model developed for this study, we assume a fully functioning cochlea. Therefore, the IHC response is always assumed to be dependent on the OHC response.

In the original formulation, the recorded cochlear microphonic collected by the extracellular electrode was used to compare the voltages recorded intracellularly from the IHC. Subsequently, Mountain and Cody found that the model based on the outer hair cell force coupling was an extremely close representation of the *in vivo* data they collected. In that study, the CM recorded from the scala media was used as a way to estimate the OHC receptor potential. Since our electro-mechanical model can predict the OHC receptor potential, we have a more direct

way of obtaining the responses of the IHCs. An equivalent circuit model of the inner hair cell suggested by Mountain and Cody is shown in Figure 4.1.

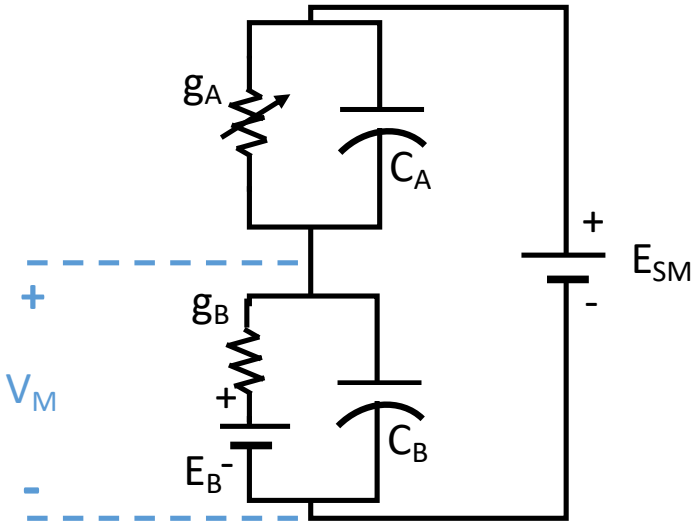

Figure 4.1: Electrical model of the inner hair cell

The model values used for the MATLAB simulation are adapted from the aboveementioned study and collected in Table 4.1.

Table 4.1: Model parameters for the IHC equivalent circuit

Parameter	Value	Notes
x_0	27nm	offset constants
x_1	27nm	offset constants
S_0	85nm	offset constants
S_1	11nm	offset constants
g_B	58.8nS	basolateral conductance
g_{max}	11.6nS	maximum conductance
C_A	2.3pF	apical membrane capacitance
C_B	8.4pF	basolateral capacitance
E_B	-45mV	basolateral electrical gradient

The apical conductance is expressed as:

$$g_A = \frac{g_{max}}{\left(1 + e^{-\frac{x-x_0}{S_0}}\right)\left(1 + e^{-\frac{x-x_1}{S_1}}\right)} \qquad (4.1)$$

The implemented code accepts the simulated displacement of the OHC in response to the stimulus as the input. If we feed the OHC displacement into the model, we can estimate the resulting conductance and the exact potential of the IHC. As an example the process is presented for three different levels of 1kHz stimulus in Figure 4.2.

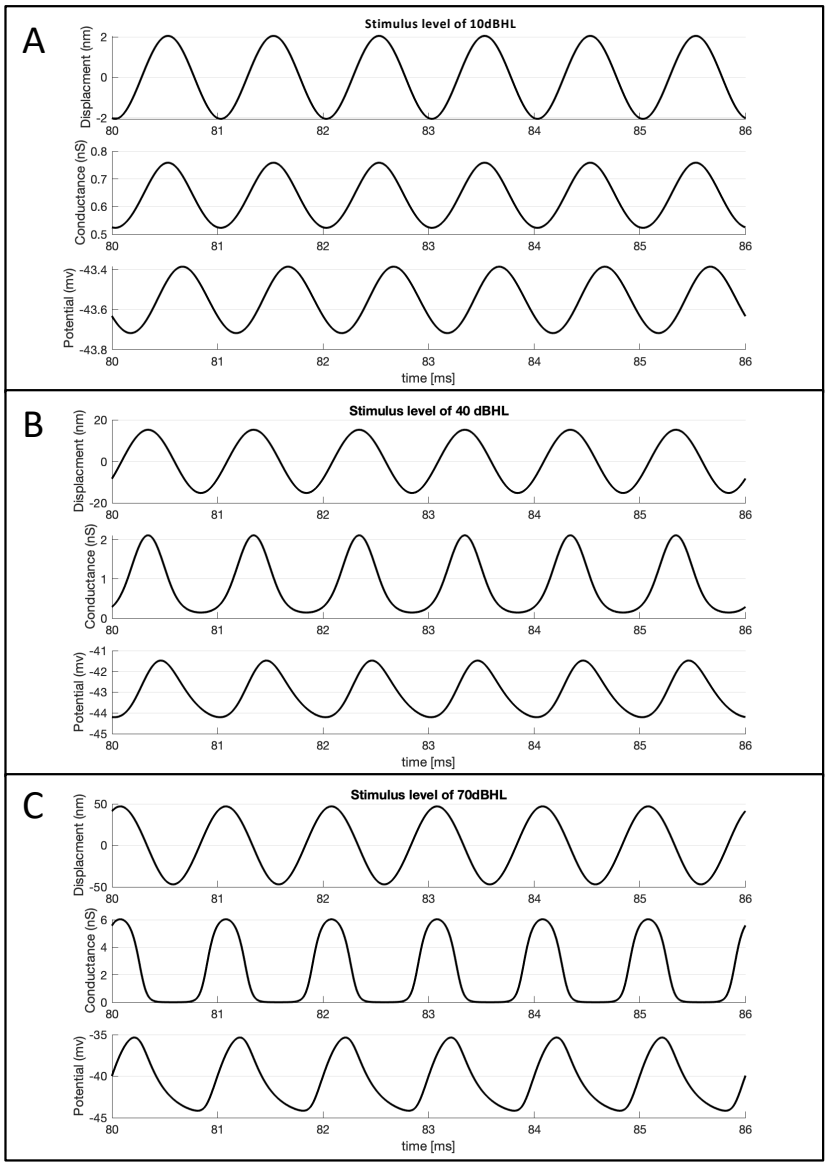

Figure 4.2: Simulated IHC potential and G_A capacitance based on the OHC displacement at the 1kHz peak location for stimulus of the following levels: A – 10dBHL , B – 40dBHL, C – 70dBHL

From the simulation graphs, we can observe the saturation taking place in the IHC potential, with the response becoming more asymmetrical as the stimulus intensity goes up.

The local IHC responses can be obtained for every single point along the basilar membrane based on the local OHC displacement. An example of the comparison between the OHC and IHC potentials evoked by a 1kHz stimulus at different levels are presented in Figure 4.3.

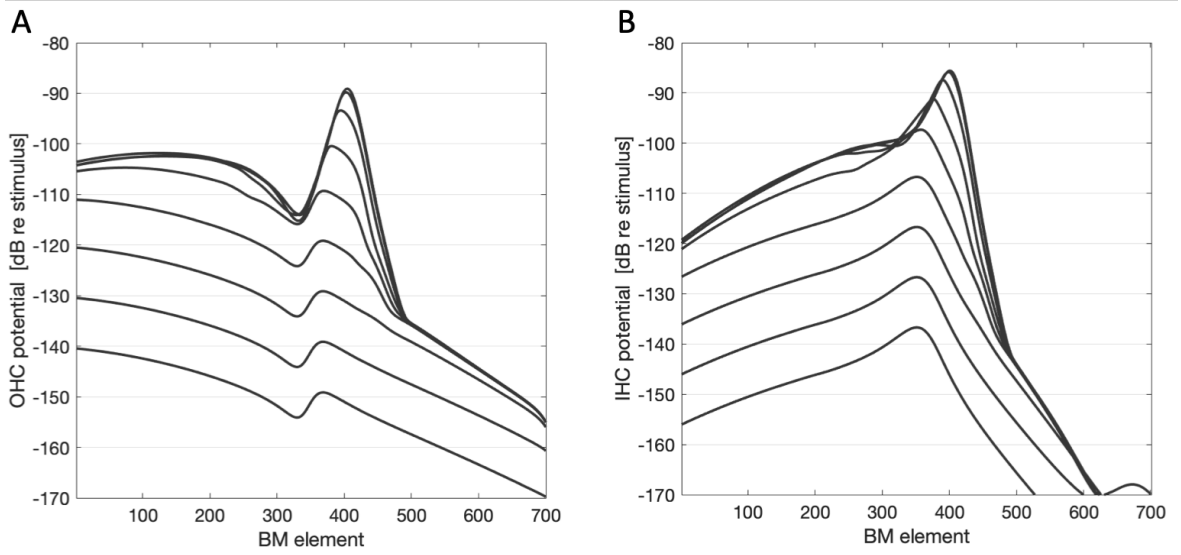

Figure 4.3: Cochlear potentials evoked in response to different levels of 1kHz stimulus. The level varies between 10 and 90dBHL in 10dB steps. A – outer hair cell potentials, B – inner hair cell potentials, both in relation to the stimulus input

The widely accepted theory is that the inner hair cell's function is purely sensory (transporting the auditory information into the brain), unlike that of the outer hair cells that exert a force on the Organ of Corti elements. Following that assumption, the IHC simulation does not need to contribute to the mechanics of the model.

Furthermore, the entire calculation of the IHC potential was done offline based purely on the OHC receptor potential after the simulation was already completed, meaning that at this point, the IHC potentials do not feed back into the model.

4.2. Two-tone suppression in mechanical responses

Two-tone suppression is one of the characteristics believed to be providing an insight into the nonlinearities of the cochlea. The simulation of this phenomenon enables us to take a closer look at how multiple stimuli are interacting with each other in the cochlea by means of observing its impact on both micromechanical responses and cochlear potentials. The presence of those nonlinear properties is said to be a quality of a healthy, functioning cochlea (Meaud and Grosh, 2014) but the significance of those results is still not particularly well understood.

In the two-tone suppression (2TS), a primary probe tone stimulating the cochlea at a frequency f_p interacts with a second stimulus - the suppressing tone of a frequency f_s. The response at the probe frequency is reduced by the presence of the suppressor. The suppression occurs for both low-side (below f_p) and high-side (above f_p) suppressors. This phenomenon is especially prominent when $0.9 \cdot f_p < f_s < 1.1 \cdot f_p$. Previous publications suggest that a cochlear amplifier is the likely source of the 2TS (Kanis and de Boer, 1994).

The two-tone suppression can be observed in both the RL and BM mechanical responses, as well as in the changes of the cochlear microphonic potential. The suppression of the mechanical responses is presented in Figure 4.4. The results were obtained by simulating model responses to a single tone input stimulus of 20dB HL first, and then simultaneously introducing a second stimulus with a 10dB higher level and comparing the FFT responses for all of the cochlear locations for both scenarios.

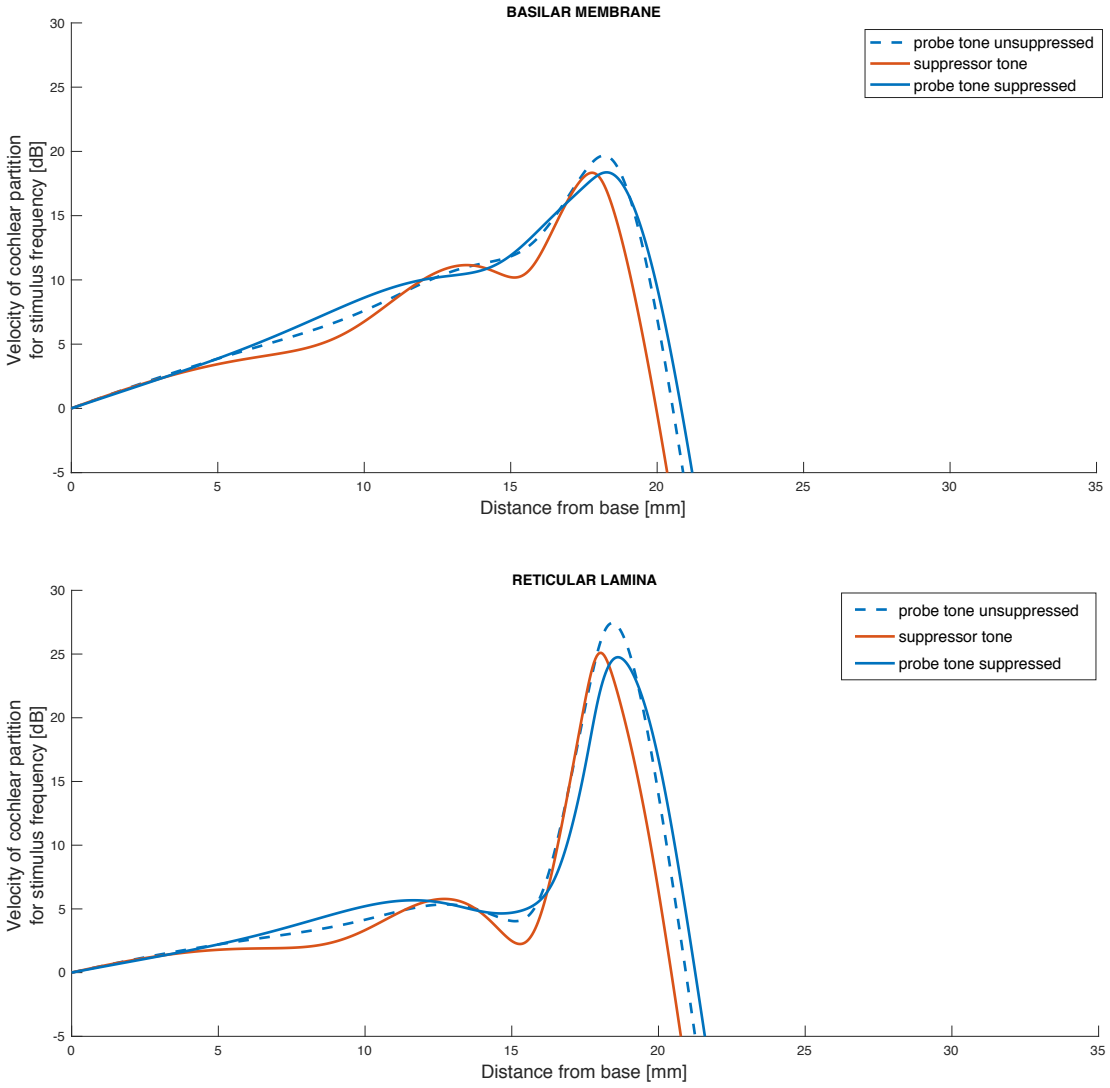

Figure 4.4: Two-tone suppression in mechanical responses of BM and RL; f_p=1300Hz, L_p=20dB, f_s=1200Hz, L_s=30dB. The probe tone peak is seen to be lowered and slightly shifted towards the base in the presence of a suppressor

To illustrate better how the suppressor frequency and level affect the mechanical responses of the BM and RL, the velocities of BM and RL responses to a two-tone stimulation can be plotted as a function of the suppressor frequency. The first step is to look at the FFT for a single point in the cochlea and track its changes depending on the presence of the suppressor frequency, as shown in Figure 4.5. In this example, we are considering the BM motion. For the RL, the procedure of obtaining the 2TS response is identical (although the peak location varies slightly). The probe frequency $f_p = 1000Hz$ of 20dBHL level is presented on its own (dashed line), and then together with the suppressor $f_s = 1100Hz$ and 30dBHL level (solid line). The FFT value at 1000Hz

is observed to be lower in the presence of the suppressor. The same principle is used to obtain the hair cell potential responses together with the V_{sm} suppression patterns in the next section.

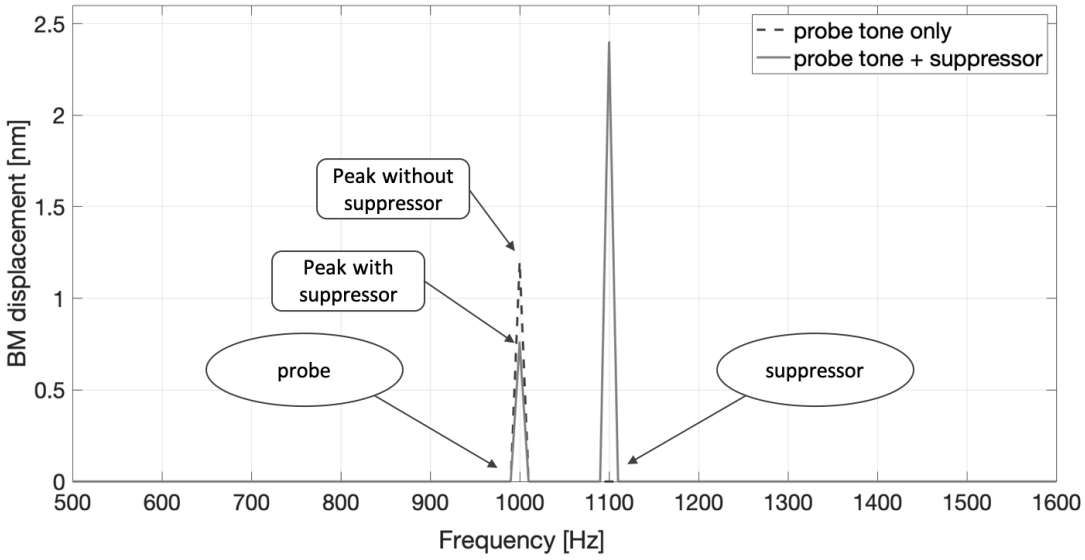

Figure 4.5: Two tone suppression in the basilar membrane displacement for a single point in the cochlea. The graph shows that the magnitude of the BM displacement is higher when there is no suppressing tone present in the stimulus (dashed line) and drops when a suppressing tone is introduced into the stimulus (solid line)

If we continue to perform simulations varying the suppressor frequency by 100Hz steps in between 100Hz – 20kHz for three selected levels, this relationship can be presented as a ratio between f_p unsuppressed and f_p suppressed as in Figure 4.6.

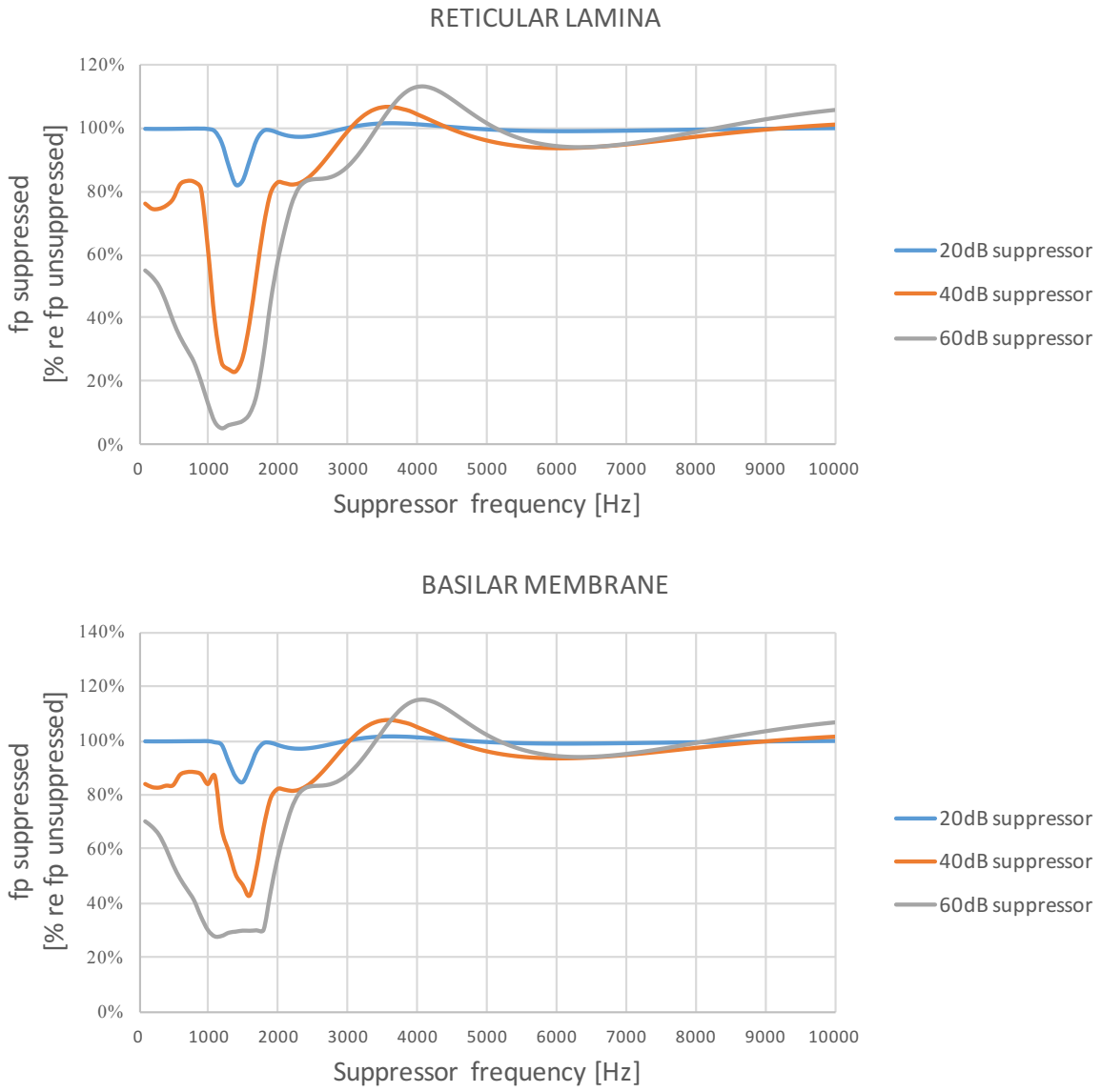

Figure 4.6: The magnitude of BM and RL responses to a 1300Hz tone as a function of suppressor frequency. A significant amount of the suppression can be seen in the motions of both RL and BM as the suppressor frequency approaches the probe tone, with the greater amount of suppression noted for higher stimulus levels.

4.3. Two-tone suppression in electrical responses

A comparable phenomenon is displayed in the individual hair cell potentials (Hudspeth, 2014). Adding stimulation at a second frequency increases the motion of the hair bundle, reducing amplification by the active processes and consequently diminishing sensitivity to the original tone. The OHC response to the two-tone stimulation is shown in Figure 4.7.

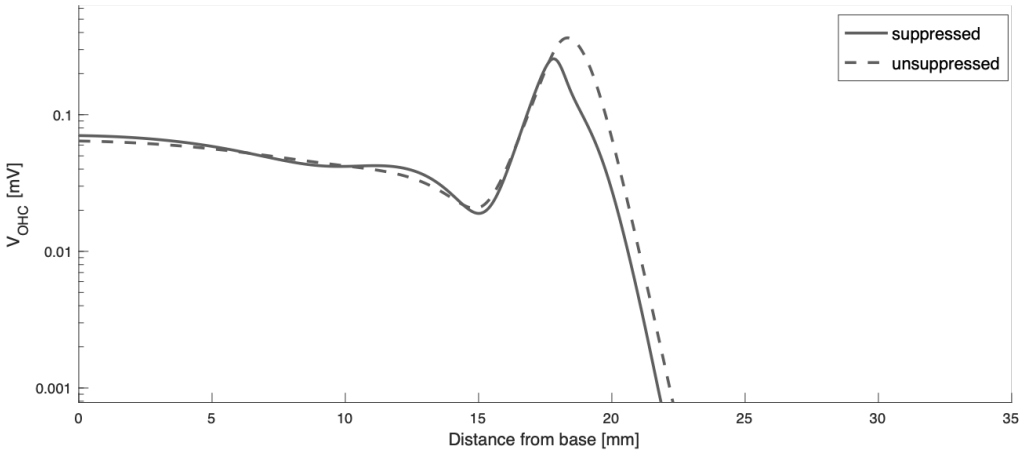

Figure 4.7: Suppression effect on outer hair cell potentials; f_p=1300Hz, 20dB, f_s=1200Hz, 30dB

According to the model, the mechanism of the 2TS is also affecting the scala media potential. Introducing the second stimulus causes the V_{sm} response to drop at the peak location, as shown in Figure 4.8.

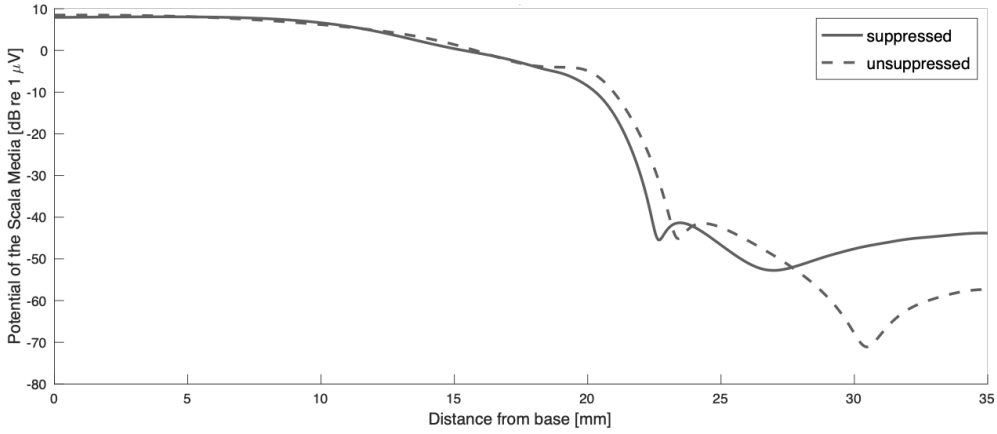

Figure 4.8: Suppression effect on cochlear microphonic; f_p=1000Hz, 20dB, f_s=1100Hz, 30dB. Slight suppression of the scala media potential can be seen at the probe tone frequency mostly around the best place.

The difficulty in comparing modelled responses to the clinical measurements lies in the way the cochlear microphonic potentials are recorded in patients. Usually, the electrode picks up responses from multiple points along the cochlea all at the same time, while the model provides us with the results specific to a single point.

As a simplification, drawing from the speculation discussed in section 1.4.3, the assumption is made that a majority of the cochlear microphonic arises from the portion of the cochlea most proximal to the stapes. Hence, we simulate responses for one of the first basal points on the cochlea to collect the V_{sm} potential from that site. To obtain a fuller picture of the two-tone suppression

mechanisms in the cochlear potentials, the simulation results are going to be recorded at the characteristic place for the probe tone frequency as well.

The frequencies selected for the suppressors are based on the setup of the two-tone suppression experiment that is going to be presented in the next chapter so that the simulation outcomes can be compared with the measurements in normal-hearing patients.

The probe tone for which the simulation was performed was 1000Hz at a level of 60dBHL. The suppressor frequencies used are: 500Hz, 1200Hz, 1800Hz, 2400Hz, 4000Hz, 4800Hz and 9600Hz. The levels of the suppressors were (all in hearing level): 0dB, 10dB, 20dB, 30dB, 40dB, 50dB, 60dB, 70dB, 80dB and 90dB.

The primary source of the cochlear microphonic is speculated to be the V_{sm} potential, therefore, its voltages were evaluated to obtain the saturation curves in Figure 4.9.

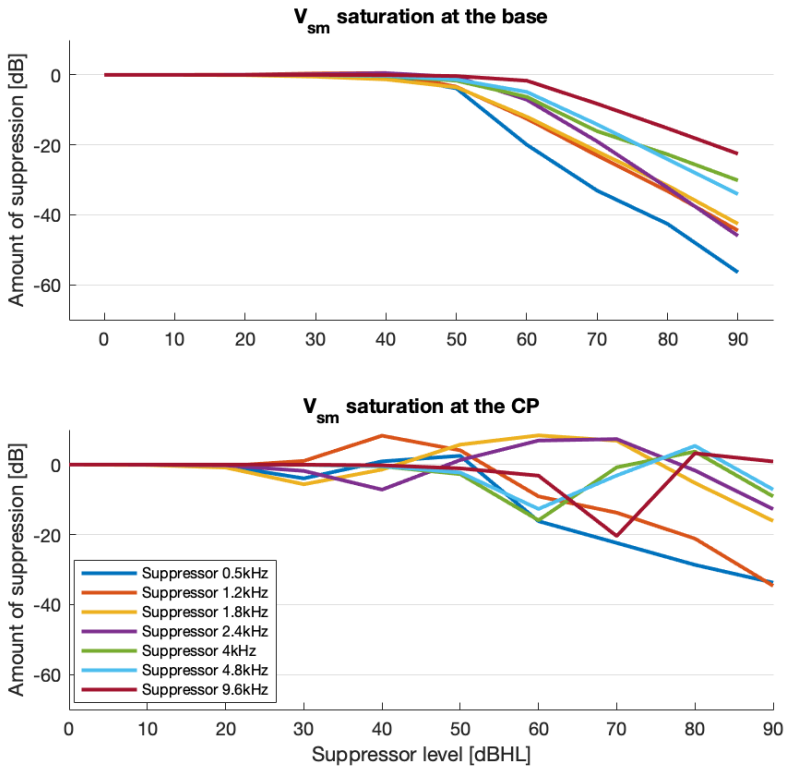

Figure 4.9: Scala media potential at the 1kHz probe frequency, in the presence of suppressing tones at the base and CP. The basal V_{sm} drops in amplitude more when the stimulus intensity gets higher, with the biggest impact of suppressors close to the probe tone (500Hz, 1.2kHz, 1.8kHz, 2.4kHz). The CM at the CP shows signs of enhancement when presented with most of the suppressors, except for the 500Hz and 1.2kHz, where the V_{sm} response is suppressed

The V_{sm} responses at the basal location are significantly dropping with the introduction of the suppressing tone. The biggest impact appears to be caused by the suppressors close to the 1kHz probe tone, namely the 500Hz, 1.2kHz, 1.8kHz and 2.4kHz.

However, this is not the case in the characteristic place where most of the suppressor frequencies appear to enhance the CM response at higher levels with exception of 500Hz and 1.2kHz.

Speculation about the source of this finding might have to do with the mechanical responses of the BM and TM. As described in Chapter 4.2, the mechanical responses are susceptible to the influence of the suppressing tone, causing the vibration of the CP to drop in amplitude. It is possible that the primary mechanism replacing the shearing motion between BM and RL is the electromotility of the OHC. As the OHCs current is directly related to the V_{sm} potential, the presence of a suppressor could then show up as an enhancement in the scala media potential caused by the excessive draining of the current from scala media into the OHC in an effort to compensate for the dampened BM and RL vibration.

To further investigate, the V_{OHC} potential at the characteristic place is presented in Figure 4.10.

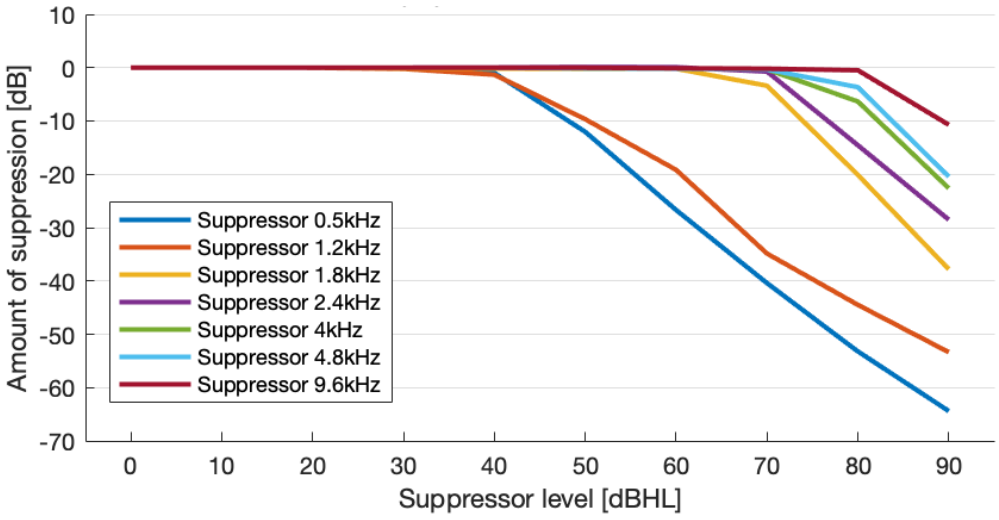

Figure 4.10: Outer hair cell potential at 1kHz probe frequency, in the presence of suppressing tones at the characteristic place. The V_{OHC} at the probe tone remains largely unchanged until the suppressor frequency reaches around 70dB, after which the response drops. The exceptions are the suppressors of 500Hz and 1.2kHz, where the suppression is visible starting from the 40dB level.

The OHC potential at the characteristic place shows that the suppressors close to the probe tone frequency have a significant impact on the response at the probe tone, while the remaining ones only affect the OHC voltage at very high stimulus intensities.

Since the IHC potential depends on the OHC, let's investigate all three of the potentials at the characteristic place, this time producing a graph showing the amount of suppression against the different suppressor frequencies in Figure 4.11.

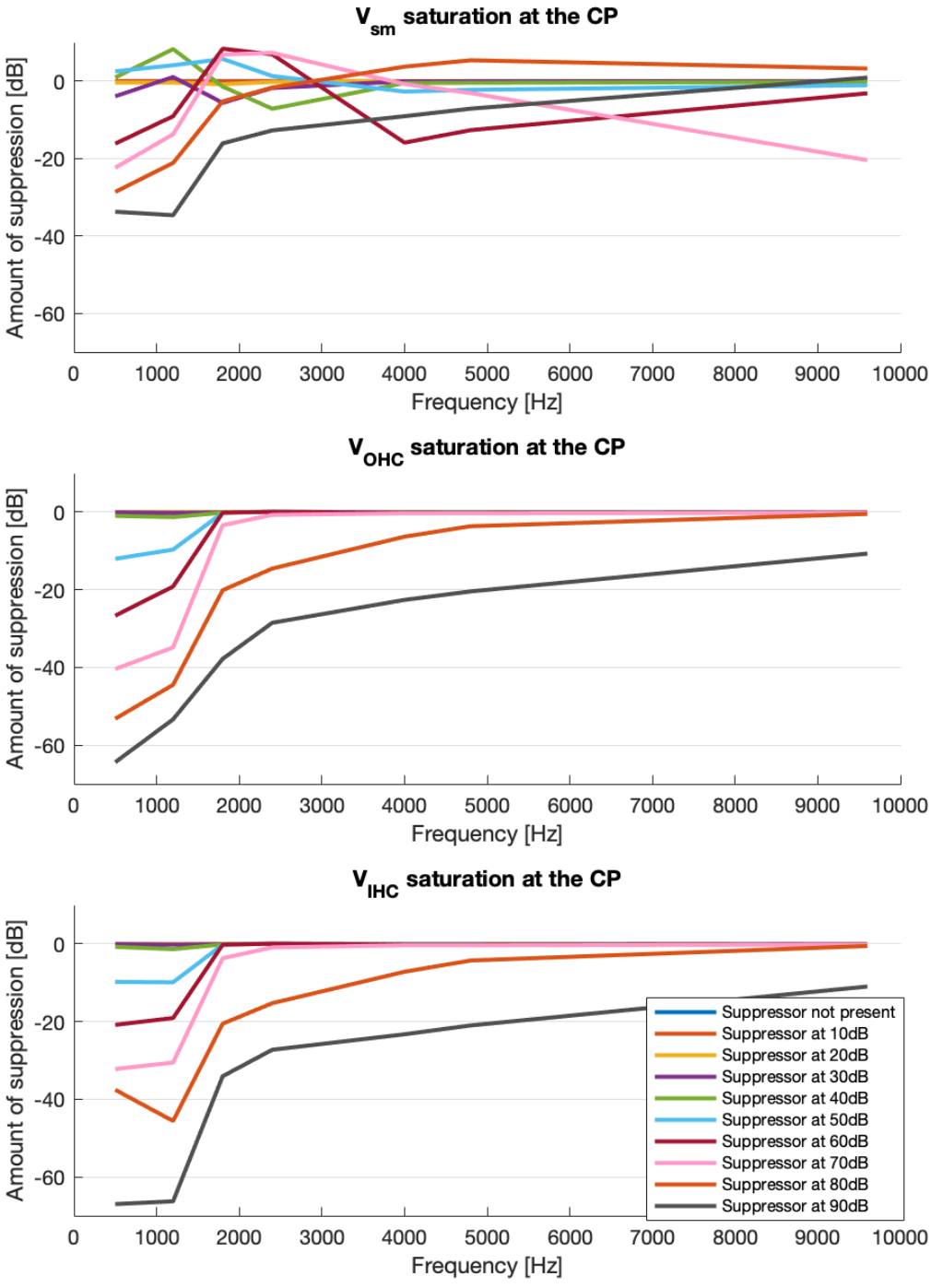

Figure 4.11: The amplitude of the cochlear potentials V_{sm}, V_{OHC} and V_{IHC} at the 1kHz probe tone characteristic place depending on the suppressing tone level and frequency. All of the potentials are affected mostly by the suppressors close of the probe tone frequency, with only a minor impact seen for the higher frequencies.

Comparing the graphs from Figure 4.11, we observe that, indeed, the enhancement in the V_{sm} potential is present primarily at the region where the V_{OHC} is affected by the suppressor frequency to a much smaller extent. The IHC potential appears to be slightly less prone to the impact of the suppressing tone, but since the OHC and IHC tuning curves are almost identical (Pickles, 1988), the difference is relatively small. All of the potentials are mostly affected by the suppressors close to the probe tone frequency with only minor impact from the higher frequencies.

The same simulation is now evaluated at the base of the cochlea in Figure 4.12.

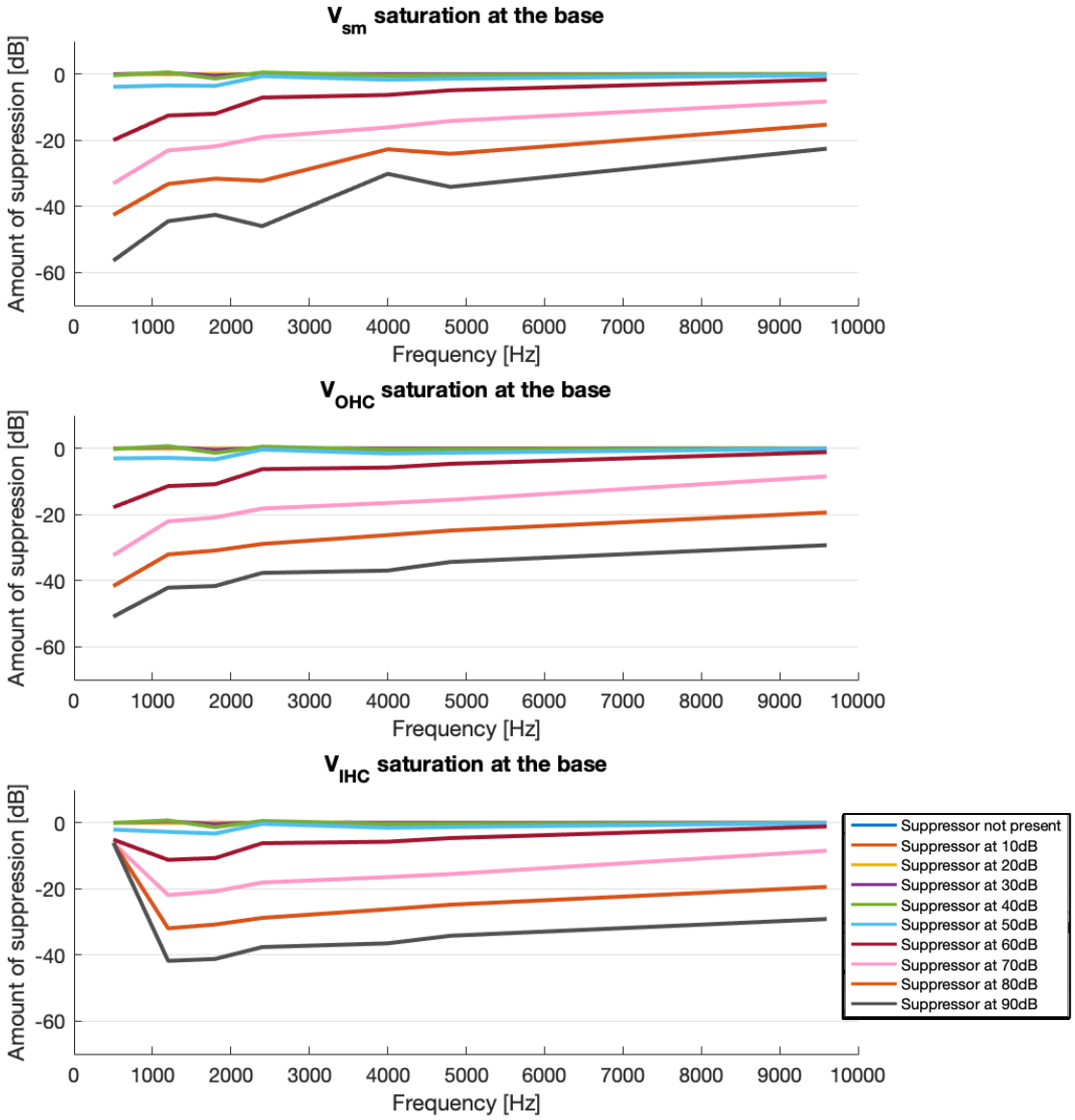

Figure 4.12: Cochlear potentials V_{sm}, V_{OHC} and V_{IHC} at the 1kHz probe tone at the base, depending on the suppressing tone level and frequency. For the suppressor tones above 60dB, the potentials at the probe tone frequency are affected by all of the suppressors.

The responses obtained from the basal point on the cochlea show that the potentials from that region are affected in a greater manner by the suppressing tones. For suppressor levels at and above 60dB, the reduction of the V_{sm}, V_{OHC} and V_{IHC} potentials is observed across all frequencies, although the ones closer to the probe tone have the biggest impact on the V_{sm} and V_{OHC}.

The assumptions outlined in the study that the model was based on (Mountain and Cody, 1999) suggests that the IHC voltages for low-frequency stimulus (below 1kHz) significantly differ from the potentials of the scala media. Therefore, the suppression effect on the IHCs observed at the presence of the 500Hz suppressor is likely the reason for the large difference between the effect a 500Hz suppressor has on the OHC compared to the IHC potentials.

The general outcome of the simulation seems to suggest that the basal responses tend to be more affected by the presence of the suppressing tones, and that impact should be seen in the potential of the scala media, which is suggested to be directly linked to the cochlear microphonic. If the assumption about the basal part of the cochlea being the primary source of the CM is correct, the measurements could show similar patterns to the ones presented in Figure 4.12. However, it is likely a considerable simplification assuming that the CM generation site is limited to that one location. Therefore, the findings from this chapter are going to be discussed further in the context of the experiments presented in Chapter 5.

5. Measuring cochlear microphonic in normal hearing patients

The main objective of this section of the project was to develop a reliable method of measuring the cochlear microphonic using non-invasive extratympanic electrodes and study the nonlinear processes within the cochlea, including saturation of the input-output function, two-tone suppression and distortion products of the cochlear microphonic. The measurements can then be validated against the modelling results presented in the previous chapter to evaluate how accurate the current model formulation is in predicting the measured cochlear potentials.

5.1. Overview and methods

The following section outlines the participant requirements and demographics, measurement setup and methods used throughout the study. The experiments were approved by the University of Southampton Ethics and Research Governance board (Ethics number = 43325).

5.1.1. Participants

10 subjects aged 20 - 40 were recruited for the purpose of the experiments. There was an equal number of male and female participants. The subjects were all healthy adults, reporting no history of hearing problems. The list of exclusion criteria included:

- otological abnormalities detected during otoscopy such as excessive wax, foreign bodies, perforations, infections, mastoid cavities, pain etc.,
- participants reporting skin sensitivity,
- participants who suffer from troublesome tinnitus,
- noise exposure in the last 48 hours,
- Hyperacusis.

Before the test session participants were asked to fill in the questionnaire to qualify for the study together with a consent form. If no contradictions against their participation were found, subjects were familiarised with the test procedures and instructions and had any of their concerns addressed. Otoscopy was carried out in each case to ensure that there were no blockages or foreign bodies in the ear canal, and the eardrum was inspected for any visible abnormalities. Pure tone audiometry for frequencies between 125Hz and 8kHz was carried out in accordance

with the BSA guidelines (BSA 2004) to warrant that the air-conduction hearing thresholds were below 15dBHL. In a situation where participants presented their normal PTA results taken no longer than 1 year ago and reported no significant events that might have had a negative impact on their hearing thresholds, the PTA procedure was omitted. Participants were paid £10 upon completion of the testing.

5.1.2. Hardware

The measurement system used for testing was the Bio-logic Navigator Pro Auditory Evoked Potential System (Natus Medical Incorporated, San Carlos, CA). The model used was the older 580-NAVPR2 version as the software version native to that system allowed for extracting the numerical data into the external file – a feature that was not available in the newer version. A slight modification to the measurement setup was introduced by exchanging the transducers for the newer version resulting in an extended dynamic range. Since the transducer was not native to that version of Biologic, its output was calibrated in accordance with ANSI standards using the Brüel & Kjær Type 2250-L Sound Level Meter / Analyser.

Two types of electrodes were used during the course of the studies:

- Ambu Neuroline 720 snap electrodes
- Etymotic gold-wrapped tiptrodes
- Sanibel TM ECochG electrode

Figure 5.1: Three types of electrodes used during experiments: mastoid pad electrode (left), golden foil tiptrode (middle), wick electrode (right)

Alligator clip leads were used to connect the EEG skin electrode to the BioLogic collection device. The tiptrode lead incorporates both an alligator clip that snaps onto the foil element and a sound delivery tube that connects directly to the transducer that emits the stimulus.

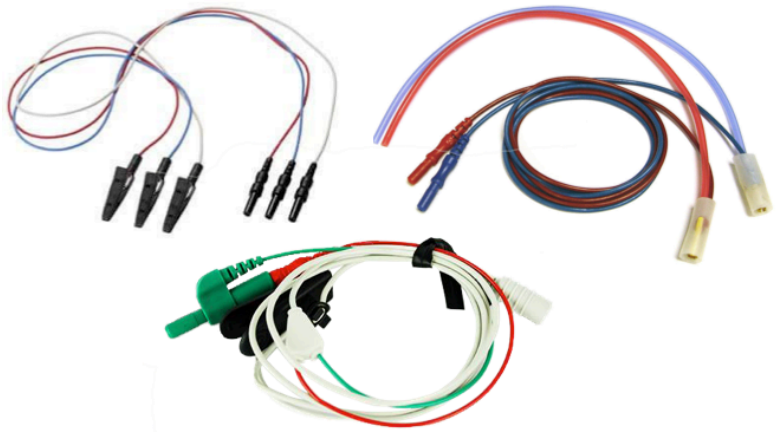

Figure 5.2: Three types of leads used during experiments: alligator clip for mastoid pad (top left), tiptrode lead combined with delivery tube (top right), wick electrode leads (bottom)

The full schematic illustrated based on the tiptrode setting is presented in the Figure 5.3.

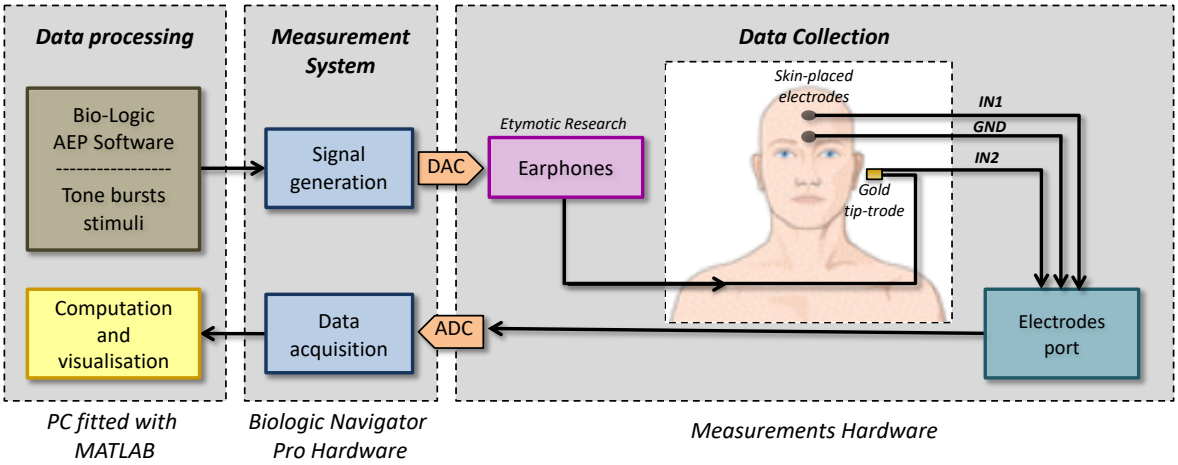

Figure 5.3: Schematic showing data collection setup: the Bio-Logic AEP Software and its GUI allows the tester to control the stimuli parameters that then gets delivered to the transducer after undergoing digital-to-analogue conversion. The transducer sends the stimulus via tubing into the foam earphone wrapped in gold foil (tiptrode) that simultaneously serves as an electrode. The tiptrode, together with two pad electrodes placed on the high- and low forehead, is connected to the electrode port that feeds the signal back through an analogue-to-digital converter into the acquisition software. The data is then analysed and visualised offline in a PC fitted with MATLAB software

5.1.3. Participant preparation

To get ready for the measurements, all participants had to have their skin prepped before the electrodes were placed. This procedure required using Nu Prep abrasive paste to gently scrub away at the skin on the low forehead and mastoid, as well as inside the ear canal, followed by cleaning out the area with a wipe saturated with isopropyl alcohol to remove any residue. To further improve the conductivity, a Ten20 conductive paste was applied to the outside of the tiptrode before being inserted into the ear canal. If a wick electrode was used, the preparation included rinsing out the ear canal with a saline solution.

It is commonly accepted that the impedance reading below 6kΩ is sufficient to ensure a substantially accurate recording, however, to make certain that any potential impact on a signal-to-noise ratio is eliminated, the impedance values for the purpose of the following experiments were always kept at or below 1kΩ on all electrodes and were repeatedly monitored throughout the course of the measurements using the pad electrode and the tiptrode. For measurements with the wick electrode, the impedance of 5kΩ was accepted as there is no easy way to lower the electrode impedance without risking damage to the eardrum.

5.1.4. Stimulus

The stimulus originated from an insert earphone (Navigator Pro, Natus Medical Incorporated) and was delivered to the ear canal through a sound delivery tube that runs through the centre of an earplug. Because of the distance the stimulus has to travel, a correction factor for the 0.8ms is applied to account for the time the sound needs to travel from the transducer to the insert earphone outlet. All of the following experiments were performed using a pure-tone stimulus as opposed to the well-studied click stimulus that is usually used in a clinical setting. For each experiment, the stimuli were slightly different, be it in a frequency or level, therefore, they are characterised in detail in each section separately.

5.1.5. Stimulus artefact and non-CM cochlear potentials

The cochlear microphonic recording is prone to interference arising from the measurement setup itself. The stimulus is delivered to the subject via a transducer unit that happens to be placed in close proximity to the electrodes. Since the transducer is a voice coil, it can emit an electromagnetic interference that might get picked up by the electrodes and recorded during the measurement. To ensure that recorded potentials are actual CM and not the electromagnetic

interference (stimulus artefact), measurements with clamped tubing (Zhang, 2012) that delivers sound to the earpiece were performed frequently throughout the course of the study. If the stimulus artefact would appear during the clamped test measurement, the results from that session would have been discarded. An example of a CM recording with negative control (blocked tubing) is presented in a section describing Experiment 2 in Figure 5.10.

CM potential arises as soon as the hair cells are activated, therefore, tracking the time between the onset of the stimulus and the onset of the CM is helpful when trying to differentiate between the CM and other auditory potentials that might be picked up by the electrodes, one of those being the neurophonic potential (FFRs – frequency following response) (Chimento and Schreiner, 1990). Previous studies report that FFRs' latency tends to be stimulus intensity-dependent (Batra, Kuwada and Maher, 1986) and not easily recorded by ear canal electrodes (Zhang, 2014) but, as an additional precaution, the latency was tracked throughout the study and did not appear to change with the change of stimulus intensity.

5.2. Experiment 1: Comparison between non-invasive measurement methods

5.2.1. Introduction

The objective of the pilot experiment was to determine what kind of electrode should be used for the main series of measurements. The evaluation included a number of considerations including the quality of the collected recordings, how safe and comfortable the procedure was for the participants considering the length of the experiment, the feasibility of repeated measurements using the selected method and its potential availability for further research and clinical setting.

The electrodes in question included all three types listed in the Hardware section in this chapter. The collection device has the possibility to record two channels at the same time, therefore two sets of measurements were performed:

- simultaneous recording from mastoid-placed pad electrode against the wick electrode: presumed lowest and highest quality setting respectively,
- simultaneous recording from mastoid-placed pad electrode against the tiptrode: the mastoid recording was collected to act as a cross-reference point for comparison with the wick electrode measurement.

5.2.2. Methods

The recordings were obtained for the stimulus level of 85dBHL for three frequencies: 1000Hz, 2000Hz and 4000Hz. Stimuli used were pure-tone bursts with a 2ms rise-decay and 6ms plateau time, totalling 10ms per one repeat as demonstrated in Figure 5.4. The same windowing applied to all three of the tested frequencies.

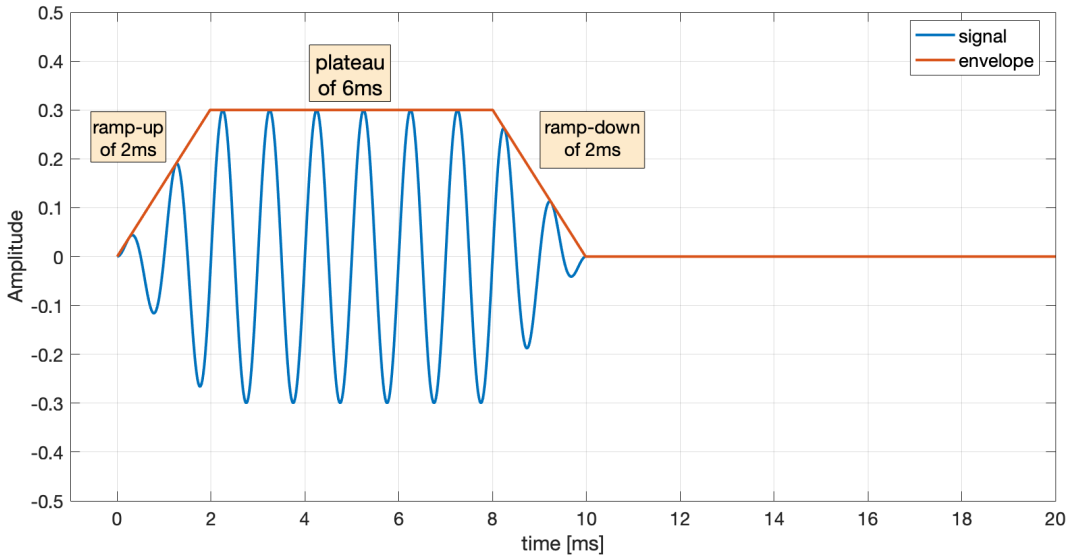

Figure 5.4: The graph shows an example of a 1000Hz pure-tone stimulus with windowing schematics consisting of a 2ms ramp-up period, followed by 6ms of a plateau and another 2ms of a ramp-down period.

The ramp-up/ramp-down characteristic of the stimulus followed by relatively long plateau time was used to mitigate the transient response as a sudden onset of the stimulus facilitates neural synchronisation. As a result, recorded neural responses can be mistaken for cochlear microphonic (Berlin, Morlet and Hood, 2003; Zeng and Liu, 2006). Applying the fade-in/fade-out windowing to the stimulus, along with the alternating polarity, ensures that the picked-up signal is not of a neural origin.

Additional measure employed to monitor the quality of the recorded responses was using the pre-stimulus feature. The pre-stimulus value defines by how much the beginning of the recording window will precede the onset of the stimulus. It can be used to track if the recorded potentials do not contain a signal that might look like a cochlear potential but actually be an artefact. In that case, the “response” might appear before the onset of the stimulus, therefore, observing the couple milliseconds ahead of the stimulus ramp-up can aid in separating reliable measurements from invalid ones.

The full measurement parameters are collected in the Table 5.1.

Table 5.1: Measurement parameters used in Experiment 1

Parameter	Value
Epoch time [ms]	21.33
Points	512
Pre-stimulus [ms]	-1.5
Post-stimulus [ms]	0.0
Polarity	Alternating
Rate [stim/s]	27.6
No. of averages	1000
Low-pass filter [Hz]	100
High-pass filter	5000

During the data collection using the tiptrode, the subjects were seated in a reclining chair. The light in the test room was switched off for the duration of the measurement and participants were asked to keep their eyes closed.

During the measurement with wick electrode, the subjects were lying down flat on a side with the tested ear positioned towards the ceiling and a pillow under the head for comfort and stability.

5.2.3. Results

For this initial experiment, a single set of measurements from one of the participants with time-domain and their frequency domain analysis is presented to demonstrate how the signals vary depending on the used electrode and to illustrate the characteristics of the noise that is present in every recording. The FFT is derived from the part of the recording, where the signal has already stabilised after the ramp-up and is already in a presumed steady-state. The results for all of the three test frequencies are illustrated in Figure 5.5, Figure 5.6 and Figure 5.7.

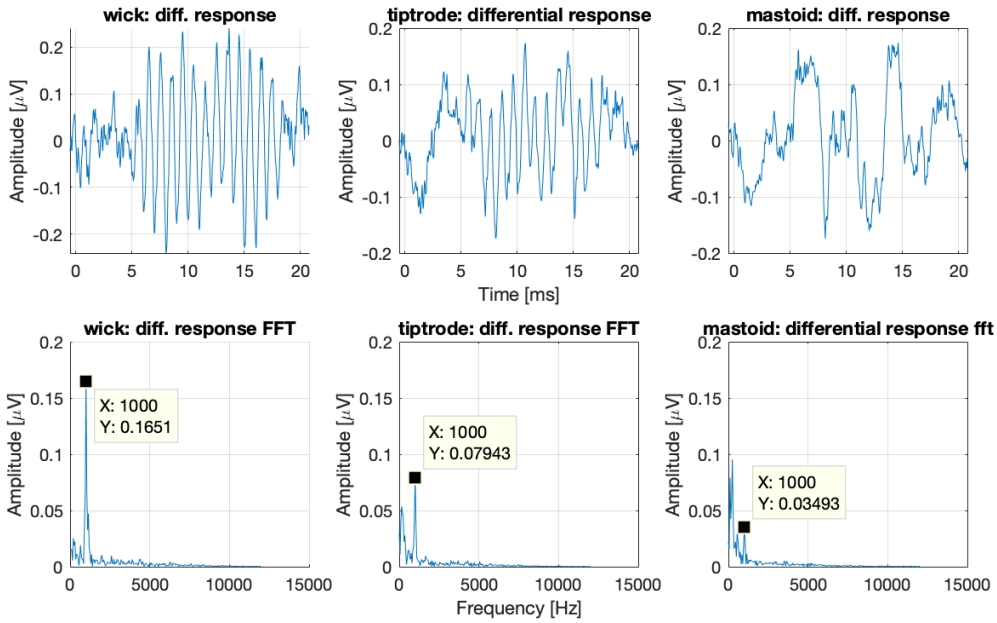

Figure 5.5: Time and frequency domain results for the stimulus of 1000Hz and intensity level of 85dBHL. The top three graphs show time domain signals obtained by deducting the rarefaction and condensation responses for all three different types of electrodes: wick, tiptrode and mastoid electrode. The three bottom graphs show the analysis of their spectral content with clearly marked peaks visible at the stimulus frequency.

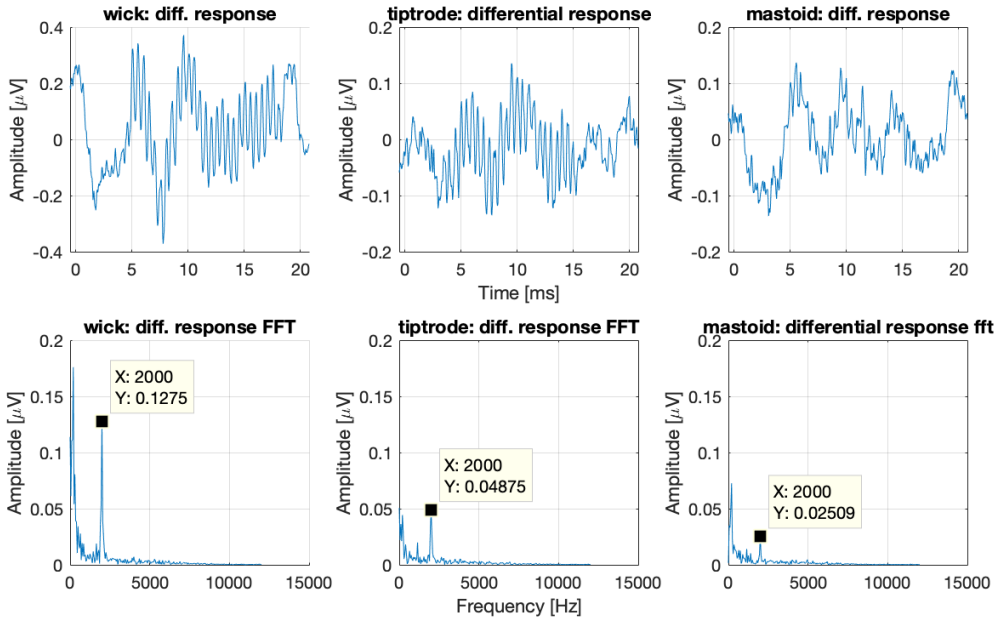

Figure 5.6: Time and frequency domain results for the stimulus of 2000Hz and intensity level of 85dBHL. The top three graphs show time domain signals obtained by deducting the rarefaction and condensation responses for all three different types of electrodes: wick, tiptrode and mastoid electrode. The three bottom graphs show the analysis of their spectral content with clearly marked peaks visible at the stimulus frequency.

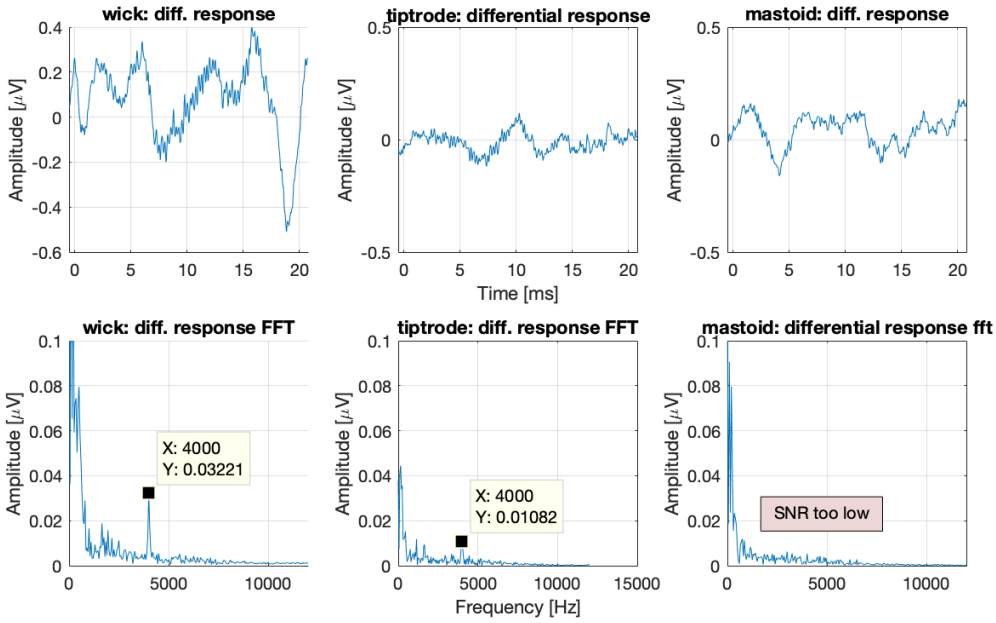

Figure 5.7: Time and frequency domain results for the stimulus of 4000Hz and intensity level of 85dBHL. The top three graphs show time domain signals obtained by deducting the rarefaction and condensation responses for all three different types of electrodes: wick, tiptrode and mastoid electrode. The three bottom graphs show the analysis of their spectral content with clearly marked peaks visible at the stimulus frequency.

To compare the three different types of electrodes to each other, the obtained results are collected in a single graph in Figure 5.8, showing the amplitude of the recorded CM depending on the type of electrode used and the frequency of the stimulus. The measurements with negative control (blocked tubing) were collected after each test run with the stimulus present and evaluated for each separate measurement for the signs of electromagnetic interference. Since there was no evidence of the stimulus artefact in any of the blocked tubing measurements, for clearer illustration, the average of the negative control recordings is pictured in Figure 5.8 as the noise floor.

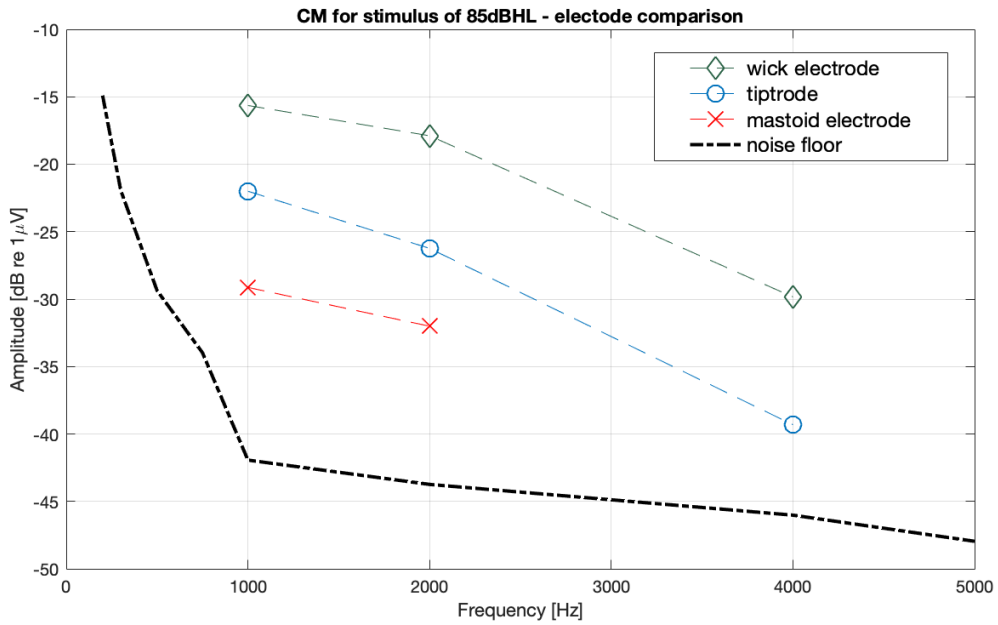

Figure 5.8: Comparison of the recorded CM amplitude depending on the electrode type and the input frequency for the 85dBHL stimulus. The CM recorded by the wick electrode has the highest amplitudes, followed by slightly lower amplitude for the tiptrode and the mastoid electrode that picks up the least amount of the response. The recorded CM drops in amplitude for all of the electrodes as the frequency goes up.

5.2.4. Discussion

From the data presented, it is evident that, as expected, the wick electrode yields the best results when it comes to SNR and therefore would be the most accurate method of measurement. However, it should be noted that the measurement using the wick electrode has a couple of significant drawbacks:

- the electrode has to be placed on the eardrum by a trained individual as, if done incorrectly, it can result in damage to the tympanic membrane,
- it is notably more difficult to obtain the required impedance using this method, and it often times includes repositioning the electrode couple of times until the reading gets to the desired value,
- the position which the subject has to assume for the time of the test (resting on a side) was reported to become uncomfortable after some time due to the pressure put on the shoulder while lying down.

Analysing the comparative graph in Figure 5.8, we can observe that the signal obtained from tiptrode is consistently well above the noise floor and follows fairly closely the frequency-amplitude trend that can be observed in the wick electrode recordings, although this dependency is not entirely linear.

Table 5.2 shows how much lower the CM amplitude picked up by the tiptrode and mastoid electrodes is if we consider the wick electrode a baseline for the non-invasive measurement method.

Table 5.2: Amplitude of the recorded CM in relation to wick the electrode (baseline)

Electrode type	**Amplitude of recorded CM vs. wick electrode**		
	1000Hz	**2000Hz**	**4000Hz**
Tiptrode	-6dB	-8dB	-9dB
Mastoid pad	-13dB	-14dB	not measurable

While the comfort of the subject might seem like a problem of a purely subjective matter, analysing the collected data, a pattern was noticed in the characteristics of the noise present in the recordings. The noise recorded by the wick electrode was becoming increasingly prominent as the test progressed, which can be seen in Figure 5.9. The noise picked up by the two remaining electrode types stayed relatively consistent throughout the duration of the measurement.

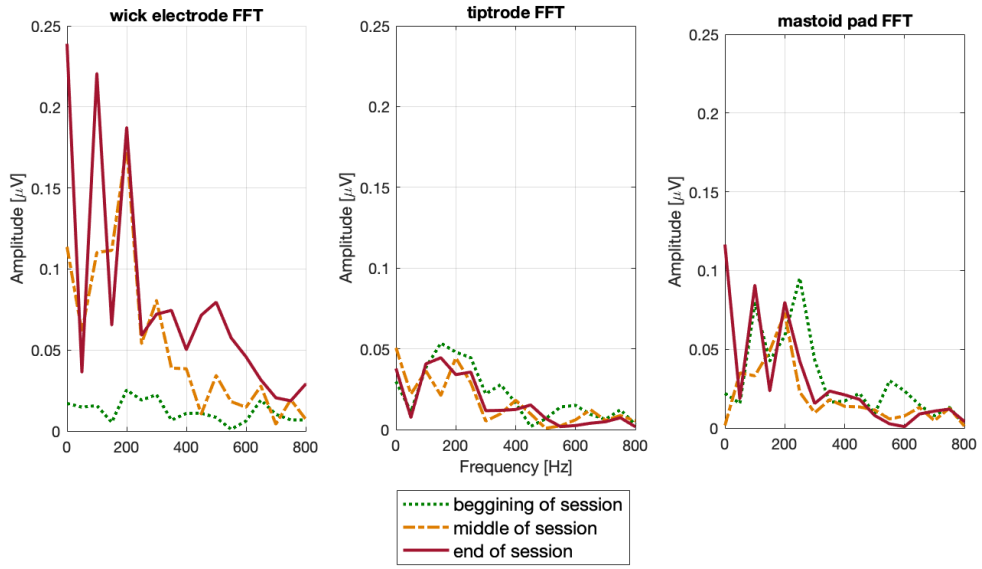

Figure 5.9: Characteristics of the noise change throughout the duration of the test for all three electrode types. The wick electrode recording shows increasing noise contribution as the measurement progresses, with little noise present at the beginning of the session to a significant amount of noise present at the end of the session. For the remaining two electrodes, the noise stays stable throughout the measurement.

In line with the data provided in Table 1.3, the increase in the noise picked up by the wick electrode is presumed to be associated with the progressing strain on the muscles affected by the uncomfortable positioning needed for the measurement which causes the subject to build up tension in the arm and neck that then gets picked up by the electrodes as a noise. When the data from tiptrode and mastoid electrodes is analysed, this effect cannot be observed as the position assumed during those measurements (lying on the back on a reclining chair) allows for easier muscle relaxation and reduces or even eliminates the discomfort the participants' experience.

The results presented are for a single participant only, however, the test was performed on two more subjects and the results across every data set were consistent with the one presented above but were not presented for the purpose of clarity in the reporting.

Based on the points outlined above, the decision was made to continue further experiments using the tiptrode. This method not only allows for good quality recordings but also does not require any significant training and therefore is more likely to be used in a conventional setting.

5.3. Experiment 2: Repeatability and input-output functions

5.3.1. Introduction

The first part of this experiment focuses on the repeatability of cochlear microphonic measurements that are presumed to be influenced by the following factors:

- immediate repeatability – the CM's amplitude is small enough that it can vary slightly from one measurement to the other due to insufficient SNR, presence of other physiological potentials not generated by the auditory system, external interference or artefacts arising from the measurement setup itself,
- repositioning of the electrodes - every time a subject is prepped for the measurement, the placement of the electrodes is going to be slightly different, which could result in changes in the picked-up potentials,
- repositioning of the earphone – the placement of the earphone inside the ear canal could affect the resonance of the cavity,
- physiological changes – due to ageing processes and/or any external factors that can cause hearing deterioration/changes over time.

Due to the limited duration of the research project, the CM stability could mainly be evaluated in regards to immediate repeatability. Where possible, the data was collected during a single session without repositioning the electrodes and the earphone to mitigate the variability within subjects and, for every participant, the earphone placement in the ear canal was as deep as possible to shift the cavity resonance towards higher frequencies.

The second part of the experiment was to observe dependencies between the stimulus input levels and resulting amplitude of the recorded pure-tone evoked cochlear microphonic across all participants. This test is also the pre-check for Experiment 3 to evaluate whether a CM recording can be obtained from all of the participants. The input-output functions were collected during the same session as repeatability measurements, therefore, if any participants got excluded from the study due to inability to obtain clear data from them, they would also be excluded from Experiment 3.

5.3.2. Methods

The stimuli used were windowed in the same manner as the stimuli from Experiment 1 with the rise-decay characteristic as seen in Figure 5.4. The decision was made to focus on two frequencies: 1000Hz and 2000Hz.

The choice of the specific probe tone frequencies was dictated by several key factors:

- the physiological and physical artefacts that were listed in Table 1.3 are more likely to affect the measurement quality for the probe tone lower than 1kHz - even at 500Hz, the muscle contractions can still introduce interference into the recorded signals having a detrimental impact on the SNR,
- the lower the probe tone is, the more likely it is for the CM to be contaminated with the auditory nerve neurophonic - because of the neural phase-locking frequency limit, the ANN response begins to roll off at around 1kHz (Fontenot, Giardina and Fitzpatrick, 2017) making it less likely to be mistaken for the CM as the stimulus frequency goes up. Additional measure implemented to ensure that the CM is not mistaken for the ANN was to track whether the recorded signal does not contain the 2^{nd} harmonic component (or higher) at the probe tone frequency that was previously reported to appear in the spectral analysis of the measured potential due to asymmetric half-wave shape of the ANN (Forgues *et al.*, 2014),
- the occlusion effect that boosts the ear canal sound pressure affects mostly frequencies below 500Hz introducing additional uncertainty into the measurement for lower frequency stimuli (Dean and Martin, 2000),
- for probe tones higher than 2kHz, the amplitude of the CM was becoming small in comparison to the noise floor (as can be seen in Figure 5.7), rendering the results unreliable,
- the lower frequency stimuli were not well represented in the cochlear model introduced in the previous chapter - the transient response was taking a very long simulation time to die down the lower the stimulus frequency. To be able to efficiently compare the simulation obtained from the model to measurements, higher frequencies were selected.

An attempt was made to obtain CM recordings from all 10 participants. Before commencing the measurement, every participant was presented with the highest intensity stimulus that would be used during the test to verify whether the loudness will not cause any discomfort. Even though the exposure dose calculated in compliance with the Ethics guideline was well within the limits, in some cases the maximum level had to be lowered by 5dB because of the stimulus being perceived by the participants as uncomfortably loud. This pre-check was a way to ensure that participants will be less likely to withdraw from the study.

The measurement parameters remained unchanged with exception of the pre-stimulus time being set to -1.5ms. The remaining values are in line with the ones presented in Table 5.1.

The experiment had two stages to it:

- collecting multiple measurements on the tone burst evoked CM at stimulus level of 80dBHL and frequencies of 1kHz and 2kHz to evaluate whether the recorded CM changes from one measurement to another (the measurements were not taken back-to-back, they were spread throughout the session of input-output measurements)
- recording CM potential for 1000Hz and 2000Hz at 4-5 different levels separated by 5dB steps ranging from 75 - 90dBHL (or 70 - 85dBHL if the participant requested to have the maximum level lowered) – the measurements were taken at least twice at every level to verify that the potentials recorded are true.

Through the entire duration of the test measurements with blocked sound delivery tube were performed as a standard check to exclude the stimulus artefact interference.

5.3.3. Results

The GUI of BioLogic Navigator Pro software allows seeing the graph containing collected data directly after each test run. Aside from recognising the stimulus artefact, based on the visual representation of recorded cochlear potential the tester can estimate whether the signal recorded indeed contains the cochlear microphonic potential. Based on that visual inspection, two of the participants got excluded from the study, as the recorded signal did not seem to contain the CM response.

An example of a stimulus and a resulting recorded response (opened tubing) in comparison to negative control measurement (clamped tubing) is shown in Figure 5.10. The recorded CM

potentials presented on the graph were filtered with a high-Q bandpass filter with a centre frequency f_0 = 1kHz for clearer illustration and was not a part of the standard data analysis.

The true cochlear microphonic potential can easily be differentiated on the graph from the stimulus artefact because of two main factors:

- a small latency in the recorded signal can be observed in relation to the input stimulus; for the artefact that latency would be close or equal to 0ms,
- the response disappears once the sound delivery tube is clamped.

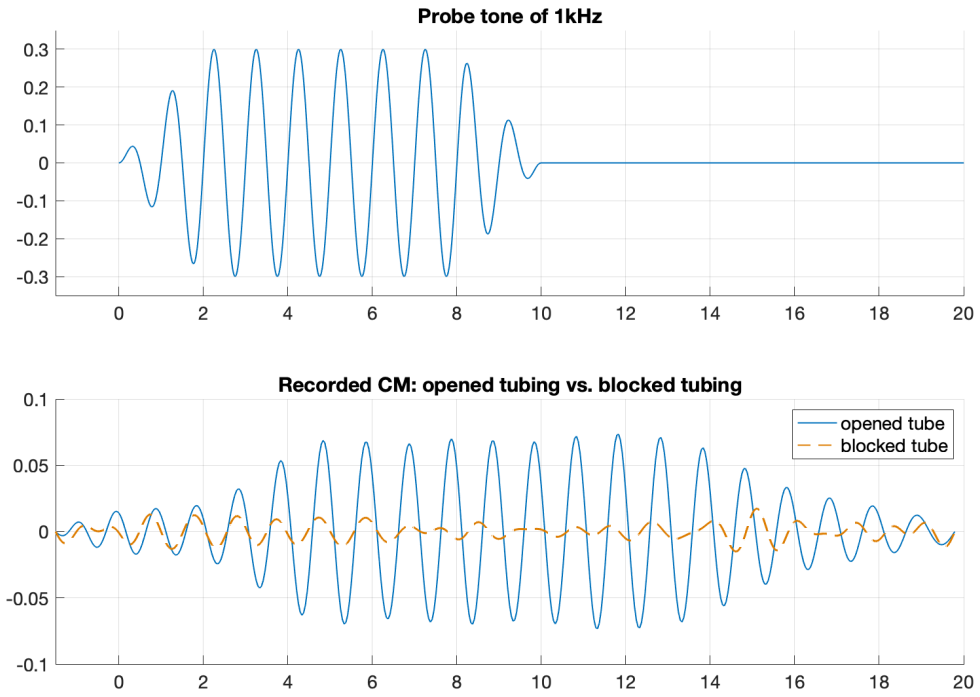

Figure 5.10: Comparison of input stimulus vs recorded CM potential and negative control measurement (blocked tubing). The signals are filtered with a high-Q bandpass filter with a centre frequency f_0 = 1kHz to extract the response at the probe frequency from the noise for illustration purposes.

As can be noted from Figure 5.10, the number of periods in the recorded CM is bigger than the number of periods present in the stimulus signal, however, that phenomenon, called "long ringing cochlear microphonic" was documented before and it was concluded that in around 69% of normal-hearing people the prolongation of the cochlear microphonic will be present (Gibbin, Mason and Kent, 1983).

Figure 5.11 and Figure 5.12 depict the statistical distribution of repeated measurements of 1kHz and 2kHz probe tones, respectively (teal boxes), all at 80dBHL recorded across 8 subjects,

in comparison to the clamped tubing measurements (red boxes) of the same stimuli frequencies and levels. For each participant and every probe frequency, in between 6 to 9 separate measurements were taken with the opened sound delivery tubing, and 4 to 5 measurements with the tubing blocked.

The purpose of presenting this graph is to investigate three main aspects of CM recordings carried out for the purpose of this research:

- the stability of the CM potential reading stays when measured repeatedly in the same subject,
- the differences in CM amplitude evoked by the exact same stimulus in between normal-hearing individuals,
- identification of the subjects for whom the CM can be recorded reliably (if opened and blocked tubing boxes are too close or overlap the reading cannot be treated with confidence).

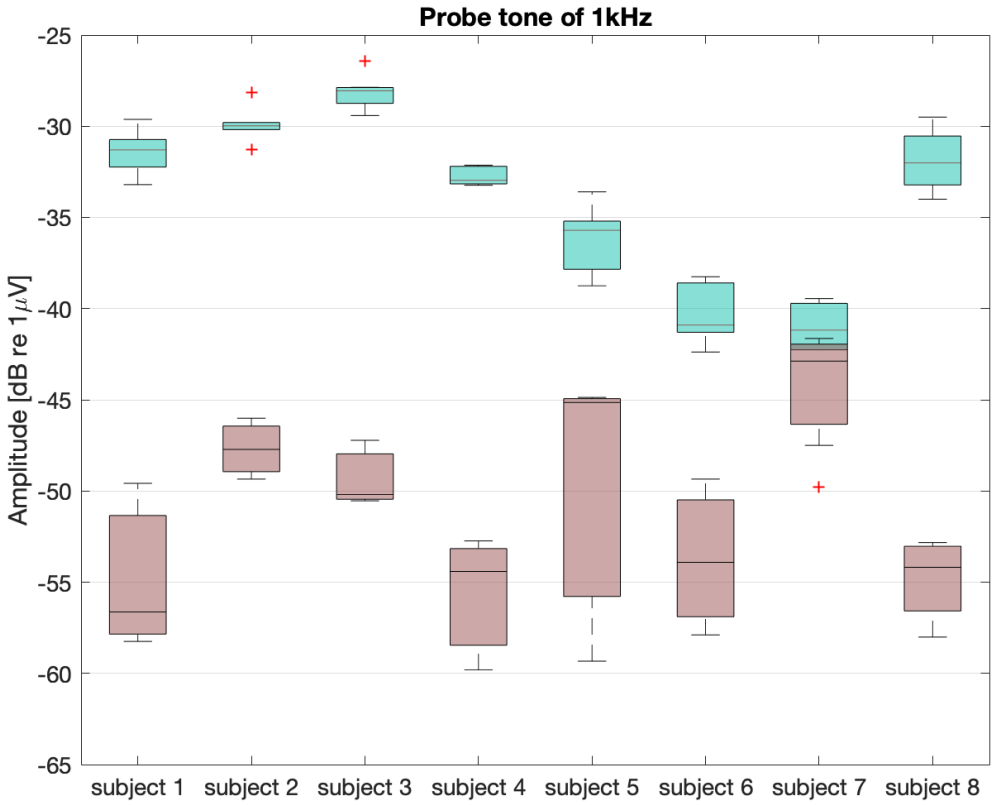

Figure 5.11: Collective results for repeatability test for 8 participants for the stimulus frequency of 1kHz. The boxplot shows a statistical analysis of CM potential and negative control measurements. The number of repeated tests for each subject varied between 6 to 9 for the measurement with probe tone present, and 5 to 6 for the negative control

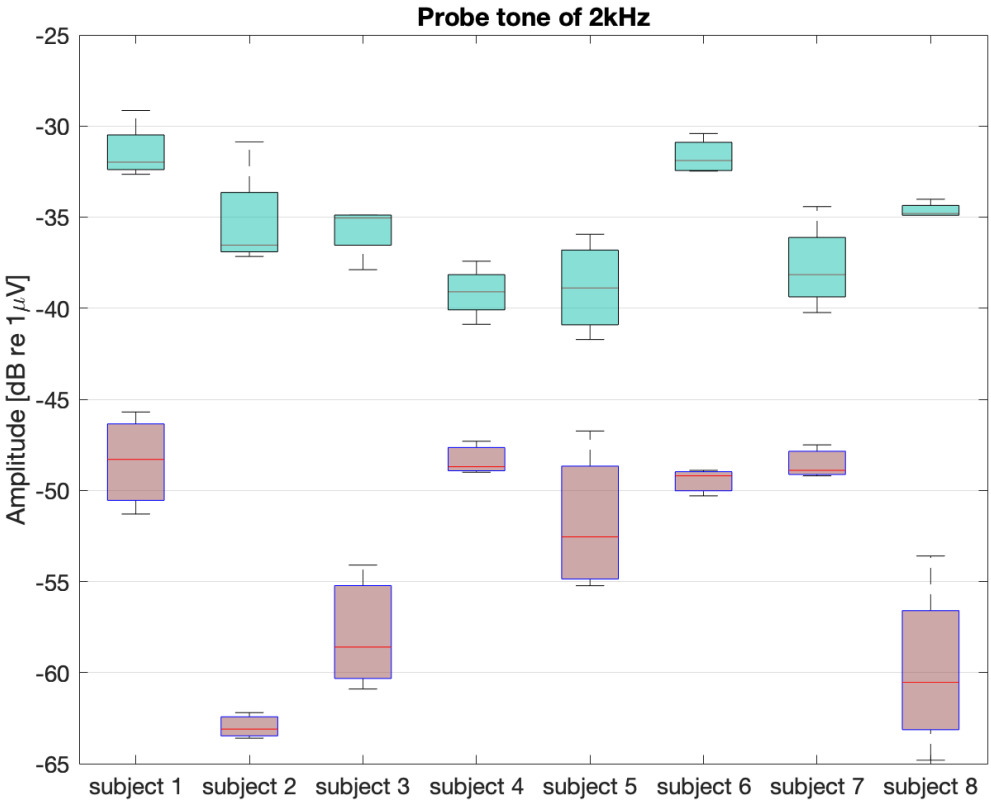

Figure 5.12: Collective results for repeatability test for 8 participants for the stimulus frequency of 2kHz. The boxplot shows a statistical analysis of CM potential and negative control measurements. The number of repeated tests for each subject varied between 5 to 7 for the measurement with probe tone present, and 4 to 5 for the negative control

The graph shows that in most cases, the CM can reliably be recorded in a non-invasive manner, using a gold foil tiptrode. In every single participant, the value of the interquartile range for the recorded CM does not exceed 2.7dB for 1kHz stimulus, and 4dB for 2kHz stimulus, which can be considered a stable value.

Based on the presented data, subject 7 was shown to present with an insufficient distance between the CM recording and negative control test for the 1kHz probe tone to consider the recording reliable. Therefore the results will not be considered. Furthermore, the SNR for subject 5 is relatively worse when compared to remaining participants for both 1kHz and 2kHz stimuli, so those recordings are going to be omitted for the purpose of more intelligible data representation but will be used in Experiment 3.

For all of the remaining subjects, the input-output functions were obtained. The collected data is presented in Figure 5.13.

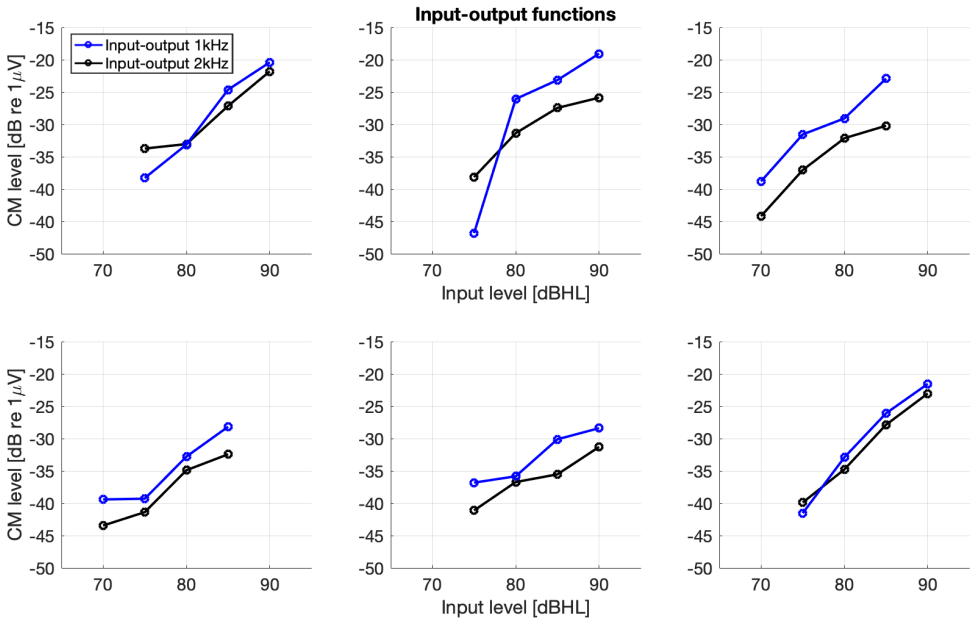

Figure 5.13: Input-output functions of cochlear microphonic for stimulus frequencies of 1kHz and 2kHz for six subjects. In all instances, the CM potentials grow as the stimulus level gets higher. The amplitude of 1kHz CM tends to be slightly higher than the 2kHz CM recorded at the same dBHL stimulus intensity

As can be seen from both repeatability and input-output measurements, the amplitude of CM varies by as much as 12dB in between tested individuals for the same exact stimulus frequency and intensity. To extract the data about the I/O function of the CM, the measurements have to be considered as being dependent on the “anchor”, in this case, decided to be set at CM value obtained for 80dBHL stimulus, and note by how much the CM amplitude recorded for every individual changes in relation to that “anchor”. An example of that conversion is illustrated in Table 5.3.

Table 5.3: Example of conversion from CM amplitude in relation to stimulus level to CM amplitude in respect to an "anchor". The “anchor” describes CM potential recorded at 80dBHL and is treated as the baseline where all of the other measurements are presented in reference to that value

	STIMULUS LEVEL [dBHL]			
	75	80	85	90
CM amplitude [dB]	-38.3	-33.1	-24.6	-20.4
		↓		
CM amplitude [re CM at 80dBHL]	-5.2	0.0	8.5	12.7
	-5	0	+5	+10
	STIMULUS LEVEL [re 80dBHL]			

A boxplot for this normalised data was obtained and an approximate input-output function for the test group was derived from the collected data and is shown in Figure 5.14. Because of the limited sample size and a relatively sparse number of different stimulus levels included in the study, drawing conclusions about the exact shape of the input-output function is difficult. However, the data shows an evident increase in the CM amplitude as the stimulus level goes up but does not appear to reach a saturation point for either of the stimulus frequencies for the stimulus levels tested. The extensive statistical analysis of the data continues in section 5.3.4.

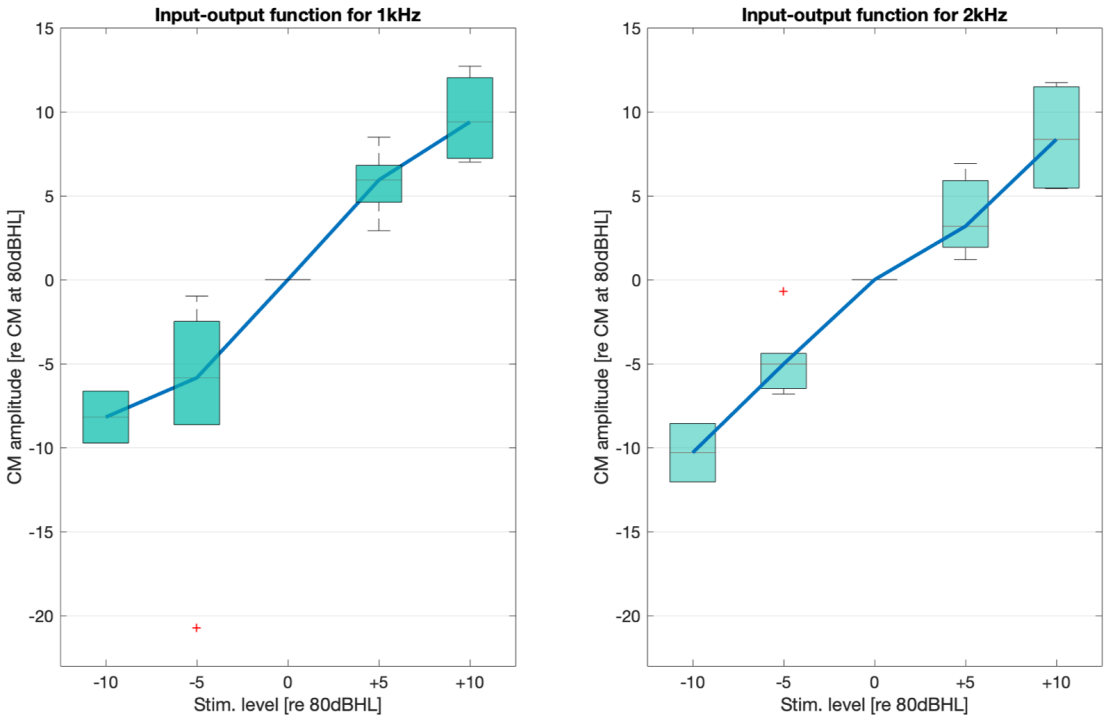

Figure 5.14: Input-output functions of CM for two test frequencies: 1kHz and 2kHz. The graph depicts the boxplot obtained by analysing the data obtained for all six subjects. The relationship appears to be non-linear and does not show clear signs of saturation towards the highest stimulus loudness

5.3.4. Statistical analysis of the results

For statistical analysis of Experiment 2, a paired samples t-test has been chosen to determine the statistical significance between the responses to different stimulus intensities. This particular study design is appropriate for statistical analysis of one dependent variable (here: recorded output level) measured on a continuous scale with one underlying independent variable (here: the stimulus input level) using two different conditions (here: input levels 75dBHL

and 85dBHL) tested on the same participants (referred to as related groups). While the actual measurements included more than two conditions, only three of these conditions were common across all participants (75dBHL, 80dBHL and 85dBHL) for reasons outlined in section 5.3.2. These three conditions allow consideration of a one-way repeated measures analysis of variance (ANOVA), however, since the absolute levels of the recorded outputs varied greatly between participants (with difference up to 15dB) and the relative changes for these measured outputs were of higher relevance for this experiment, the recorded CM value in each participant for the 80dB input level was again used as an "anchor" leaving the 75dB and 85dB levels as conditions for further analysis thus making the paired-samples t-test the most suitable statistical test method. This also meant that for each of the stimulus frequencies (1kHz and 2kHz) a separate paired-samples t-test had to be performed and analysed independently.

Table 5.4 Statistical tests overview for input-output experiment

Statistical test method:	paired-samples t-test
Assumptions:	checking for outliers using boxplot, confirming normality using Shapiro-Wilk test of normality and Normal Q-Q plot
Dependent variable:	recorded pure-tone evoked CM (output)
Cases:	participants 1-6 (pre-selected using boxplot method and SNR)
Independent variable:	stimulus input at 1kHz and 2kHz (analysed independently)
Conditions:	75dBHL and 85dBHL input level (using 80dB input as an „anchor")

A paired-samples t-test sets out a number of requirements that must be fulfilled to ensure that the data sets qualify for subsequent statistical analysis. This includes the detection of outliers using boxplot as well as confirming normality with either numerical methods like the Shapiro-Wilk test of normality, a graphical method such as visual inspection of a Normal Quantile-Quantile plot or a combination of both – a common method for small sample sizes (Easton and McCulloch, 1990). According to standard procedure, these checks have to be performed on the values of differences between the two related data groups rather than the individual values.

After the difference values are calculated a boxplot can be computed in SPSS to check for outliers for both sets of data referring to stimulus signals of 1kHz and 2kHz. Outliers are defined as points falling outside the Inter Quartile Range (IQR) by more than $1.5 \times IQR$ from the edge of the box.

The results presented in Figure 5.15 show that there are no outliers present for either data set satisfying the prerequisite to proceed with an investigation of normal distribution.

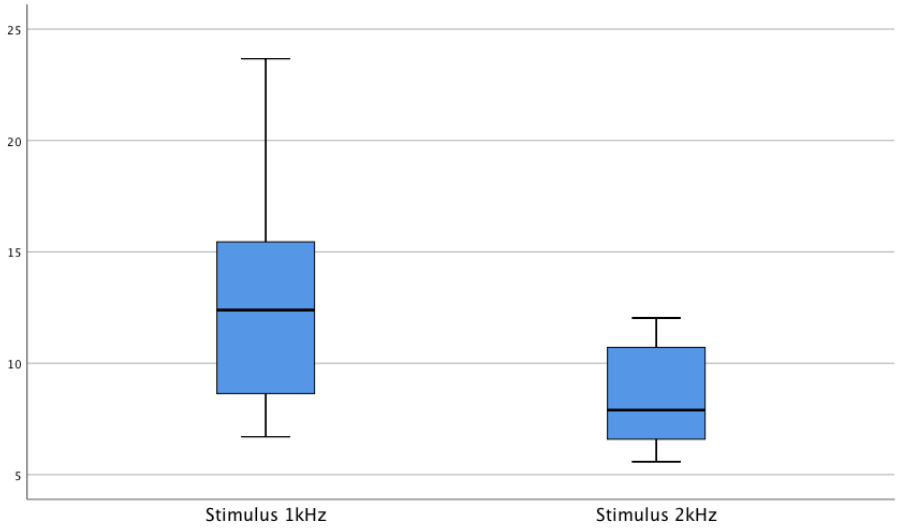

Figure 5.15 Boxplot with Experiment 2 data for 1kHz and 2kHz stimulus frequencies. The y-axis of the plot shows the CM level increase in decibels in response to the stimulus level increase from 75dBHL to 85dBHL

Due to the small sample size (N=6) normality is assessed using both: visual inspection by means of Normal Quantile-Quantile plots (also called Normal Q-Q plots) and a numerical verification through the Shapiro-Wilk test of normality. Assuming a perfect normal distribution, data points are expected to fall exactly on the diagonal line in the Q-Q plot. However, with experimental data, such assumptions are rather unrealistic, and the objective is to make sure that points are distributed closely along the diagonal line. This is the case for both data groups, and normality can be assumed based on the visual inspection of the Q-Q plots shown in Figure 5.16.

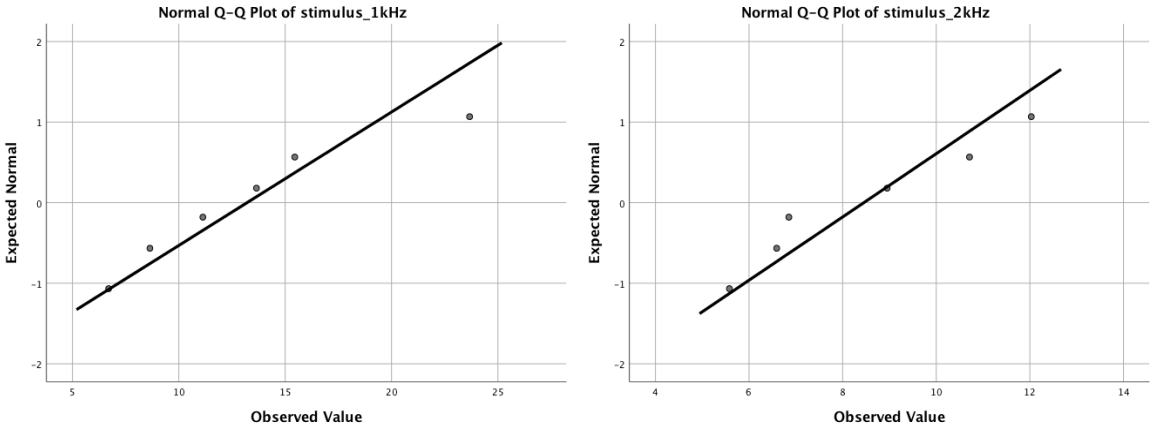

Figure 5.16 Normal Q-Q plot for 1kHz and 2kHz stimuli. All data points appear to be located in close proximity to the diagonal line

The numerical results for the Shapiro-Wilk test of normality are listed in Table 5.5 for each of the two stimulus frequencies. Based on this method normality can be assumed if the significance is higher than 0.05 (p > 0.05). In this case, the significance is equal to 0.611 and 0.573 for the 1kHz stimulus and 2kHz stimulus, respectively. Therefore, the threshold of normality is also confirmed numerically. With these tests successfully completed, all requirements for statistical analysis can be considered fulfilled.

Table 5.5 Numerical results for the Shapiro-Wilk test of normality for input-output experiment data

Tests of Normality

	Kolmogorov-Smirnov[a]			Shapiro-Wilk		
	Statistic	df	Sig.	Statistic	df	Sig.
stimulus_1kHz	.188	6	.200*	.934	6	.611
stimulus_2kHz	.235	6	.200*	.929	6	.573

*. This is a lower bound of the true significance.

a. Lilliefors Significance Correction

A paired-samples t-test was conducted to establish whether there was a statistically significant difference between the CM responses to the stimulus inputs of 75dB and 85dB for the stimulus frequencies of 1kHz and 2kHz. For this analysis, responses were anchored using the CM responses to the 80dB stimulus. As assessed through boxplot analysis, no outliers were detected. All data sets were normally distributed as confirmed visually through inspection of Q-Q plots and numerically through the Shapiro-Wilk test of normality (p > 0.05).

As presented in Table 5.6 and Table 5.7 participants' CM responses showed a statistically significant increase of 13.2dB, 95% CI [6.9, 19.5], $t(5) = 5.4$, p <0.05, $d = 2.2$ when exposed to a stimulus level of 85dB ($M = 5.8$, $SD = 1.9$) as opposed to stimulus level of 75dB ($M = -7.4$, $SD = 7.1$) in the case of stimulus frequency of 1kHz. Similarly, for 2kHz stimulus the CM responses of participants also indicated a statistically significant increase of 8.4dB, 95% CI [5.8, 11.1], $t(5) = 8.1$, p <0.05, $d = 3.3$ when exposed to a stimulus level of 85dB ($M = 3.7$, $SD = 2.3$) versus stimulus level of 75dB ($M = -4.7$, $SD = 2.2$).

Table 5.6 Estimated marginal means for input-output experiment

Paired Samples Statistics

		Mean	N	Std. Deviation	Std. Error Mean
Pair 1	Output_85dB_1kHz	5.7850	6	1.90270	.77677
	Output_75dB_1kHz	-7.4217	6	7.08480	2.89236
Pair 2	Output_85dB_2kHz	3.7167	6	2.28597	.93324
	Output_75dB_2kHz	-4.7350	6	2.19154	.89469

Table 5.7 Statistical results for input-output experiment

Paired Samples Test

		Paired Differences					t	df	Sig. (2-tailed)
		Mean	Std. Deviation	Std. Error Mean	95% Confidence Interval of the Difference Lower	Upper			
Pair 1	Output_85dB_1kHz - Output_75dB_1kHz	13.20667	6.03679	2.46451	6.87144	19.54189	5.359	5	.003
Pair 2	Output_85dB_2kHz - Output_75dB_2kHz	8.45167	2.54678	1.03972	5.77898	11.12435	8.129	5	.000

It can be concluded that for both stimulus frequencies: 1kHz and 2kHz there was a statistically significant increase ($p < 0.05$) of the CM responses to the 85dB stimulus as opposed to the 75dB stimulus.

5.3.5. Discussion

The repeatability experiment data presented in Figure 5.11 and Figure 5.12 shows that the amplitude of the evoked CM varies by as much as 12dB in between the tested group of individuals if recorded at the same stimulus level. For the probe tone of 1kHz, that variation is slightly bigger than for 2kHz. At the same time, the difference is not consistent for both of the probe tones. As an example, if we compare subject 1 and subject 2, the amplitude of 1kHz evoked CM is bigger for subject 1, however, the amplitude of the 2kHz evoked CM is bigger for subject 2. The suggested aetiology of that observation is geometrical differences in skulls, namely the bony structures surrounding the inner ear that undoubtedly will be non-identical in different subjects. This will lead to the electrical potential propagating to the tiptrode in a slightly different manner. Interestingly, when we compare the CM levels presented in Figure 5.11 and Figure 5.12, and I/O functions from Figure 5.13 for subjects 2 and 3, a similarity can be noticed that could stem from the fact that subjects 2 and 3 are monozygotic twins. That could be a further indicator that the recorded CM potential could be influenced by the skull geometry.

The aforementioned inability to record pure-tone evoked CM in two of the participants was further investigated in a series of additional studies, where, on separate occasions, the attempt was made to re-run the test. Consistently, the pure-tone evoked CM was undetectable in all of the follow-up tests in the same subjects, even when using the highly sensitive wick electrode. The confidence in the validity of those results can be further reinforced by another observation that was made - in subjects where CM was present during this measurement, the potential could be recorded in every single test thereafter, which virtually rules out the possibility that the inability to detect the CM was random. However, there is no clear explanation as to why the pure-tone evoked CM was not present in the recordings as the subjects in question did not show any signs of hearing impairment that could explain the absence of cochlear microphonic.

5.4. Experiment 3: Two-tone suppression in cochlear microphonic

5.4.1. Introduction

The final experiment was designed to evaluate how the two-tone suppression (2TS) is going to show up in the measurements of cochlear microphonic potentials in normal-hearing humans using non-invasive measurement methods. Two-tone interactions within the cochlea have the potential to carry information about local activity of the inner ear, and while they have been studied in animals like gerbils (He *et al.*, 2012) or chinchillas (Charaziak, Shera and Siegel, 2017b), there was little research targeted specifically towards human cochlea. In Experiment 3, the aforementioned non-linear interactions are being tested and evaluated.

5.4.2. Methods

The experiment is yet again focused on two main probe frequencies: 1kHz and 2kHz. The probe tones used throughout the study are constructed in the same way, as was described in Experiment 1 with the rise-decay windowing applied. However, this time, a second tone burst in added to the stimulus, namely the suppressing tone. The suppressor's onset is delayed by 3ms in relation to the probe tone, and its exact windowing operation is further explained in Figure 5.17.

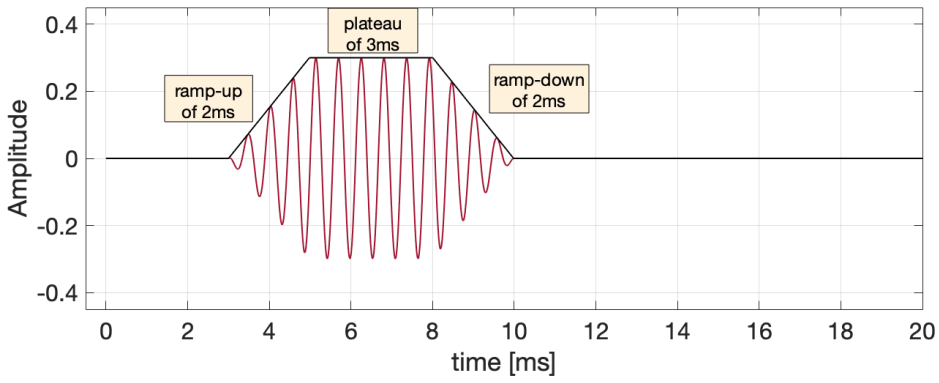

Figure 5.17: Windowing of the 2kHz suppressor tone showing the 2ms ramp-up, 3ms plateau and another 2ms ramp down.

The construction of the entire stimulus is illustrated in Figure 5.18, based on an example of a probe tone of 1000Hz and a suppressor of 1200Hz.

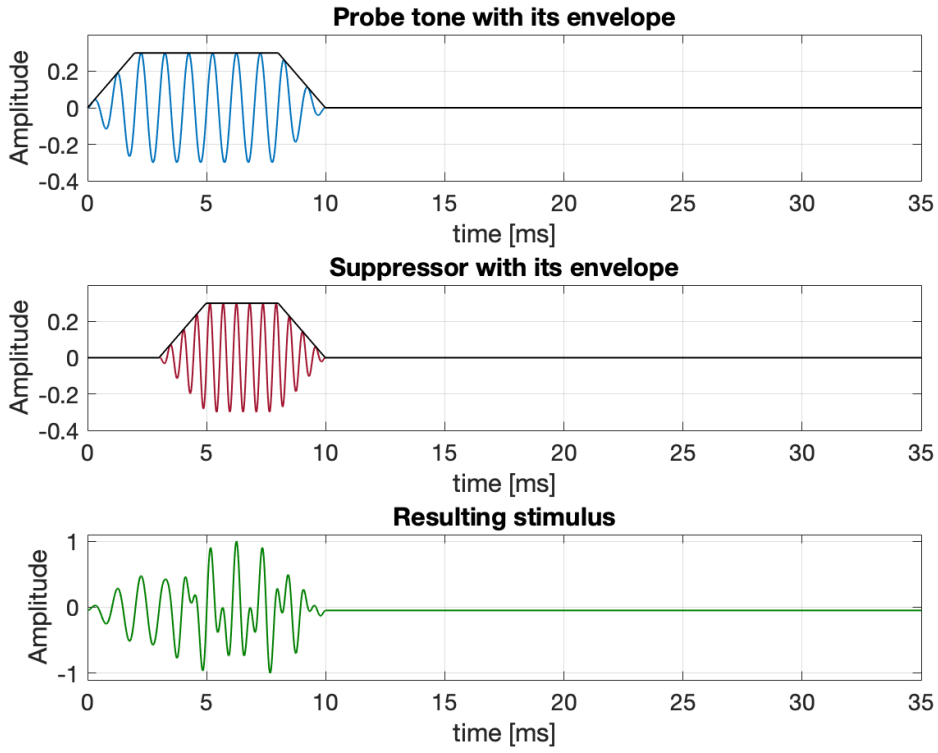

Figure 5.18: Generation of the probe tone with the suppressing tone. The graph depicts a 1kHz probe tone and a 1.2kHz suppressing tone, with their relevant windowing applied, and the resulting stimulus that is a sum of the probe and suppressor tones.

The probe tones were kept at 80dBHL during the entire study. The frequencies selected for the suppressing tones were: 1200Hz, 1800Hz, 2400Hz, 4000Hz, 4800Hz and 9600Hz. For the probe tone of 1kHz, they were presented at 5 different intensities: 62dBHL, 68dBHL,

74dBHL, 80dBHL and 86dBHL. For the probe tone of 2kHz, they were presented only at the three highest levels: 74dBHL, 80dBHL and 86dBHL, as the preliminary studies showed no evidence of suppression for lower levels at that probe tone frequency.

Every couple of test runs the amplitude of the probe tone without the presence of the suppressor was collected, together with the negative control measurement for the purpose of further validation of the results.

All of the recordings were collected from each participant during a single session. The entire procedure took around 90 minutes, during which, on average, 100 recordings were obtained from every participant.

The earphones used for measurement were checked before the experiment to exclude the possibility of distortion being introduced upon presenting the two-tone stimulus by the transducer itself and no evidence of such non-linear behaviour was found.

5.4.3. Results

The results were obtained by tracking the changes in the amplitude of the recorded cochlear microphonic using FFT analysis. There are three key components that are presented on the graph depicting obtained results:

- the CM amplitude obtained for a probe tone without the presence of the suppressing tone – recorded multiple times throughout the session, informs on what is the CM amplitude for tone burst at the probe frequency and is the baseline,
- the CM amplitude obtained for a probe tone with the presence of the suppressing tone – obtained twice for each suppressor frequency and each suppressor level,
- the negative control test – also recorded multiple times during the session, shows the noise floor in the measurement with the clamped tubing (noise floor).

For illustration purposes, an example of a time domain signal from the obtained CM measurement is presented in Figure 5.19. The suppression mechanism can clearly be seen in between the 8ms and 15ms mark, where the amplitude of the CM drops from a peak value of around 0.6μV to 0.3μV.

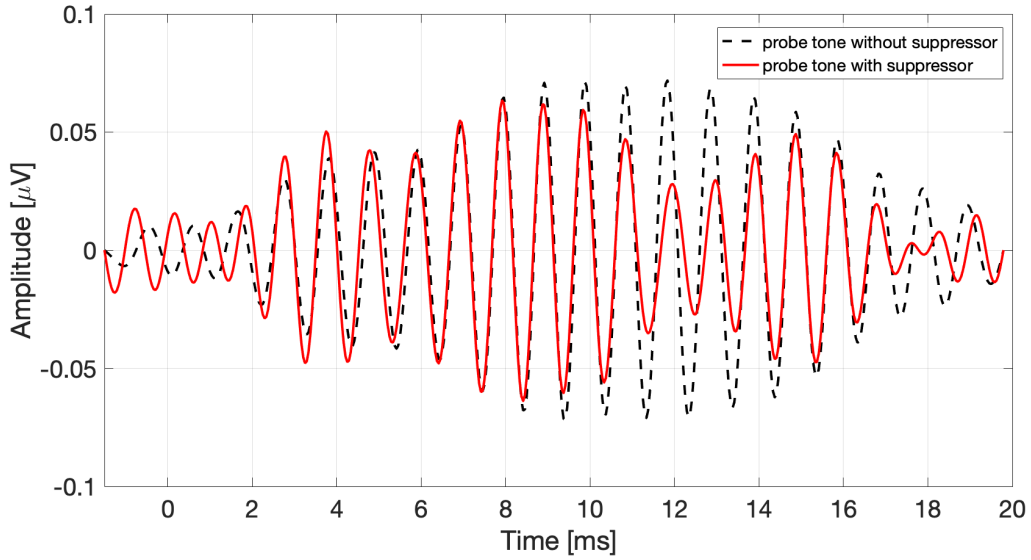

Figure 5.19: Time domain recording of the CM response at 1kHz with and without the 4kHz suppressing tone 4kHz. When the suppressor is introduced, a drop in the amplitude of the probe tone induced CM can be observed. The signal is filtered with a high-Q bandpass filter with a centre frequency f_0 = 1kHz to extract the response at the probe frequency from the noise for illustration purpose

A further FFT analysis allows extracting the exact amplitude of the CM at the probe tone for every probe + suppressor combination. An example of the frequency domain analysis is shown in Figure 5.20

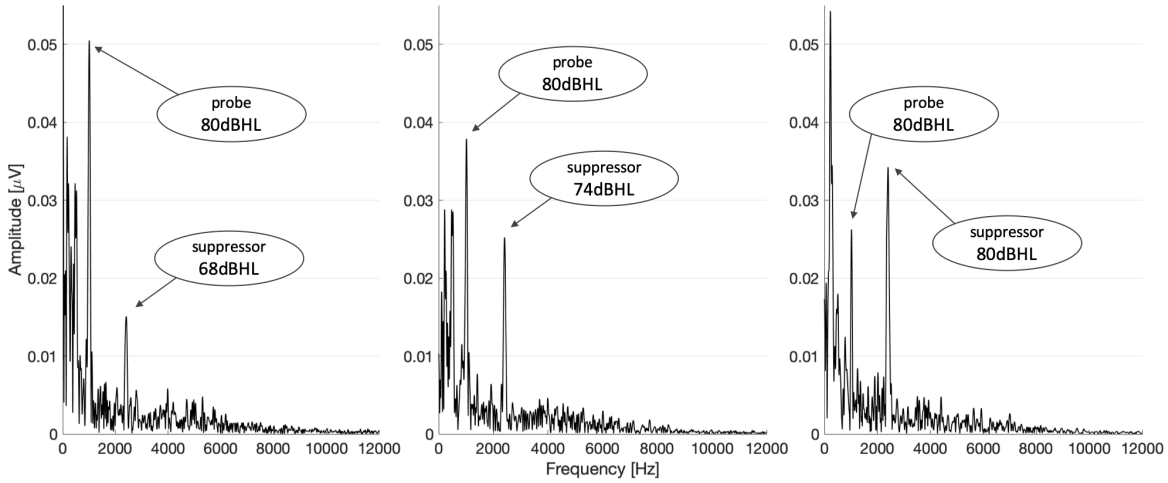

Figure 5.20 The effect of the 2.4kHz suppressing tone on the CM at the probe tone of 1kHz. The three graphs show the FFT analysis of the impact the suppressor's loudness has on the amplitude of the probe tone

All measurements from each subject were evaluated in the same way as demonstrated in the example for every probe-tone + suppressor combination. The collective responses from a single subject for all of the suppressor frequencies and levels are presented, as an example, in Figure 5.21.

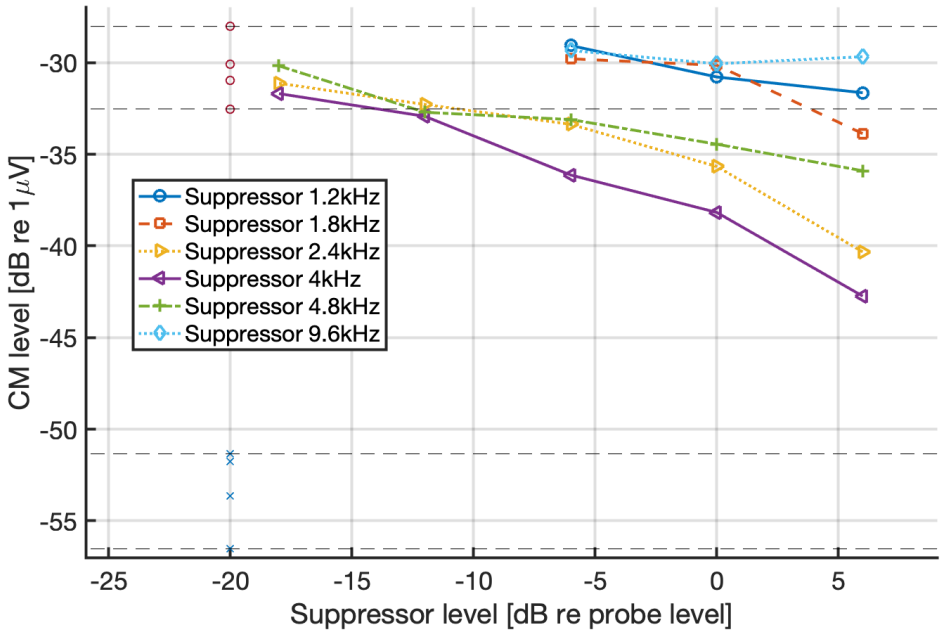

Figure 5.21: Influence of the suppressor tone frequency and level on the amplitude of the CM at the probe tone of 1kHz. Marked in between the bottom dash lines are the negative control run result, and in between the top dash lines are the amplitudes of the CM at the probe tone frequency without any suppressor present. The graph shows an apparent CM suppression, especially in the presence of 2.4 and 4kHz suppressing tones by (on average) 10dB and a slightly smaller suppression for 4.8kHz and 1.8kHz suppressing tone, at around 3dB. The 1.2kHz and 9.6kHz suppressors appear to have little to no impact on the probe tone

Based on the presented data, a clear suppression pattern can be seen for some of the suppressors. To better illustrate the effect of each frequency and level of the suppressor on the cochlear microphonic at 1kHz probe tone, a graph comparing the amount of achieved suppression in decibels at each stimulus level is presented in Figure 5.22.

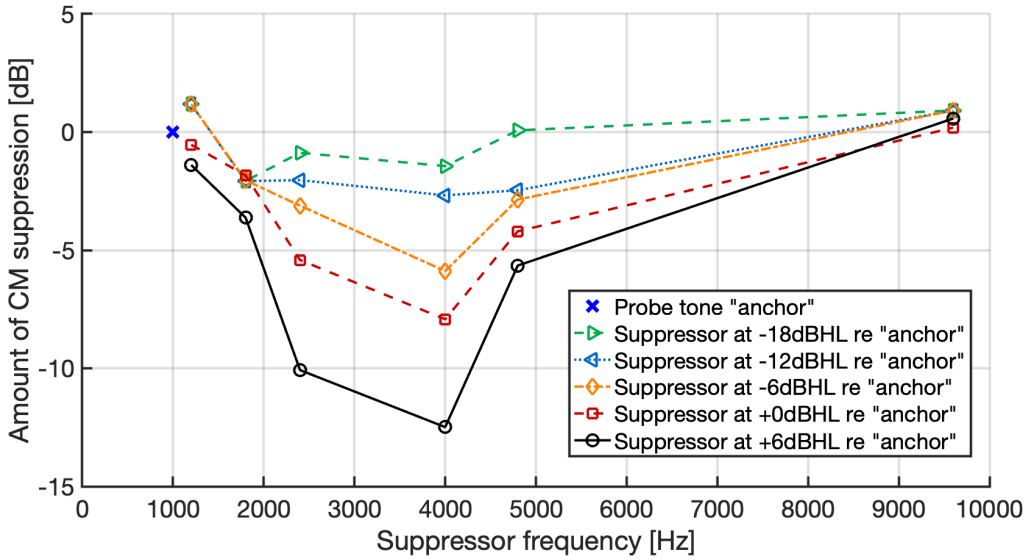

Figure 5.22: The amount of suppression achieved at each suppressing tone level as a function of frequency for a single subject. A clear correlation between the suppressor level and the amount of achieved suppression can be seen. The biggest CM attenuation is visible for 2.4kHz and 4kHz suppressing tones

A distinct correlation between the suppressor level and the recorded CM at the probe tone frequency can be observed from the presented data. In the given example, two of the suppressor frequencies: 2.4kHz and 4kHz, appear to have the largest impact on the CM at the probe tone, with suppression reaching -10dB and -12.5dB, respectively. For suppressors at 1.8kHz and 4.8kHz, the drop in recorded CM amplitude was less significant at -3.5dB and -5.5dB, respectively, while for 1.2kHz and 9.6kHz, no significant impact can be noted. A full statistical analysis of the collected data is described in the following section.

5.4.4. Statistical analysis of the results

For statistical analysis of Experiment 3, a one-way repeated measures analysis of variance (ANOVA) has been selected to assess if the suppressor signal at different frequencies has a statistically significant impact on the amount of suppression. The full statistical analysis was limited to the 1kHz probe tone with the suppressor at the highest intensity (+86dBHL) as a representative case since a more extensive set of measurements was collected for the 1kHz probe compared to the 2kHz.

One-way repeated measures ANOVA is suitable for statistical analysis of one dependent variable (here: suppression level) measured on a continuous scale with one underlying independent variable also referred to as ‘within-subject factor’ (here: the suppressor signal at different frequencies) using three or more different conditions (here: 1.2kHz, 1.8kHz, 2.4kHz, 4.0kHz, 4.8kHz and 9.6kHz) tested on the same group of participants.

Table 5.8 Statistical tests overview for 2TS experiment

Statistical test method:	one-way repeated measures ANOVA
Assumptions:	checking for outliers using boxplot, confirming normality using Shapiro-Wilk test of normality and Normal Q-Q plot, testing sphericity using Mauchly's test of sphericity
Dependent variable:	Recorded suppression levels
Cases:	Participants 1-7
Independent variable:	Suppressor signal at different frequencies
Conditions:	1.2kHz, 1.8kHz, 2.4kHz, 4.0kHz, 4.8kHz and 9.6kHz

There are specific requirements data must satisfy before a one-way repeated measures ANOVA can be performed. This includes outlier detection using boxplot, checking for normality with the help of numerical methods like the Shapiro-Wilk test of normality, a visual inspection method such as a Normal Quantile-Quantile plot (or both if the sample size is small) and, finally, sphericity test using Mauchly's test of sphericity.

A boxplot was obtained from SPSS to detect potential outliers in the data.

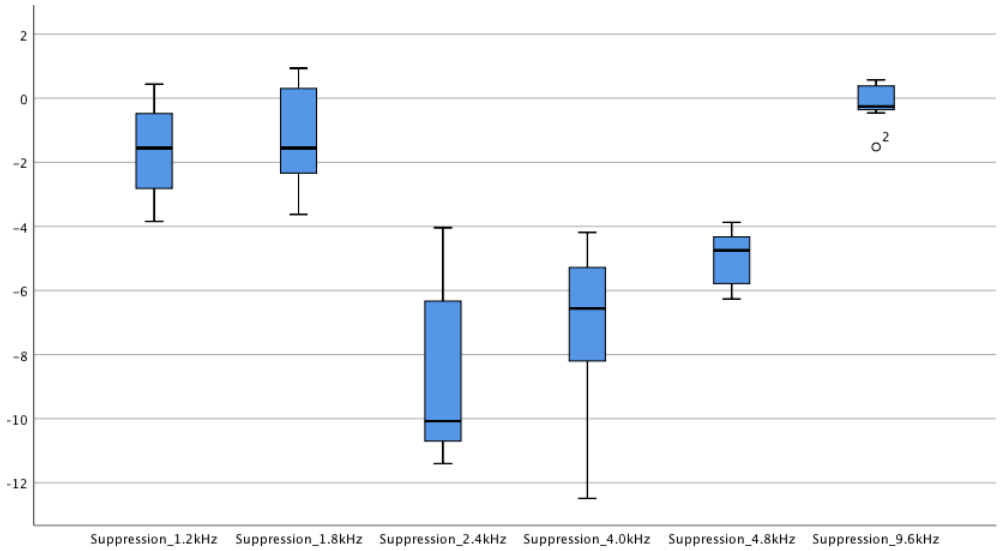

Figure 5.23 Boxplot with 2TS experiment data for all suppressor frequencies. The y-axis of the plot shows the probe-tone evoked CM level decrease in decibels when presented together with a suppressing tone at +6dB relative to the probe tone level

The boxplot in Figure 5.23 indicates a presence of one outlier for participant 2 for the suppressor frequency of 9.6kHz. No additional outliers were detected for remaining suppressor frequencies or participants. To ensure that the outlier point is genuine and that no errors were made leading up to the processing of the data, all steps were revised to identify possible errors such as mistakes made during data entry, but after careful revision, all of the data was deemed valid.

There are several approaches to deal with outliers. They include:

- keeping the outlier point and continue with the further analysis regardless,
- removing the whole data set of the participant related to this outlier,
- manipulate the data point according to ANOVA requirements if it is expected that the outlier would materially affect the results.

The removal of data sets is a possibility that should only be exercised if all of the other options are exhausted, as discarding the outlier can skew the statistical results.

It is possible to conduct ANOVA with the outlier if it is not expected to cause major uncertainties. Alternatively, the outlier can be replaced with another value, such as the closest data point to the outlier that would be still within the $1.5\ x\ IQR$ or run a Friedman test (Friedman, 1937). The Friedman test is a non-parametric alternative to the repeated measures ANOVA and, as such, has fundamental implications on the study design. For this case, a decision was made to keep the data point, and to proceed with the verification of normal distribution since the outlier was only present in one condition and is thus not expected to cause major uncertainties.

Due to the small sample size (N=7), normality has been evaluated using both a visual inspection of the normal Q-Q plots and a numerical check through the Shapiro-Wilk test of normality. Close attention has been paid to the inspection of the data set referring to condition 6 (responses to suppressor at a frequency of 9.6kHz), which contains the outlier data point as detected in the boxplot in Figure 5.23. The normal Q-Q plots show that for all six conditions, the data points appear to be located near the diagonal line indicating normal distribution shown in Figure 5.24, however, a Shapiro-Wilk test of normality has been conducted to provide additional confidence to validate this assumption.

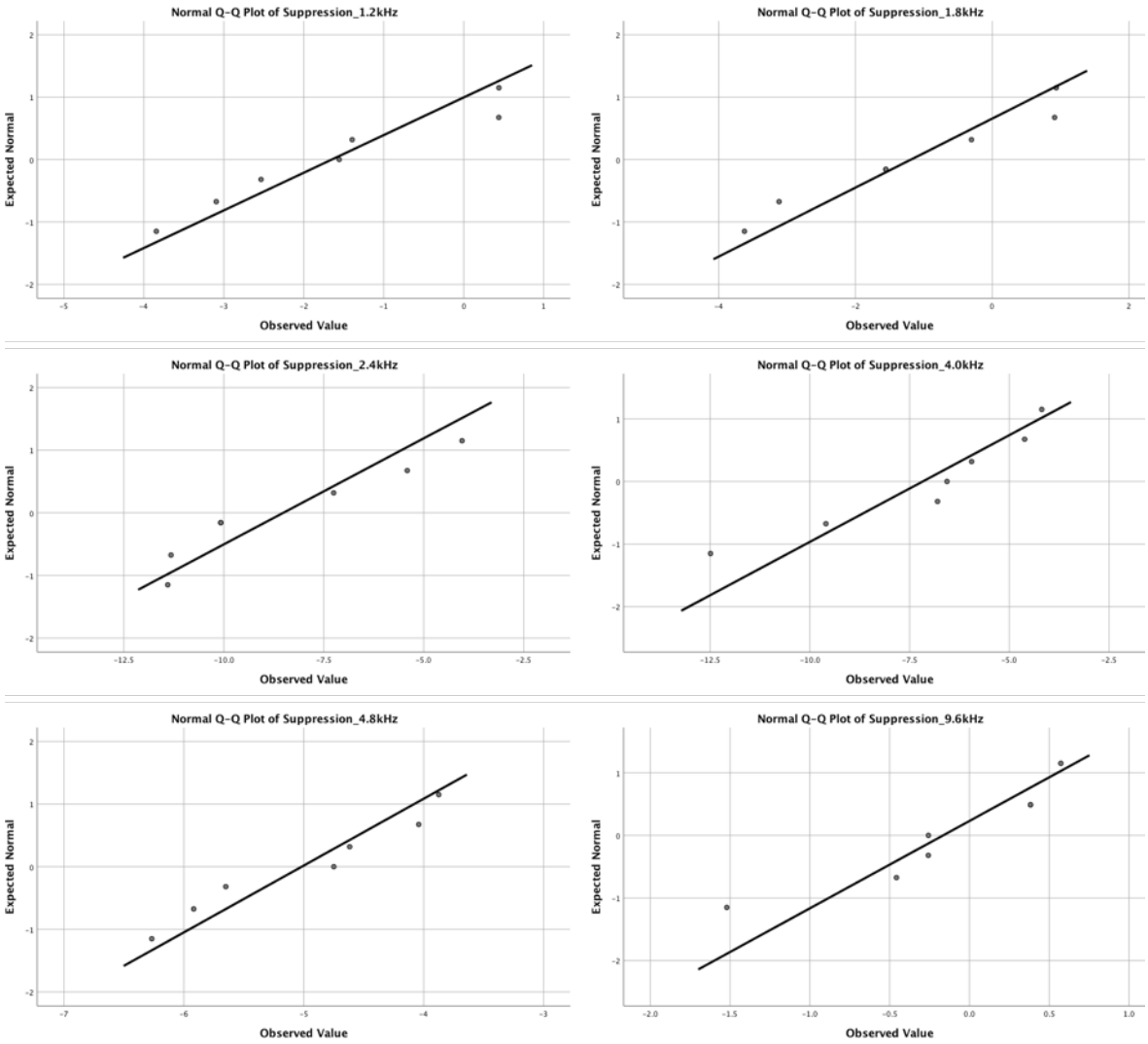

Figure 5.24 Normal Q-Q plot for all suppressor frequencies: 1.2kHz, 1.8kHz, 2.4kHz, 4kHz, 4.8kHz and 9.6kHz. All data points appear to be located in close proximity to the diagonal line including the identified outlier

The numerical results for the Shapiro-Wilk test of normality are listed in Table 5.9 for all of the different conditions. The normal distribution can be implied if the significance is higher than 0.05 ($p > 0.05$) for each of the six conditions. In this case, all of the significance values are well above the threshold, therefore, the normality is proven numerically.

Table 5.9 Numerical results for Shapiro-Wilk test of normality for 2TS experiment data

Tests of Normality

	Kolmogorov-Smirnov[a]			Shapiro-Wilk		
	Statistic	df	Sig.	Statistic	df	Sig.
Suppression_1.2kHz	.182	7	.200*	.923	7	.493
Suppression_1.8kHz	.163	7	.200*	.915	7	.434
Suppression_2.4kHz	.273	7	.123	.877	7	.215
Suppression_4.0kHz	.265	7	.148	.897	7	.312
Suppression_4.8kHz	.184	7	.200*	.924	7	.501
Suppression_9.6kHz	.206	7	.200*	.882	7	.235

*. This is a lower bound of the true significance.

a. Lilliefors Significance Correction

Lastly, the sphericity evaluation is tested before proceeding to the statistical analysis. A routine method is Mauchly's test of sphericity, which allows for testing of the hypothesis whether the differences between the conditions of the within-subject factor have equal variances. If Mauchly's test is not statistically significant ($p > 0.05$), the assumption of sphericity is met. On the other hand, if the test indicates statistical significance ($p < 0.05$), the assumption of sphericity is violated, implying that there are significant variances of the differences between the conditions. In case that sphericity is violated, an adjustment has to be applied to the degrees of freedom using estimates for the sphericity, like the Greenhouse-Geisser (Greenhouse and Geisser, 1959), Huynh-Feldt (Huynh and Feldt, 1976) and the lower-bound estimates.

Table 5.10 Results of Mauchly's test of sphericity for 2TS experiment data

Mauchly's Test of Sphericity[a]

Measure: suppression

Within Subjects Effect	Mauchly's W	Approx. Chi-Square	df	Sig.	Epsilon[b]		
					Greenhouse-Geisser	Huynh-Feldt	Lower-bound
suppressor	.003	23.494	14	.087	.409	.622	.200

Tests the null hypothesis that the error covariance matrix of the orthonormalized transformed dependent variables is proportional to an identity matrix.

a. Design: Intercept
Within Subjects Design: suppressor

b. May be used to adjust the degrees of freedom for the averaged tests of significance. Corrected tests are displayed in the Tests of Within-Subjects Effects table.

For the data of Experiment 3, the result of Mauchly's test of sphericity shown in Table 5.10 was not statistically significant ($p > 0.05$), meaning that the assumption for sphericity had not been violated ($\chi^2(2) = 23.494$, $p = 0.087$). Hence, no adjustment was necessary for further analysis. With the sphericity confirmed, all conditions all assumptions to carry out the repeated measures ANOVA have been fulfilled.

The results of the one-way repeated measures ANOVA are shown in Table 5.11 and Table 5.12.

Table 5.11 Estimated marginal means of suppression

Estimates

Measure: suppression

suppressor	Mean	Std. Error	95% Confidence Interval	
			Lower Bound	Upper Bound
1.2kHz	-1.650	.627	-3.183	-.117
1.8kHz	-1.187	.683	-2.860	.485
2.4kHz	-8.512	1.116	-11.243	-5.781
4.0kHz	-7.172	1.108	-9.884	-4.460
4.8kHz	-5.017	.354	-5.883	-4.151
9.6kHz	-.165	.271	-.828	.498

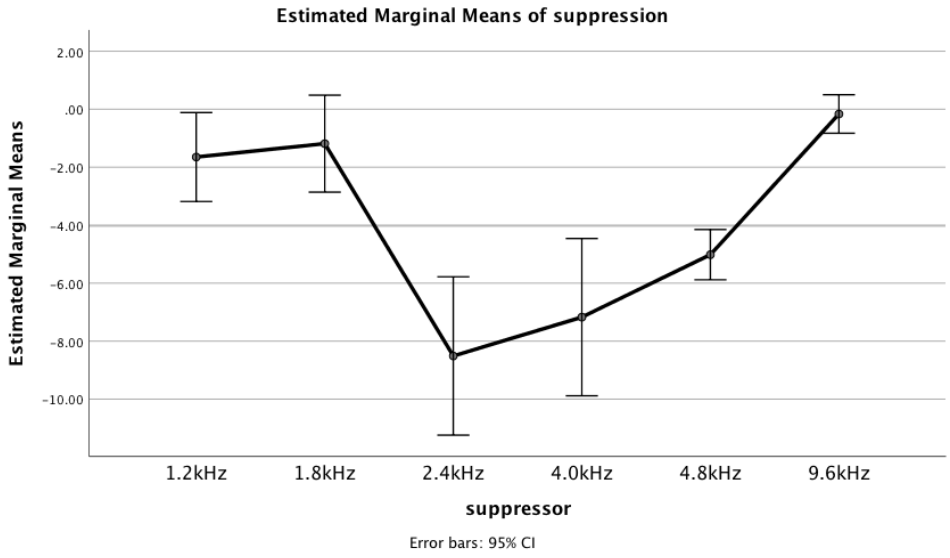

Figure 5.25 Graphical representation of the estimated marginal means of suppression

Table 5.12 Statistical results for 2TS experiment

Tests of Within-Subjects Effects

Measure: suppression

Source		Type III Sum of Squares	df	Mean Square	F	Sig.	Partial Eta Squared
suppressor	Sphericity Assumed	417.052	5	83.410	20.976	.000	.778
	Greenhouse-Geisser	417.052	2.043	204.141	20.976	.000	.778
	Huynh-Feldt	417.052	3.109	134.162	20.976	.000	.778
	Lower-bound	417.052	1.000	417.052	20.976	.004	.778
Error(suppressor)	Sphericity Assumed	119.291	30	3.976			
	Greenhouse-Geisser	119.291	12.258	9.732			
	Huynh-Feldt	119.291	18.651	6.396			
	Lower-bound	119.291	6.000	19.882			

The analysis revealed that there were statistically significant differences in suppression levels for different suppressor frequencies, $F(5, 30) = 20.976, p < 0.05, partial\ \eta^2 = 0.778$ with participants' responses varying from (*M* = -1.7, *SD* = 0.6) for suppressor of 1.2kHz, over (*M* = -1.2, *SD* = 0.7) for suppressor of 1.8kHz, over (*M* = -8.5, *SD* = 1.1) for suppressor of 2.4kHz, over (*M* = -7.2, *SD* = 1.1) for suppressor frequency of 4.0kHz, over (*M* = -5.0, *SD* = 0.4) for suppressor of 4.8kHz to (*M* = -0.2, *SD* = 0.3) for suppressor of 9.6kHz.

In summary, it was demonstrated that there were statistically significant differences in suppression levels in between different suppressor frequencies. The suppressing tones of 2.4kHz, 4kHz and 4.8kHz were effective at lowering the amplitude of the CM evoked by the 1kHz probe tone, while the 1.2kHz, 1.8kHz and 9.6kHz suppressing tones did not have a noticeable impact.

5.4.5. Additional analysis – CM in males vs. females

During visual inspection of the suppression graphs collected from each of the participants an observation was made that, when the data were analysed according to the sex of the subjects, two distinct suppression patterns could be observed. The results were therefore split into two categories and shown separately to investigate the correlation. The possible explanation of this phenomenon will be discussed in the following section.

Figure 5.26 depicts the suppression pattern depending on the suppressor frequencies presented at 86dBHL (meaning +6dB in relation to the probe tone) separated into two categories according to the participant's sex. The results continue to be displayed as the "anchored" values. The 0dB value on the y-axis of the plots indicates the normalised level of the CM response evoked by 80dBHL probe tone without the suppressor present. Therefore, any negative dB values on the y-axis mean suppression of the CM at the probe tone, while any positive dB values would indicate enhancement of the response.

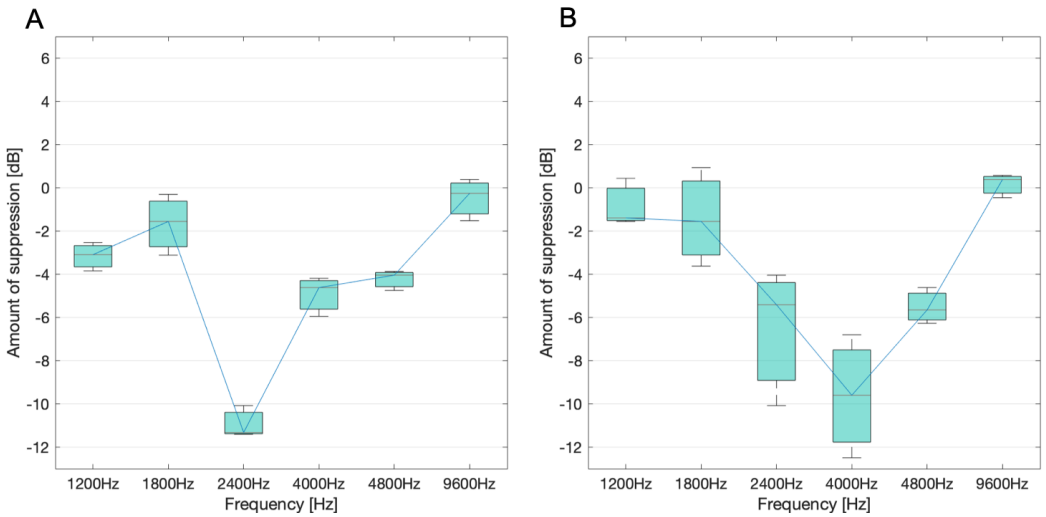

Figure 5.26: Suppression patterns for 1kHz probe tone and suppressor level of 86dBHL presented on two separate graphs; A – (sample size N=3) females, where the biggest amount of suppression can be observed for the suppressor frequency of 2.4kHz, and B – (sample size N=4) males, where the biggest amount of suppression can be observed for the suppressor frequency of 4kHz

While the interquartile ranges of the boxplots are indicating quite significant differences between participants, especially for males, there is still a visible trend showing that for females, the suppressor at 2.4kHz has the biggest impact on the CM recorded at the probe tone, around 11dB drop, while for the males that suppressor frequency is 4kHz at around 10dB drop. The data depicting median values for all suppressor levels (62dBHL, 68dBHL, 74dBHL, 80dBHL and 86dBHL) and frequencies are presented in Figure 5.27.

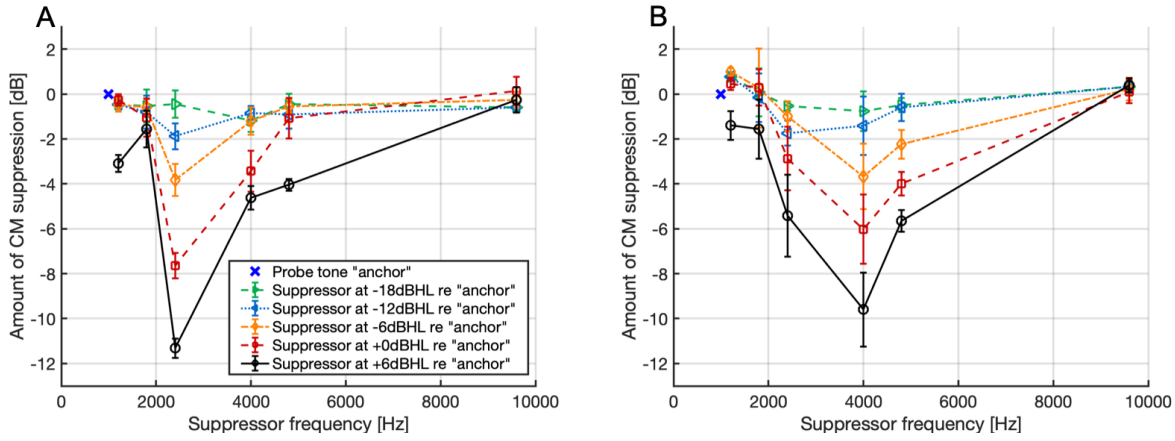

Figure 5.27: Suppression patterns at 1kHz probe tone for suppressor levels of 62dBHL, 68dBHL, 74dBHL, 80dBHL and 86dBHL divided by sex; A – 3 females, where the largest amount of suppression is noted for the 2.4kHz, and B – 4 males, where the largest amount of suppression is observed for the 4kHz. In both groups, the amount of suppression present clearly depends on the level of the suppressing tone

Similarly, the same set of measurements was repeated for the 2kHz probe tone. The suppressor levels were limited to 74dBHL, 80dBHL and 86dBHL as preliminary tests showed that for lower-level suppressors, there was no significant impact on the probe tone. All measurements were evaluated in the same way as demonstrated in the example for 1kHz probe tone. Collective results for probe tone of 2kHz and highest suppressor level at 86dBHL are illustrated in Figure 5.28.

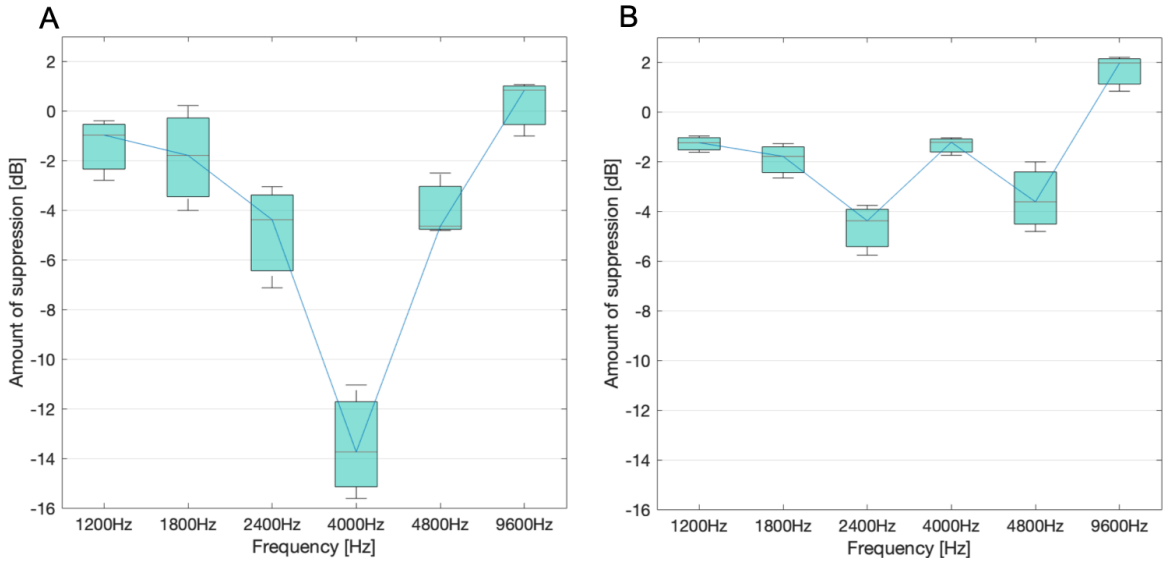

Figure 5.28: Suppression patterns for 2kHz probe tone and suppressor level of 86dBHL presented on two separate graphs divided by gender; A – (sample size N=3) females, where the largest amount of suppression can be observed for the suppressor frequency of 4kHz, and B – (sample size N=4) males, where a relatively small amount of suppression can be noted for the suppressor frequencies of 2.4kHz and 4.8kHz

The interquartile ranges of the boxplots are a lot more narrow than those obtained for 1kHz probe tone. For females, the amount of suppression at 4kHz is quite significant at around 14dB, while for the males, none of the suppressor frequencies affect the probe tone in a significant way, with around 4dB drop at 2.4kHz and 4.8kHz.

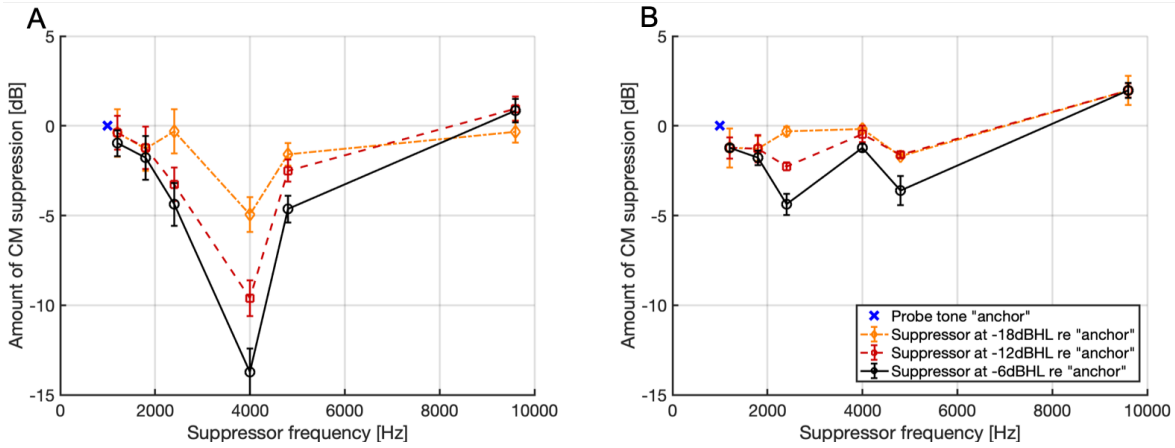

Figure 5.29: Suppression patterns at 2kHz probe tone for suppressor levels of 74dBHL, 80dBHL and 86dBHL divided by gender; A – 3 females, where the biggest amount of suppression is noted for the 4kHz, and B – 4 males, where a small amount of suppression is observed for the 2.4kHz and 4.8kHz.

The suppression patterns for the probe tone of 2kHz are noticeably different from each other. The measurements obtained from male participants show hardly any suppression characteristic. On the contrary, a well-defined drop in CM amplitude is visible at 4kHz in results obtained from female participants.

The full statistical analysis of the between-gender differences was omitted because of the extremely limited sample size: N=3 for female participants and N=4 for male participants. With data sets containing very few samples, the analyses carry low statistical power, therefore, a visual inspection of the boxplots is an appropriate method to aid in deciding on whether a given research question should be explored further but it cannot provide a definitive answer whether the correlation is statistically significant.

5.4.6. Discussion

The data collected from the study participants allowed us to observe the two-tone interactions present in normal hearing subjects and recoded with non-invasive methods. The probe tone evoked cochlear microphonic amplitude was affected by the presence of the suppressing tone in every participant that took part in this experiment. The suppressor frequencies that appeared to have the most significant influence on the 1kHz evoked CM were 2.4kHz and 4kHz. The results obtained for the 2kHz probe tone were not as conclusive.

A certainly interesting aspect are the presumed differences between the CM recorded male and female participants, so it is worth considering what could be the possible origin of those variations.

In the recently published study (Potrusil *et al.*, 2020) a finite element analysis and reconstruction of the tonotopical organisation of the cochlea was evaluated in 3-dimensional space. A micro-CT imaging was used to obtain an accurate representation of the cochlea and couple the 3D scan with the exact locations of 30 nerve fibre bundles and their corresponding excitation frequencies. As a result, they derived a table showing the location of the best place for selected 30 frequencies in a three-dimensional space and expressed those locations as an angle measured from the round window. The graph in Figure 5.30 is based on the data presented in the abovementioned study.

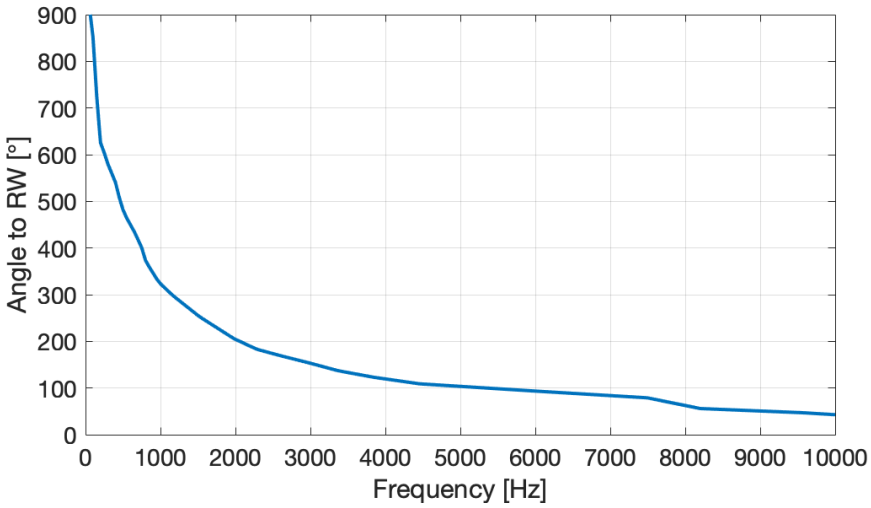

Figure 5.30: Distribution of the frequencies along the cochlea spiral as a function of their angle in relation to the round window

Since the function was not specified for the exact frequencies that were used in this two-tone suppression experiment, the values were obtained using linear interpolation and a look-up table for selected frequencies and their corresponding angles is presented in Table 5.13.

Table 5.13: Frequencies used in 2TS experiment and their corresponding angles in relation to the RW

Frequency [Hz]	Angle to RW [°]
1000	***323***
1200	294
1800	224
2000	***204***
2400	178
4000	120
4800	106
9600	47

According to the study on centiles for adult head size (D Bushby *et al.*, 1992), males tend to have their head circumference on average bigger by 1.38cm than females of the same height. The difference between genders applied as well to the length of the cochlea that in males averaged at 37.1mm compared to females at 32.3mm (Sato, Sando and Takahashi, 1991). Based on that information, it can be assumed, that this frequency distribution is going to be different, both because of the average height and head size variation between females and males. Therefore, it is not unreasonable to assume as well that the tonotopic organisation of the cochlea is going to differ in those two groups.

If we consider the two of the most efficient suppressors: 2.4kHz and 4kHz, and their placement in relation to the probe tone of 1kHz, using Table 5.13, we can observe that they are the closest to the 180° shift from the 1kHz place. That placement schematic is drawn in Figure 5.31. Considering that spatial distribution, it is likely that the two suppressors can be responsible for causing the destructive interference to the probe tone potential when picked up by the extratympanic electrode that will record the vector sum of the potentials arising from multiple places along the cochlea. Considering that the male and female cochlear lengths vary by as much as 13%, the locations will shift slightly, and that shift might cause the differences seen in Experiment 3.

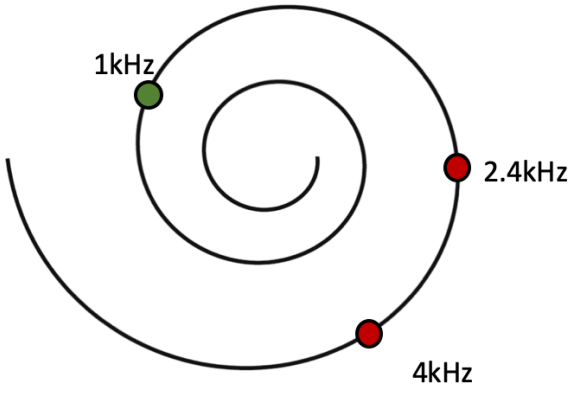

Figure 5.31: Schematic placement of the 1kHz probe tone and 2.4kHz and 4kHz suppressors and their placement along the cochlea spiral

Further evidence of how much the suppression patterns picked up by an extratympanic electrode depends on the temporal bone geometry can be seen when analysing curves obtained from the female monozygotic twins against the curves obtained from males unrelated to each other.

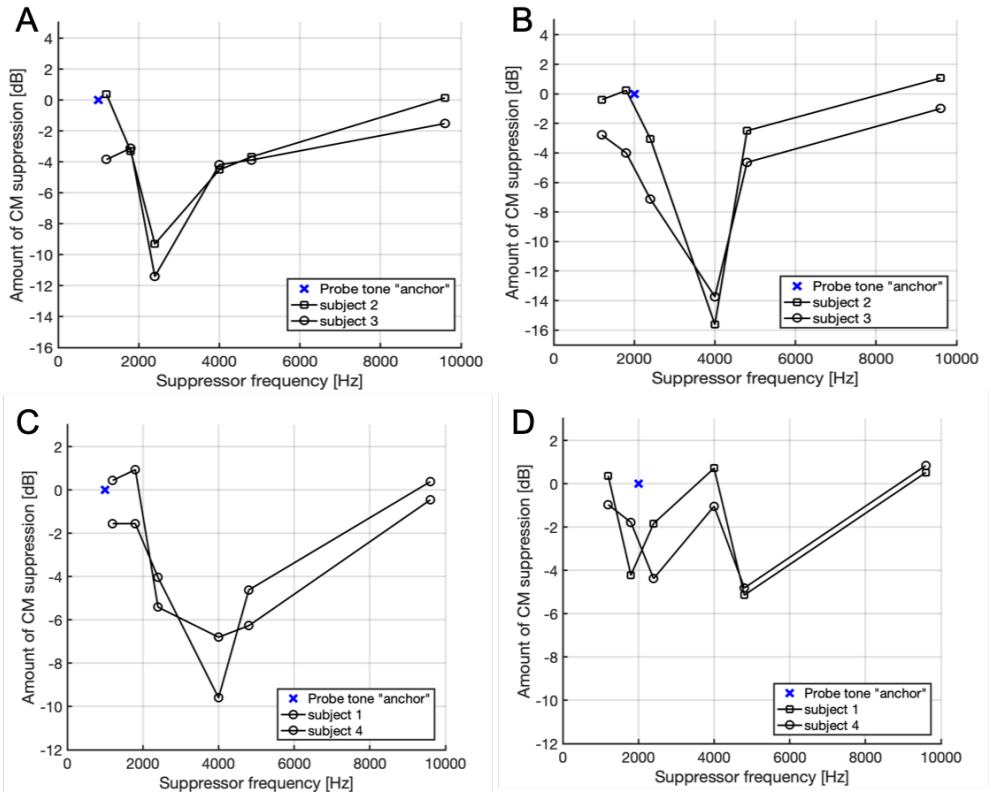

Figure 5.32: Comparison of the suppression patterns obtained for: A - female monozygotic twins for the probe tone of 1kHz, B - female monozygotic twins for the probe tone of 2kHz, C - unrelated males for the probe tone of 1kHz, D - unrelated males for the probe tone of 2kHz. The A and B graphs show similarity while the graphs C and D follow a similar general pattern but are nowhere near as correlated

The two data sets collected from the monozygotic twins appear to be closely correlated, while the data obtained from unrelated males is characterised by a much broader variation in the responses recorded for all of the probe-suppressor combinations. This finding underlines the importance of incorporating the geometry and the medium-specific lossy transmission model of the temporal bone into the models aimed at predicting remotely-recorded cochlear microphonic, as, based on the results shown in Figure 5.32, we can anticipate that the propagation of the cochlear potentials is heavily influenced by the bone and the soft tissue distribution within the skull.

6. Findings, future research and conclusions

This chapter reviews the link between the findings outlined in this thesis with the published literature, as well as discusses the outcome of the simulation work in the context of the measurements in normal-hearing patients reported in the previous chapter.

6.1. Cochlear model, measurements and literature – comparative analysis

6.1.1. Measurement results in context of published research

To compare the results of simulation and experiments detailed in chapters 4 and 5 to a previously published research, two types of data collection protocols have to be considered: the single-point, invasive measurements and the less invasive gross potential measurements recorded in the proximity of the cochlea (specifically the two-tone suppression measurements).

6.1.2.1. Single-point measurements

Single-point measurements can be considered to be the most correlated with the simulation results obtained from a cochlear model as the element under investigation is a single location along the Organ of Corti. These measurements can be a tool allowing for investigation of both types of responses:

- mechanical - where a reflective bead is placed on the basilar membrane and a laser beam emitted by an interferometer is used to track the displacement of the membrane,
- electrical – measurements where an electrode picks up potential from a single hair cell (outer or inner) that, depending on the electrode location, can be divided into two types:
  - extracellular – where the recording is collected from a place above the epithelial surface in close proximity to the hair bundle to track the potential changes in the medium surrounding the hair cell (Hudspeth, 1982);
  - intracellular - where the electrode is inserted into the body of the hair cell (Weiss, Mulroy and Altmann, 1974)

The difficulty in comparing the results obtained during the course of this research with the published literature stems from a couple of reasons:

- the *in-vivo* data is obtained from different species – understandably, the measurements obtained from a living cochlea using invasive methods will not be available for humans and, while the data from species with similar inner ear anatomy is contributing a great deal to the understanding of the hearing processes, the findings can be problematic when attempting to apply them to a model of a human cochlea as the characteristics of the cochlea as well as the surrounding tissues undoubtedly differ in between species (Fallah, Strimbu and Olson, 2021);
- a limited number of locations along the Organ of Corti can be tested – when using the invasive methods to measure displacements or receptor potentials within the OC, an overwhelming amount of data is collected only for the basal turn of the cochlea as it is the most accessible part that can be reached through the round window (Russell and Sellick, 1978; Brown *et al.*, 1983; Cooper, 1998), although measurements for more apical locations are also available ;
- invasive measurements introduce uncertainty into the results - the impact of both placement of the measurement instruments and the preparation protocols that oftentimes involve dissecting parts of the inner ear, draining the cochlear fluids, piercing the cell membranes, etc. might affect the physiology of the cochlea altering the outcome of the experiments.

The basic responses of the cochlear model were shown in chapters 2 and 3 and were in good agreement with the published data as they are well-established formulations that have been used and verified in numerous studies. The novel addition to the model was investigating how the two-tone interactions are going to show up in mechanical and electrical responses of the model. The two-tone interactions of the responses obtained from the model were discussed in chapter 4 but to reiterate the findings a short summarising discussion is included in this section.

The basilar membrane and reticular lamina responses presented in Figure 4.6 in section 4.2 showed that for both BM and RL, the suppressing effect of the saturating tone added to the probe tone stimulus was the most impactful as the f_p/f_s ratio was getting close to 1. This observation appears to be in good agreement with the responses recorded from BM in living cochleae in several studies (Rhode, 2007; Versteegh and van der Heijden, 2013), however, the modelled responses show no suppressing activity for the saturating tones of frequencies greater than $\sim 4f_p$

even for the highest suppressor levels. This is in contrast to the cited publications where the saturation of the BM motion could be seen even for high saturating tones, albeit a less prominent one.

A similar dependency was found in the hair bundle displacement described in a study evaluating the hair cells of a bullfrog's sacculus (Barral and Martin, 2012). The magnitude of the bundle motion was significantly decreased in a presence of a second tone at a nearby frequency. That impact was becoming less prominent as the frequency separation between the probe and suppressor increased. Additionally, the authors of the paper noted that the suppressing effect was significantly larger when the hair bundle was stimulated at or near its characteristic frequency, compared to a stimulation off-resonance.

Analysing data obtained from the model, similar conclusions can be drawn when we analyse the simulated hair cells. In Figure 6.1, responses from a single point at the basal location and the characteristic place for 1kHz are shown for an outer and inner hair cell. For saturating tones closest to the probe tone, the amplitude reduction is more prominent at the characteristic place. This trend reverses somewhat as the saturating tone frequency gets higher.

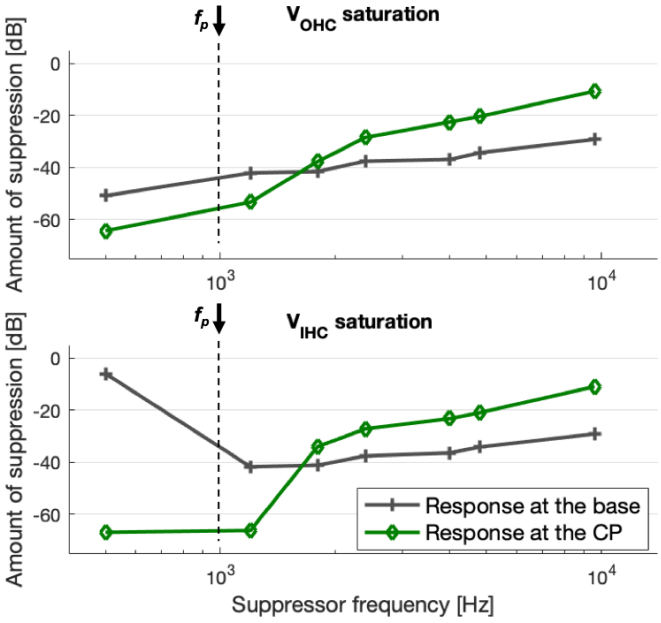

Figure 6.1: Two-tone suppression patterns in OHC and IHC responses from a basal location and a characteristic place at the probe tone frequency f_p=1kHz. The observed impact on the 1kHz evoked CM at the characteristic place shows bigger amounts of suppression for saturating tones close to the probe frequency than the suppression at the base for the same stimuli combination

Additionally, when analysing the IHC response at the base against response at the CP, a much bigger suppression can be seen at the CP than at the base for suppressor frequencies close to the probe tone. A similar observation was noted before (Cheatham and Dallos, 1982, 1992) when a notch-like suppressed response could be observed *in-vivo* in an IHC potential when the saturating tone was presented at a frequency near the probe.

All of those findings correlate well with the results presented in sections 4.2 and 4.3, where the impact of the saturating tone on the responses at the probe tone frequency was the most prominent when the two tones were closest to each other, leading to a conclusion that overall, the model can be used to obtain information about two-tone interactions at a single point along the cochlea, although some adjustment to the model parameters might be required to match the saturation characteristics measured in living cochleae

6.1.2.2. Two-tone suppression measurements

In a majority of the experiments referenced in this chapter, the cochlear microphonic potential was measured by an electrode placed in a round window niche. While this method ensures the best possible SNR in the recordings because of the close proximity of the source to the recording site, it also means that if we consider the geometrical distance ratio between electrode-to-base and electrode-to-apex, intrinsically, the contribution of the cochlear potentials arising from the hook region is going to be greater than those of the apical region. This is contrary to the experiments described in this thesis, where the difference in distance from the base and apex of the cochlea to the electrode placed in the ear canal is going to be much smaller. As a consequence, a direct comparison of the results presented in Chapter 5 to the published literature would not be entirely appropriate but is nonetheless helpful in discussing how the two-tone suppression is expected to show up in the cochlear microphonic measurements.

Contribution of different cochlear locations to round window CM

In a study where an impact of a high-pass filtered noise on cochlear microphonic responses of a gerbil was assessed the authors investigated if place-specific information about the cochlear microphonic can be extracted by saturating the OHCs in the basal part of the Organ of Corti using a high-pass filtered noise with varying cut-off frequencies (Chertoff, Earl and Diaz, 2012). The amplitude of the CM at the probe tone of 733Hz was shown to be suppressed the most (with only 20% of the unsuppressed response amplitude remaining) when the cut-off frequency

of the noise filter was the lowest. The suppressor had the biggest impact on the probe frequency f_p for cut-off frequencies lower than ~3f_p or 2.3kHz. For higher cut-off frequencies, the impact systematically decreased until little to no effect could be seen for the filtered noise that the most basal cochlear locations would respond to.

A lot of the emphasis in Chertoff's study has been on discussing the need of assigning the spiral geometry of the cochlea and modelling the conductivity of the bones and soft tissues surrounding the inner ear. In an attempt to compare a simple exponential decay of the potentials propagated along the longitudinal axis of the cochlea (with a space constant defined as 1mm) to the measured CM amplitude function, the authors showed that the two were in agreement only for a limited number of locations emphasising the need for a more complex model of the cochlear potentials' propagation in the three-dimensional space. Additionally, the authors suggested it might be beneficial to consider all of the three scalae potentials: scala media, scala vestibuli and scala tympani as sources contributing to the generation of the CM rather than using the scala media potential alone as a CM approximation.

Similarly, another study was recently published that evaluated the round window cochlear microphonic in a response to a combination of two pure tone stimuli (probe tone and saturating tone), with a single pure tone stimulus without the presence of the suppressor as a baseline (Charaziak, Siegel and Shera, 2018). A characteristic "ripples" were observed in the collected spectra obtained in response to probe tones f_p in between 0.5kHz and 16kHz. The rippling was not present when the saturating tones were added to the stimulus, with its frequencies at $f_s = f_p$ - 43Hz. Based on that observation the authors concluded that the notches seen during the frequency analysis are caused by the interference between the CM evoked at multiple locations from both basal and apical regions of the cochlea. A direct comparison to the results of this study is not possible as the investigated frequencies were starting at 5kHz and were presented at a much lower stimulus intensity where the cochlea is still operating at a linear region, whereas the experiments detailed in section 5.4 used moderate-to-high stimulus intensities. Nonetheless, the general outtake of both of the experiments appears to suggest that the responses recorded as a cochlear microphonic are a complex sum of multiple potentials generated by the elements of the Organ of Corti, rather than simply the responses arising solely from the basal locations of the cochlea.

Suppression patterns for a low-frequency round window cochlear microphonic

A research paper detailing a study that carries the most similarity to the one described in section 5.4 was a study in gerbils (He et al., 2012), where the round window cochlear microphonic evoked by a probe tone of 500Hz was recorded in a presence of the suppressing tone of multiple frequencies and intensities.

The main results of this study are re-printed in Figure 6.2 to facilitate better comparison with the data obtained from Experiment 3 detailed in section 5.4.

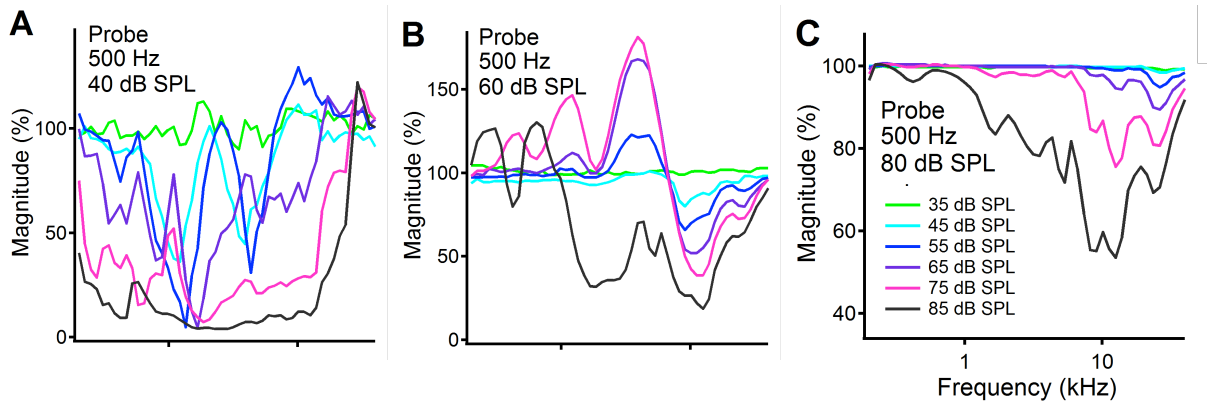

Figure 6.2: The magnitude of the RW CM as a function of suppressor frequency; from (He et al., 2012), A – probe tone at 500Hz and 40dB SPL, B - probe tone at 500Hz and 60dB SPL, C- probe tone at 500Hz and 80dB SPL, all plotted against the suppressor frequency at different suppressor levels

Figure 6.2.C shows the 500Hz probe tone at a moderate-to-high level at 80dB SPL with the saturating tones frequencies spanning between 0.2kHz and 40kHz and intensities between 35dB SPL and 85dB SPL in 10dB increments. Those measurement conditions, though not exactly the same, are the closest to the assumptions of Experiment 3, therefore, a comparison of the data obtained from both of the experiments can be made.

For the probe tone of 500Hz and 80dB SPL, as seen in Figure 6.2.C, the probe tone is mainly suppressed when the suppressor reaches frequencies around 10kHz. As a reference, the gerbil's inner ear responds to frequencies up the 60kHz (Ryan, 1976) and the total length of the cochlea averages at about 12mm. According to Greenwood's tonotopic mapping, the 500Hz probe tone is going to have its best place at ca. 10mm from the stapes (83% of the total length) and the 10kHz – at ca. 4mm (25% of the total length). The corresponding angles along the cochlear spiral relative to the round window are 748° (or 28°) for 500Hz and 200° for 10kHz, meaning that the angular shift in between those two frequencies is 172° (Hutson *et al.*, 2021).

The results from Experiment 3 were plotted in Figure 6.3 in the same way as Figure 6.2.C, showing the magnitude change of the probe-tone CM in the presence of a saturating tone.

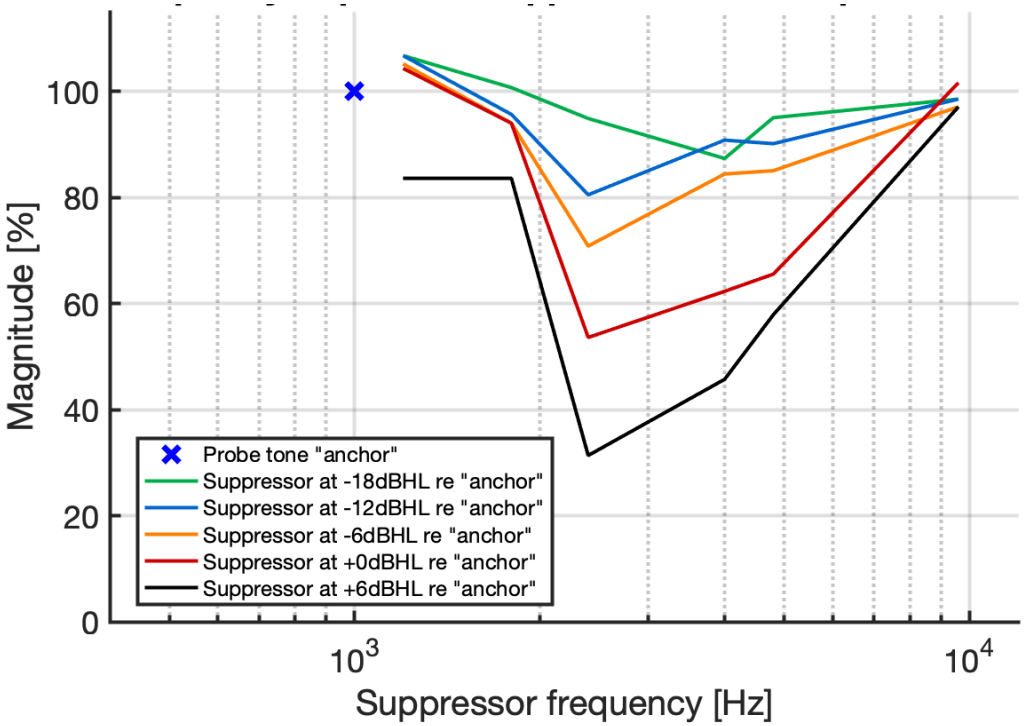

Figure 6.3: Ear canal recorded CM as a function of suppressor frequency and level

The probe tone is affected by the saturating tone mainly when it is presented at 2.4kHz and 4kHz. If we consider that the human inner ear responds to frequencies up the 20kHz and the total length of the cochlea averages at about 35mm, the 1kHz probe tone is going to have its best place at ca. 21mm from the stapes (60% of the total length), the 2.4kHz at ca.16mm (45% of the total length) and the 4kHz at 10mm (28% of the total length). The corresponding angles along the cochlear spiral relative to the round window are 323° for 1kHz, 178° for 2.4kHz and 120° for 4kHz, meaning that the angular shift in between those two pairs is 145° and 200° respectively.

He's study, much like the data obtained from experiment 3 and shown in Figure 6.3, does not show the saturation effect for the suppressor frequencies closest to the probe tone. Instead, it is primarily the suppressors with best places significantly more basal to that of the probe tone that appear to affect the amplitude of the CM at the probe tone the most. At this point, it is not clear what exactly determines the effectiveness of the suppressor and if that dependency can be described in simple terms like the angle shift between the probe and suppressor's best place (even though in both studies the angle between the two tones was close to 180°), whether it's the ratio between the f_p and f_s, or, most likely, an intricate combination of many interlocking mechanisms

and geometries of the inner ear and the surrounding tissues. Nevertheless, the general characteristics of the two tone suppression patterns obtained from the non-invasive measurements detailed in this thesis show similarities to the results obtained through more invasive methods implemented by He.

Overall, the outcomes from all of the studies detailed in the literature mentioned in this section lead to the conclusions that the broader region of the cochlea contributes to the generation of the CM and the basal location is not the primary source, as it has been speculated (Patuzzi, Yates and Johnstone, 1989), but just one of the multiple locations that all contribute to the gross potential recorded in the proximity of the round window.

6.1.2.3. Two-tone suppression in model predictions against the measured data

The initial assumption for using the cochlear model to simulate the cochlear microphonic was that the majority of the contributions to the potential come from the basal part of the cochlea. In that case, a simple vector summation of the simulated voltages across several most basal points would have been able to predict the CM response. However, the critical analysis of the model outputs showed that while the model is able to reproduce data collected from a living cochlea at a single point, it cannot be utilised to predict the gross cochlear potentials like the CM since the propagation paths are much more complicated than initially hoped for.

The model would certainly benefit from incorporating it into a three-dimensional spiral map (Li *et al.*, 2021) that would allow simulating the cancellation effects caused by the shifting phase of the potentials as the excitation reaches the more distal cochlear regions, and possibly a model of the surrounding tissues and their effect on the potentials' propagation. At the moment, the model in its simpliest form cannot successfully predict auditory evoked potentials.

6.1.2.4. Difference between CM recorded in males and females

In section 5.4.5 of Experiment 3, a possible difference in the shape of the suppression curve depending on the sex of the participants was discussed.

Although it was not in the context of the two-tone suppression measurements, a recently published study suggested this correlation as well (Coraci and Beynon, 2021). The experiment evaluated CM recordings from 24 normal-hearing participants (10 males and 14 females) evoked by clicks, broad band CE-chirp (a stimulus designed to compensate for frequency-dependent delays

in the cochlea (Pushpalatha and Konadath, 2016)) and 2kHz tone bursts using a wick electrode. The results showed a statistically significant difference in the CM amplitude evoked by the click stimulus between males and females with the amplitude recorded in male participants being nearly double that of females. However, the differences were not observed for the tone burst or the BB CE-chirp stimulus.

Those findings could be an additional argument for the variability of the cochlear microphonic responses between males and females to be investigated further, and that identifying the source of those differences could provide valuable insight into a better understanding of the underlying mechanisms of the CM generation and propagation within the skull.

Additionally, as a more general remark on the reliability of the CM recordings, the same study provided information about the proportion of the normal-hearing participants in which the cochlear microphonic response to a tone burst stimulus was recognisable in the ECochG traces. While the click-evoked CM appeared in 92-100% of the collected responses, that number dropped to 75-83% for the 2kHz tone burst evoked CM. That estimation appears to be reflected in the experiments that were a part of this research thesis, as the tone burst evoked CM was recognisable in 80% of the participants recruited for the study.

6.2. Suggestions for future research

The simulations of cochlear mechanics in frequency and time domain were successfully implemented in MATLAB, compared with literature findings and with one another, resulting in their performance being determined as satisfactory. Introducing the electrical elements into the model provided some insightful results that can be a helpful tool in the following research. That being said, the model is far from being able to simulate the real-life situation as the primary outputs are only concerning the single cochlear partition responses, rather than the complex dependencies that can be seen in *in vivo* measurements.

Some of the suggestions for further research are outlined in the following chapters.

6.2.1. Reformulation of the model

Models currently in use (Liu and Neely, 2010) assume that the fluid motion is driven by the reticular lamina (rather than the basilar membrane, like in the mechanical model presented in Chapter 2). If the RL is locked stationary, the model formulation would implicate that the fluid motion would

no longer be possible in any of the scalae. Since the fluid in the cochlea is almost incompressible, it is leading to an assumption that the volume velocity at the oval window is equal and opposite to the volume velocity of the round window, unless we consider a “third window” in the cochlea. The assumptions of the model suggest also that if equal and opposite movements of RL and BM would be considered, there would be no flow through stapes, helicotrema or round window despite the deflection of the BM. Those are only a few of many weaknesses in current mathematical formulations of the cochlea.

In the correspondence with Professor Yi-Wen Liu, he suggested that those problems can be solved by introducing a “pseudo 2D” model presented in Figure 6.4.

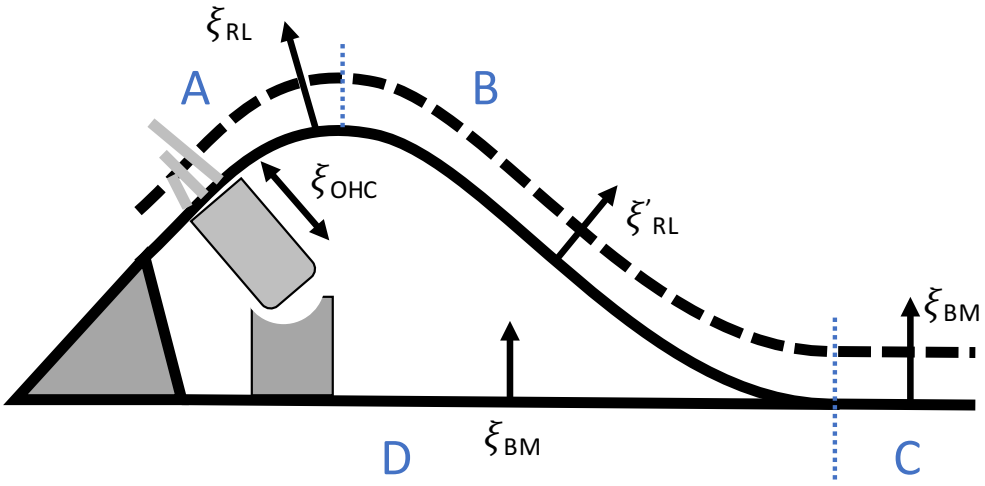

Figure 6.4: "Pseudo 2D" model of the Organ of Corti showing enclosed space in between basilar and reticular membranes with no flow through the tunnel of Corti

It assumes that the total area enclosed by A, B and D is fixed so that there is no flow through the tunnel of Corti. The equations describing the model could be as follows:

$$1D: \qquad \xi_{OHC} = 0 \tag{6.1}$$

$$2D: \qquad \int_A \xi_{RL}(y)\,dy + \int_B \xi'_{RL}(y)\,dy - \int_D \xi_{BM}(y)\,dy = 0 \tag{6.2}$$

$$\partial_x U = \int_A \xi_{RL}(y)\,dy + \int_B \xi'_{RL}(y)\,dy + \int_C \xi_{BM}(y)\,dy \qquad (6.3)$$

However, this complicated definition does not solve all the discrepancies of the model while significantly increasing the computational burden as it requires additional dimensions added to the state vector.

If we consider the anatomy of the Organ of Corti as shown in Figure 1.6, a simplified model could look as presented in Figure 6.5.

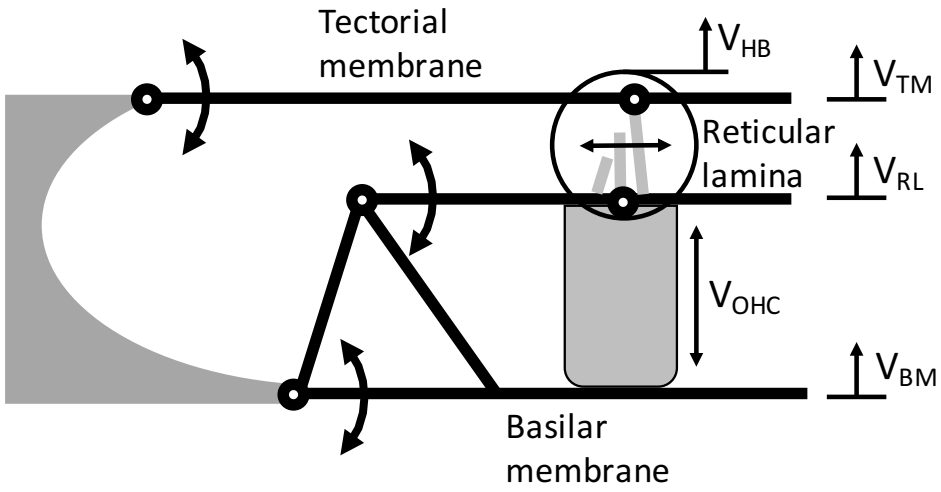

Figure 6.5: Micromechanics of the Organ of Corti featuring basilar, reticular and tectorial membrane fixed on one side, allowing for pivoting motion. The outer hair cell is embedded in between BM and RL, and stereocilia between RL and TM

As shown above, the more realistic formulation should consist of a three-degrees of freedom system to include all three: basilar membrane, reticular lamina and tectorial membrane. However, modifying the model this way would significantly complicate the formulation and extend the calculation time, therefore it should first be evaluated how to achieve the most accurate results with the simplest solution available.

6.2.2. Predictions of the auditory evoked potentials in 3-dimensional space

The current formulation of the models have the possibility for making predictions about the potentials like the cochlear microphonic only when one of two assumptions is made:

- the CM arises primarily from the characteristic place for the stimulus frequency, therefore to acquire its amplitude, the values of the cochlear potential for a single cochlear partition should be tracked to obtain the predicted potential, or
- the CM arises primarily from the basal part of the cochlea independent of the stimulus frequency, therefore to acquire its amplitude, the values of the cochlear potential should be tracked at the basal cochlear partitions

Aside from the unrealistic 2D representation of the cochlea, none of those assumptions can approximate the propagation of the cochlear potentials in the skull. While it has been speculated that the CM recorded by the intratympanic electrodes is arising primarily from the base of the cochlea, the experiments using the extratympanic measurements presented in this document results appear to suggest that the CM reaching the recording electrode arises from multiple locations across the cochlea.

This difference might be a matter of using the extratympanic electrode itself. If we consider the golden tiptrode placed in the ear canal, the vector sum of the potentials arising from the cochlea is going to be less influenced by the specific locations, since the electrode already is placed farther away from the cochlea. However, all of the recordings presented in section 6.1 were collected using an electrode placed in the round window niche, and yet the results seem to suggest that the basal part of the cochlea might not be the primary source of the cochlear microphonic potential.

To understand the mechanism better, the mechanoelectrical model of the cochlea would have to be integrated into the 3-dimensional representation of the outer, middle and inner ear. A good starting point could be to simply sum the potentials generated at each cochlear partition considering the distance. An added difficulty would be to simulate the lossy transmission in a non-uniform medium in between the origin point and the electrode.

6.2.3. Measurements in normal hearing and hearing-impaired patients

The presented measurements are showing promising results when it comes to further evaluation of the cochlear microphonic using non-invasive techniques. Because of the safety and accessibility of the procedure, the scope of data collection could be expanded to include more combinations of the stimuli types and their levels, and be used to create a link in between other clinical findings, like ABR, AP and SP.

Additionally, the anthropometric cranial indices, including head circumference, head breadth and ear canal length, could be collected and analysed in correlation with the measurements results in an effort to better understand the causes of variability in recorded cochlear potentials and to establish whether skull geometry can, in fact, contribute to those differences.

A similar set of measurements could be performed on people with hearing impairment, specifically ANSD, where the cochlear microphonic is one of the main diagnostic tools. With expanding the measurement database, the statistical analysis of the obtained results would become increasingly more accurate and meaningful.

During the data collection process, it became apparent that the measurement system itself was lacking in flexibility and quality. Therefore, a custom-built measurement system with dedicated software would significantly improve future experimental work.

6.3. Conclusions

The main conclusions of this PhD thesis are as follows:

- the electromechanical model of the cochlea is able to successfully simulate responses obtained from single points along the cochlea, and the simulation is in good agreement with the clinical data documented in the literature, however
- at this point, the model cannot predict the auditory evoked potentials obtained during *in vivo* measurements because it lacks the three-dimensional formulation and does not account for lossy transmission between the cochlea and extratympanic electrodes;
- from Experiment 1: out of the three types of electrodes commonly used for non-invasive measurements of the cochlear microphonic, the golden tip-trode is the optimal choice when it comes to the ease of use, patient comfort and good SNR in recorded responses. The wick electrode can be used to obtain high fidelity recordings provided that we re-evaluate the patient's position during the measurement that would have to be both safe and comfortable;
- from Experiment 2: when the CM was measured repeatedly in the same subject using the golden tip-trode the collected CM amplitude remained stable with a maximum standard deviation of 1.8dB for the 1kHz probe tone, and 3dB for the 2kHz probe tone within subjects;
- from Experiment 2: the amplitude of the recorded CM evoked by the same stimulus level differed between study participants by as much as 13dB for both 1kHz and 2kHz probe tones;
- from Experiment 2: the shape of the input-output functions of the measured CM varied between subjects but the function tended to have a similar shape within subjects for both of the probe tone frequencies;
- from Experiment 3: when the 1kHz probe tone was presented together with the suppressing tone, the amplitude of the CM at 1kHz was:
  - affected the most by the 2.4kHz and 4kHz suppressors,
  - affected moderately by the 4.8kHz suppressor,
  - scarcely affected by the 1.8kHz suppressor,
  - virtually unaffected by the 1.2kHz and 9.6kHz suppressors;
- from Experiment 3: the CM obtained from an electrode placed in an ear canal does not pick up solely the potential arising at the base of the cochlea but contains contributions from multiple locations along the Organ of Corti.

APPENDICES

Appendix A: Kanis & de Boer model formulation

The model developed by Kanis and de Boer (Kanis and de Boer, 1993) broadly follows the assumptions from earlier active models (Neely and Kim, 1986) but changes the way a basilar membrane impedance is implemented. Kanis & de Boer model defines it incorporating an active term that causes the resistance to go negative and, in consequence, allows sharp response in characteristic place for stimulus frequency.

The long-wave model is considered. The one dimensional linear cochlear fluid dynamics can be described by wave equation:

$$\frac{d^2}{dx^2}p(x,\omega) - \frac{2i\omega\rho}{HZ_{act}(x,\omega)} = 0,$$

where $p(x,\omega)$ - complex pressure in one of the scalae, ω - radian frequency, ρ - cochlear fluid density, h – the height of the scalae, $Z_{act}(x,\omega)$ – impedance describing basilar membrane with active elements. First of the boundary conditions for $p(0,\omega)$ describes coupling to the middle ear and the driving source. For simplicity, this is not mentioned in the method description as it is not the main focus in cochlear modelling. The second boundary condition assumes $p(L,\omega) = 0$. Once the wave equation is solved, the BM velocity is calculated as:

$$v_{BM}(x,\omega) = \frac{-2p(x,\omega)}{Z_{act}(x,\omega)},$$

The $Z_{act}(x,\omega)$ impedance has two components – passive BM impedance function $Z_{pass}(x,\omega)$, and a transfer impedance $Z_{OHC}(x,\omega)$ that considers a resonance of the tectorial membrane and the stereocilia of the OHCs.

The passive BM impedance is described as:

$$Z_{pass}(x,\omega) = i\omega M_0 + R(x) + \frac{S(x)}{i\omega}$$

for stiffness *S(x)* and damping *R(x)* given as:

$$S(x) = S_0 e^{-ax},$$

$$R(x) = \delta\sqrt{M_0 S_0}\, e^{-\frac{ax}{2}}.$$

The active part is a somewhat simplified expression of Neely & Kim model, being defined as:

$$Z_{OHC}(x,\omega) = c_0 CF(x) \frac{1 + i\beta(x,\omega)}{\delta_{sc} + i\left[\beta(x,\omega) - \frac{\sigma^2}{\beta(x,\omega)}\right]},$$

$$\beta(x,\omega) = \frac{\omega}{CF(x)}$$

Model parameters are gathered in table below. The physical parameters follow the N&K model.

Parameter	Value/Formula	Units	Notes
b	0.4	—	N&K BM bending shape factor
S_0	10^{10}	$kg \cdot m^{-2} \cdot s^{-2}$	stiffness per unit area of BM
M_0	0.5	$kg \cdot m^{-2}$	areal density of BM
d_0	1404	$kg \cdot s^{-1}$	active OHC impedance parameter
e_0	$4.28 \cdot 10^{-5}$	$kg \cdot m^{-2}$	active OHC impedance parameter
σ	0.7	—	shift of OHC resonance
δ	0.4	—	damping ratio
δ_{sc}	0.14	$N \cdot s \cdot m^{-3}$	stereocilia damping
R_0	$\sqrt{(s_0 \cdot e^{-300x} \cdot m_0)} \cdot \delta$	$N \cdot s \cdot m^{-3}$	damping per unit area of BM
CF_{st}	$\sqrt{s_0 \cdot m_0^{-1}}$	s^{-1}	characteristic frequency at stapes
CF	$CF_{st} \cdot e^{-150x}$	s^{-1}	characteristic frequency along BM
m_1	$b \cdot m_0$	$kg \cdot m^{-2}$	—
m_2	$m_1 \cdot 10^{-2}$	$kg \cdot m^{-2}$	—
k_1	$b \cdot s_0 \cdot e^{-300x}$	$N \cdot m^{-3}$	—
k_2	0	$N \cdot m^{-3}$	—
k_3	$m_2 \cdot \sigma^2 \cdot CF^2$	$N \cdot m^{-3}$	—
k_4	$e_0 \cdot d_0 \cdot b \cdot CF^2$	$N \cdot m^{-3}$	—

c_1	$b_0 \cdot r_0$	$N \cdot s \cdot m^{-3}$	—
c_2	0	$N \cdot s \cdot m^{-3}$	—
c_3	$m_2 \cdot \delta_{sc} \cdot CF$	$N \cdot s \cdot m^{-3}$	—
c_4	$e_0 \cdot d_0 \cdot b \cdot CF$	$N \cdot s \cdot m^{-3}$	—

The model described above was implemented in MATLAB. The results show system response to a single tone stimulus of frequency 6kHz in both active (γ=1) and passive (γ=0) cases. In the figure below, the upper plot shows the magnitude of basilar membrane velocity, and the lower one illustrates the basilar membrane resistance of a locally active model. The negative resistance component shows the position on the basilar membrane where the active force is 'injected' into the system.

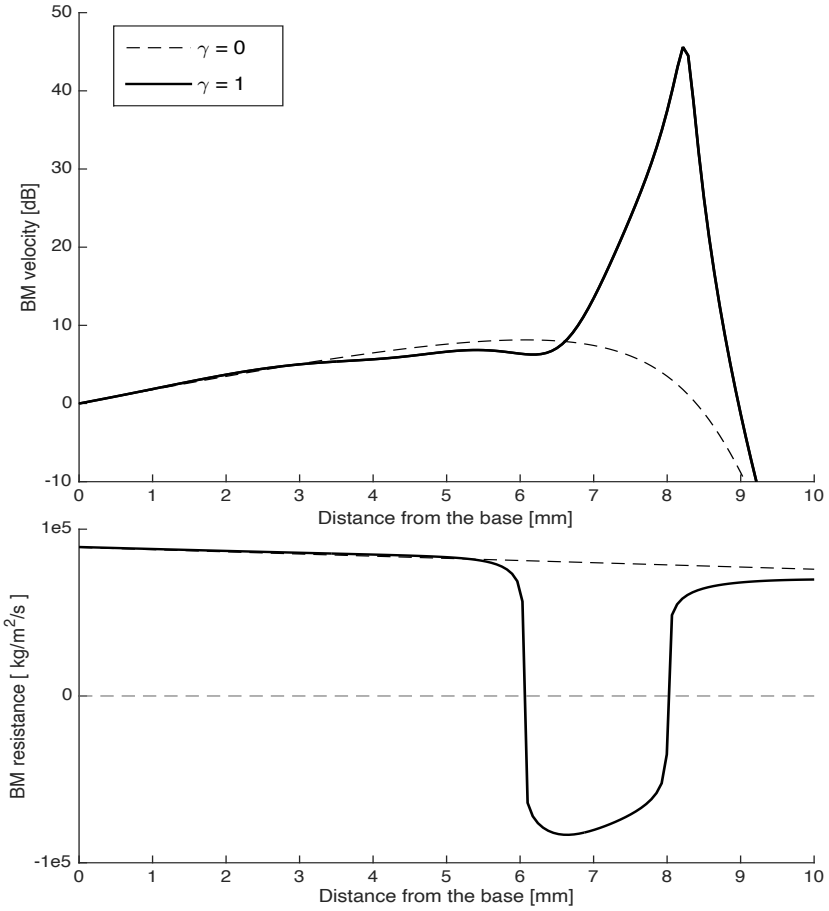

Appendix B: State space formulation of the Neely & Kim model

The following section contains the details about state space representation of the time-domain model introduced in Chapter 2.2.

Using the concept of the discretized cochlea proposed by Neely (1981), the length *L=25mm* of the cochlea is divided into *N=500* sections, each with length $\Delta = \frac{L}{N}$. Equations (2.11) - (2.13) are being rewritten as discretised spatial derivatives:

$$\frac{p_{n-1}(t) - 2p_n(t) + p_{n+1}(t)}{\Delta^2} - \frac{2\rho}{H}\ddot{\xi}_p(t) = 0, \tag{AB.1}$$

$$\frac{p_2(t) - p_1(t)}{\Delta} - 2\rho\ddot{\xi}_{SR}(t) = 2\rho\ddot{\xi}_{SO}(t), \tag{AB.2}$$

$$\frac{H}{\Delta^2}\left[\frac{\Delta}{H}p_{N-1}(t) - \left(\frac{\Delta}{H} - \frac{\Delta^2}{H^2}\right)p_N(t)\right] = 2\rho\ddot{\xi}_N. \tag{AB.3}$$

The equations (AB.1) – (AB.3) may then be written in matrix form:

$$\mathbf{F}\mathbf{p}(t) - \ddot{\boldsymbol{\xi}}(t) = \mathbf{q}. \tag{AB.4}$$

The expanded matrix equation has a following form:

$$\frac{H}{2\rho\Delta^2}\begin{bmatrix} -\frac{\Delta}{H} & \frac{\Delta}{H} & & & & & 0 \\ 1 & -2 & 1 & & & & \\ 0 & 1 & -2 & 1 & & & \\ & & \ddots & \ddots & \ddots & & \\ & & & 1 & -2 & 1 & 0 \\ & & & & 1 & -2 & 1 \\ 0 & & & & & 0 & -\frac{2\rho\Delta^2}{H} \end{bmatrix}\begin{bmatrix} p_1(t) \\ p_2(t) \\ \vdots \\ p_{N-1}(t) \\ p_N(t) \end{bmatrix} - \begin{bmatrix} \ddot{\xi}_{SR}(t) \\ \ddot{\xi}_2(t) \\ \vdots \\ \ddot{\xi}_{N-1}(t) \\ \ddot{\xi}_N{}' \end{bmatrix} = \begin{bmatrix} \ddot{\xi}_{SO}(t) \\ 0 \\ \vdots \\ 0 \\ 0 \end{bmatrix} \tag{AB.5}$$

Following the derivation proposed by Elliot et al. (2007), a coupled cochlea with distributed micromechanics and dynamic boundary conditions can be represented in a general state space form:

$$\dot{\mathbf{x}}(t) = \mathbf{A}\mathbf{x}(t) + \mathbf{B}\mathbf{u}(t), \tag{AB.7}$$

where $\mathbf{x}(t)$ is a vector of state variables, and:

$$\mathbf{A} = \left[\mathbf{I} - \mathbf{B_E F^{-1} C_E}\right]^{-1} \mathbf{A_E}, \tag{AB.8}$$

$$\mathbf{B} = \left[\mathbf{I} - \mathbf{B_E F^{-1} C_E}\right]^{-1} \mathbf{B_E}, \tag{AB.9}$$

$$\mathbf{u}(t) = \mathbf{F^{-1}} \mathbf{q}(t). \tag{AB.10}$$

The Neely & Kim model has two states associated with each degree of freedom, and the chosen four state variables are defined as:

$$\begin{aligned} \dot{\xi}_b &= \dot{x}_1(t), \\ \xi_b &= x_1(t), \\ \dot{\xi}_t &= \dot{x}_2(t), \\ \xi_t &= x_2(t). \end{aligned} \tag{AB.11}$$

Dynamics of the system is described by coupled differential equations defined in terms of $x_1(t)$ and $x_2(t)$

$$\begin{aligned} \ddot{x}_1(t) = \frac{1}{m_1}\{ & p(t) + g\gamma\left[c_4\left(\dot{x}_2(t) - \dot{x}_1(t)\right) + k_4\left(x_2(t) - x_1(t)\right)\right] \\ & -\dot{x}_1(t)(c_1 + c_3) - x_1(t)(k_1 + k_3) + \dot{x}_2(t)c_3 + x_2(t)k_3\} \end{aligned} \tag{AB.12}$$

$$\begin{aligned} \ddot{x}_2(t) = \frac{1}{m_2}\{ & -\dot{x}_2(t)(c_2 + c_3) - x_2(t)(k_2 + k_3) + \dot{x}_1(t)c_3 \\ & + x_1(t)k_3\} \end{aligned} \tag{AB.13}$$

If a state variable vector is defined as

$$\mathbf{x_n} = \begin{bmatrix} \dot{x}_1(t) \\ x_1(t) \\ \dot{x}_2(t) \\ x_2(t) \end{bmatrix}_n, \tag{AB.14}$$

where *n* subscript is the index number of the cochlear partition, the equations describing the dynamics of the system can be written in a form

$$\dot{\mathbf{x}}_\mathbf{n}(t) = \mathbf{A}_\mathbf{n}\mathbf{x}_\mathbf{n}(t) + \mathbf{B}_\mathbf{n}\mathbf{p}(t), \tag{AB.15}$$

where

$$\mathbf{p}(t) = \mathbf{F}^{-1}\boldsymbol{C}_E\dot{\mathbf{x}}(t) + \mathbf{F}^{-1}\mathbf{q}(t). \tag{AB.16}$$

The matrices used for solving above equations are defined as

$$A_E = \begin{bmatrix} \begin{bmatrix} \frac{-C_S}{M_S} & \frac{-K_S}{M_S} \\ 1 & 0 \end{bmatrix} & 0 & \cdots & 0 \\ 0 & \begin{bmatrix} -\frac{(c_1+c_3-g\gamma c_4)}{m_1} & \frac{(k_1+k_3-g\gamma k_4)}{m_1} & \frac{c_3-\gamma c_4}{m_1} & \frac{k_3-\gamma k_4}{m_1} \\ 1 & 0 & 0 & 0 \\ \frac{c_3}{m_2} & \frac{k_3}{m_2} & -\frac{(c_2+c_3)}{m_2} & \frac{(k_2+k_3)}{m_2} \\ 0 & 0 & 1 & 0 \end{bmatrix}_n & & \vdots \\ \vdots & & \ddots & \\ 0 & \cdots & & \begin{bmatrix} \frac{-C_H}{M_H} & 0 \\ 1 & 0 \end{bmatrix} \end{bmatrix} \tag{AB.17}$$

$$B_E = \begin{bmatrix} \begin{bmatrix} \frac{1}{M_S} \\ 0 \end{bmatrix} & 0 & \cdots & 0 \\ 0 & \begin{bmatrix} \frac{1}{m_1} \\ 0 \\ 0 \\ 0 \end{bmatrix}_n & & \vdots \\ \vdots & & \ddots & \\ 0 & \cdots & & \begin{bmatrix} \frac{1}{M_H} \\ 0 \end{bmatrix} \end{bmatrix}, \tag{AB.18 }$$

$$C_E = \begin{bmatrix} [1 \quad 0] & & 0 & \cdots & 0 \\ 0 & [b \quad 0 \quad 0 \quad 0]_n & & & \vdots \\ \vdots & & & \ddots & \\ 0 & & \cdots & & [1 \quad 0] \end{bmatrix}, \tag{AB19}$$

where *n* subscript is the index number of the cochlear partition for $2 \leq n \leq N-1$, and $\mathbf{I}$ is the identity matrix. The boundary conditions are included in the table below.

Parameter	Value
M_s	$45 \cdot 10^{-2}\ [kg \cdot m^{-2}]$
K_s	$4 \cdot 10^{3}\ [kg \cdot m^{-3}]$
C_s	$2.16 \cdot 10^{6}\ [kg \cdot s \cdot m^{-3}]$
M_H	$0.2\ [kg \cdot m^{-2}]$
C_H	$21\ [kg \cdot s \cdot m^{-3}]$

Appendix C: State space representation of the electromechanical model

We are assuming a state space formulation with state vector:

$$x = \left(\xi_r(1), Q(1), u_r(1), u_o(1), v_{ohc}(1), \xi_r(2), \dots, v_{ohc}(N)\right)^T \quad \text{(AC.1)}$$

The linearized system equation is given by:

$$\dot{x} = A_M(x) + B_F p \quad \text{(AC.2)}$$

A_M is a 5 x 5 matrix in a form of

$$A_M(n) = \begin{bmatrix} 0 & 0 & 1 & 0 & 0 \\ 0 & 0 & 0 & \frac{1}{T} & 0 \\ -\frac{k}{m} & \frac{KT}{M} + \frac{1}{C_g TM} - \frac{kT}{m} & -\frac{r}{m} & \frac{R}{M} - \frac{r}{m} & -\frac{1}{TM} \\ 0 & -\frac{KT}{M} + \frac{1}{C_g TM} & 0 & -\frac{R}{M} & \frac{1}{TM} \\ \frac{\alpha_d}{C_4} & 0 & \frac{\alpha_d}{C_4} & -\frac{1}{TC_4} & -\frac{G_4}{C_4} \end{bmatrix} \quad \text{(AC.3)}$$

The conductances $G_1, G_2, \dots, G_{11}$ are equal to $\frac{1}{R_1}, \frac{1}{R_2}, \dots, \frac{1}{R_{11}}$.

B_F is a 5 x 1 matrix

$$B_F(n) = \begin{bmatrix} 0 \\ 0 \\ -\frac{1}{m} \\ 0 \\ 0 \end{bmatrix} \quad \text{(AC.4)}$$

while p is a pressure vector obeying the fluid coupling

$$Fp - q = C_F \dot{x} \quad \text{(AC.5)}$$

where q indicated the stapes acceleration due to stimulus containing all zero elements, except for the first one

$$q = [1 \quad 0 \quad \dots \quad 0]^T \qquad \text{(AC.6)}$$

F is a tridiagonal finite difference approximation of the second derivative:

$$F = -\begin{bmatrix} -\frac{1}{\delta} & \frac{1}{\delta} & & & & \\ \frac{A(2)}{\rho w(2)} - \frac{1}{\delta^2} & -\frac{A(2)}{\rho w(2)} - \frac{2}{\delta^2} & \frac{A(2)}{\rho w(2)} - \frac{1}{\delta^2} & & & \\ 0 & \frac{A(3)}{\rho w(3)} - \frac{1}{\delta^2} & -\frac{A(3)}{\rho w(3)} - \frac{2}{\delta^2} & \frac{A(3)}{\rho w(3)} - \frac{1}{\delta^2} & & \\ & \ddots & \ddots & \ddots & & \\ & & & \frac{A(N-1)}{\rho w(N-1)} - \frac{1}{\delta^2} & -\frac{A(N-1)}{\rho w(N-1)} - \frac{2}{\delta^2} & \frac{A(N-1)}{\rho w(N-1)} - \frac{1}{\delta^2} \\ & & & & -\frac{1}{\delta} & \frac{1}{\delta} + \frac{\rho}{A(N) m_h} \end{bmatrix} \qquad \text{(AC. 7)}$$

C_F is a 1 x 5 matrix responsible for selecting reticular lamina accelerations from $C_F(n)\dot{x}$ in a form of

$$C_F(n) = [0 \quad 0 \quad 1 \quad 0 \quad 0] \qquad \text{(AC.8)}$$

The equations (3.11) - (3.15) can be written in a matrix form

$$Gv = i \qquad \text{(AC.9)}$$

The capacitor C_3 represents hair bundle capacitance and might or might not be present in simulations. When we do not include the HB capacitance ($C_3(n) = 0$) our matrix block takes form of:

$$\begin{bmatrix} G(1) & G_+(1) & & & \\ G_-(2) & G(2) & G_+(2) & & \\ & G_-(3) & G(3) & G_+(3) & \\ & & \ddots & & \\ & & & G_-(N) & G(N) \end{bmatrix} \begin{bmatrix} \begin{bmatrix} v_{sv}(1) \\ v_{sm}(1) \\ v_{st}(1) \\ v_{hb}(1) \\ \dot{v}_{ohc}(1) \end{bmatrix} \\ \begin{bmatrix} v_{sv}(2) \\ \vdots \\ \dot{v}_{ohc}(2) \end{bmatrix} \\ \vdots \\ \begin{bmatrix} \vdots \\ \dot{v}_{ohc}(N) \end{bmatrix} \end{bmatrix} \quad \text{(AC.10)}$$

$$= \begin{bmatrix} \begin{bmatrix} 0 \\ G_6(1)V_2(1) - i_3(1) \\ i_4(1) + G_4(1)v_{ohc}(1) \\ i_4(1) - i_3(1) + G_4(1)v_{ohc}(1) \\ v_{ohc}(1) - V_1(1) \end{bmatrix} \\ \begin{bmatrix} \vdots \\ v_{ohc}(2) - V_1(2) \end{bmatrix} \\ \vdots \\ \begin{bmatrix} \vdots \\ v_{ohc}(N) - V_1(N) \end{bmatrix} \end{bmatrix}$$

where

$$G(n) = \begin{bmatrix} G_1(n) + G_2(n) & -G_2(n) & 0 & 0 & 0 \\ +G_8(n-1) + G_8(n) & & & & \\ -G_2(n) & G_2(n) + G_6(n) & 0 & G_3(n) & 0 \\ & +G_9(n-1) + G_9(n) & & & \\ 0 & 0 & G_5(n) + G_{11}(n-1) & 0 & -C_4(n) \\ & & G_{11}(n) & & \\ 0 & 0 & 0 & G_3(n) & -C_4(n) \\ 0 & 1 & -1 & -1 & 0 \end{bmatrix} \quad \text{(AC.11)}$$

$$G_-(n) = \begin{bmatrix} -G_8(n-1) & 0 & 0 & 0 & 0 \\ 0 & -G_9(n-1) & 0 & 0 & 0 \\ 0 & 0 & -G_{11}(n-1) & 0 & 0 \\ 0 & 0 & 0 & 0 & 0 \\ 0 & 0 & 0 & 0 & 0 \end{bmatrix} \quad \text{(AC.12)}$$

$$G_+(n) = \begin{bmatrix} -G_8(n) & 0 & 0 & 0 & 0 \\ 0 & -G_9(n) & 0 & 0 & 0 \\ 0 & 0 & -G_{11}(n) & 0 & 0 \\ 0 & 0 & 0 & 0 & 0 \\ 0 & 0 & 0 & 0 & 0 \end{bmatrix} \quad \text{(AC.13)}$$

Boundary conditions are defined as follows

$$G(N)=\begin{bmatrix} G_1(N)+G_2(N) \\ +G_8(N-1) \\ +\left(\frac{1}{G_8(N)}+\frac{1}{G_{11}(N)}\right)^{-1} & -G_2(N) & -\left(\frac{1}{G_8(N)}+\frac{1}{G_{11}(N)}\right)^{-1} & 0 & 0 \\ -G_2(N) & G_2(N)+G_6(N) \\ & +G_9(N-1) & 0 & G_3(N) & 0 \\ -\left(\frac{1}{G_8(N)}+\frac{1}{G_{11}(N)}\right)^{-1} & 0 & G_5(N)+G_{11}(N-1) \\ & & +\left(\frac{1}{G_8(N)}+\frac{1}{G_{11}(N)}\right)^{-1} & 0 & -C_4(N) \\ 0 & 0 & 0 & G_3(N) & -C_4(N) \\ 0 & 1 & -1 & -1 & 0 \end{bmatrix} \quad \text{(AC.14)}$$

Right hand side of the equation (AC.10) is then calculated from the state vector as follows:

$$\begin{bmatrix} 0 \\ G_6(1)V_2(1)-i_3(1) \\ i_4(1)+G_4(1)v_{ohc}(1) \\ i_4(1)-i_3(1)+G_4(1)v_{ohc}(1) \\ v_{ohc}(1)-V_1(1) \end{bmatrix} = C_E(n)\begin{bmatrix} \xi_r(n) \\ Q(n) \\ u_r(n) \\ u_o(n) \\ v_{ohc}(n) \end{bmatrix} \quad \text{(AC.15)}$$

where C_E is defined as

$$C_E(n)=\begin{bmatrix} 0 & 0 & 0 & 0 & 0 \\ -\alpha_d & 0 & -\alpha_v & 0 & 0 \\ 0 & 0 & 0 & \frac{1}{T} & G_4(n) \\ -\alpha_d & 0 & -\alpha_v & \frac{1}{T} & G_4(n) \\ 0 & 0 & 0 & 0 & 1 \end{bmatrix} \quad \text{(AC.16)}$$

If we decide to include HB capacitance ($C3(n) \neq 0$) the equation (AC.10) slightly changes to:

$$\begin{bmatrix} G(1) & G_+(1) & & & \\ G_-(2) & G(2) & G_+(2) & & \\ & G_-(3) & G(3) & G_+(3) & \\ & & \ddots & & \\ & & & G_-(N) & G(N) \end{bmatrix} \begin{bmatrix} \begin{bmatrix} v_{sv}(1) \\ v_{sm}(1) \\ v_{st}(1) \\ \dot{v}_{hb}(1) \\ \dot{v}_{ohc}(1) \end{bmatrix} \\ \begin{bmatrix} v_{sv}(2) \\ \vdots \\ \dot{v}_{ohc}(2) \end{bmatrix} \\ \vdots \\ \begin{bmatrix} \vdots \\ \dot{v}_{ohc}(N) \end{bmatrix} \end{bmatrix} \quad \text{(AC.17)}$$

$$= \begin{bmatrix} \begin{bmatrix} 0 \\ G_6(1)V_2(1) - i_3(1) - G_3(1)v_{hb}(1) \\ i_4(1) + G_4(1)v_{ohc}(1) \\ i_4(1) - i_3(1) + G_4(1)v_{ohc}(1) - G_3(1)v_{hb}(1) \\ v_{ohc}(1) - V_1(1) + v_{hb}(1) \end{bmatrix} \\ \begin{bmatrix} \vdots \\ v_{ohc}(2) - V_1(2) + v_{hb}(2) \end{bmatrix} \\ \vdots \\ \begin{bmatrix} \vdots \\ v_{ohc}(N) - V_1(N) + +v_{hb}(N) \end{bmatrix} \end{bmatrix}$$

Consecutively, matrix (AC.11) now is defined as:

$$G(n) = \begin{bmatrix} G_1(n) + G_2(n) & -G_2(n) & 0 & 0 & 0 \\ +G_8(n-1) + G_8(n) & & & & \\ -G_2(n) & G_2(n) + G_6(n) & 0 & C_3(n) & 0 \\ & +G_9(n-1) + G_9(n) & & & \\ 0 & 0 & G_5(n) + G_{11}(n-1) & 0 & -C_4(n) \\ & & G_{11}(n) & & \\ 0 & 0 & 0 & C_3(n) & -C_4(n) \\ 0 & 1 & -1 & 0 & 0 \end{bmatrix} \quad \text{(AC.18)}$$

And boundary conditions change to

$$G(N)$$

$$= \begin{bmatrix} G_1(N)+G_2(N) & -G_2(N) & -\left(\frac{1}{G_8(N)} + \frac{1}{G_{11}(N)}\right)^{-1} & 0 & 0 \\ +G_8(N-1) & & & & \\ +\left(\frac{1}{G_8(N)} + \frac{1}{G_{11}(N)}\right)^{-1} & & & & \\ -G_2(N) & G_2(N) + G_6(N) & 0 & C_3(N) & 0 \\ & +G_9(N-1) & & & \\ -\left(\frac{1}{G_8(N)} + \frac{1}{G_{11}(N)}\right)^{-1} & 0 & G_5(N) + G_{11}(N-1) & 0 & -C_4(N) \\ & & +\left(\frac{1}{G_8(N)} + \frac{1}{G_{11}(N)}\right)^{-1} & & \\ 0 & 0 & 0 & C_3(N) & -C_4(N) \\ 0 & 1 & -1 & 0 & 0 \end{bmatrix} \quad \text{(AC.19)}$$

Matrices $G_-(n)$ and $G_+(n)$ remain unchanged.

Right hand side of the equation (AC.15) is then calculated from the state vector as follows:

$$\begin{bmatrix} 0 \\ G_6(1)V_2(1) - i_3(1) - G_3(1)v_{hb}(1) \\ i_4(1) + G_4(1)v_{ohc}(1) \\ i_4(1) - i_3(1) + G_4(1)v_{ohc}(1) - G_3(1)v_{hb}(1) \\ v_{ohc}(1) - V_1(1) + v_{hb}(1) \end{bmatrix} = C_E(n) \begin{bmatrix} \xi_r(n) \\ Q(n) \\ u_r(n) \\ u_o(n) \\ v_{ohc}(n) \\ v_{hb}(n) \end{bmatrix} \quad \text{(AC.20)}$$

where C_E is defined as

$$C_E(n) = \begin{bmatrix} 0 & 0 & 0 & 0 & 0 & 0 \\ -\alpha_d & 0 & -\alpha_d & 0 & 0 & -G_3(n) \\ 0 & 0 & 0 & \frac{1}{T} & G_4(n) & 0 \\ -\alpha_d & 0 & -\alpha_v & \frac{1}{T} & G_4(n) & -G_3(n) \\ 0 & 0 & 0 & 0 & 1 & 1 \end{bmatrix} \quad \text{(AC.21)}$$

Finally, combining equations (AC.2), (AC.5) and (AC.9) we obtain:

$$p(F - C_F B_F) = C_F A_M x + q \quad \text{(AC.22)}$$

therefore

$$\dot{x} = A_M x + B_F (F - C_F B_F)^{-1} (C_F A_M x + q) \quad \text{(AC.23)}$$

Appendix D: Measurements of two-tone suppression in cochlear microphonic – results

Male participants

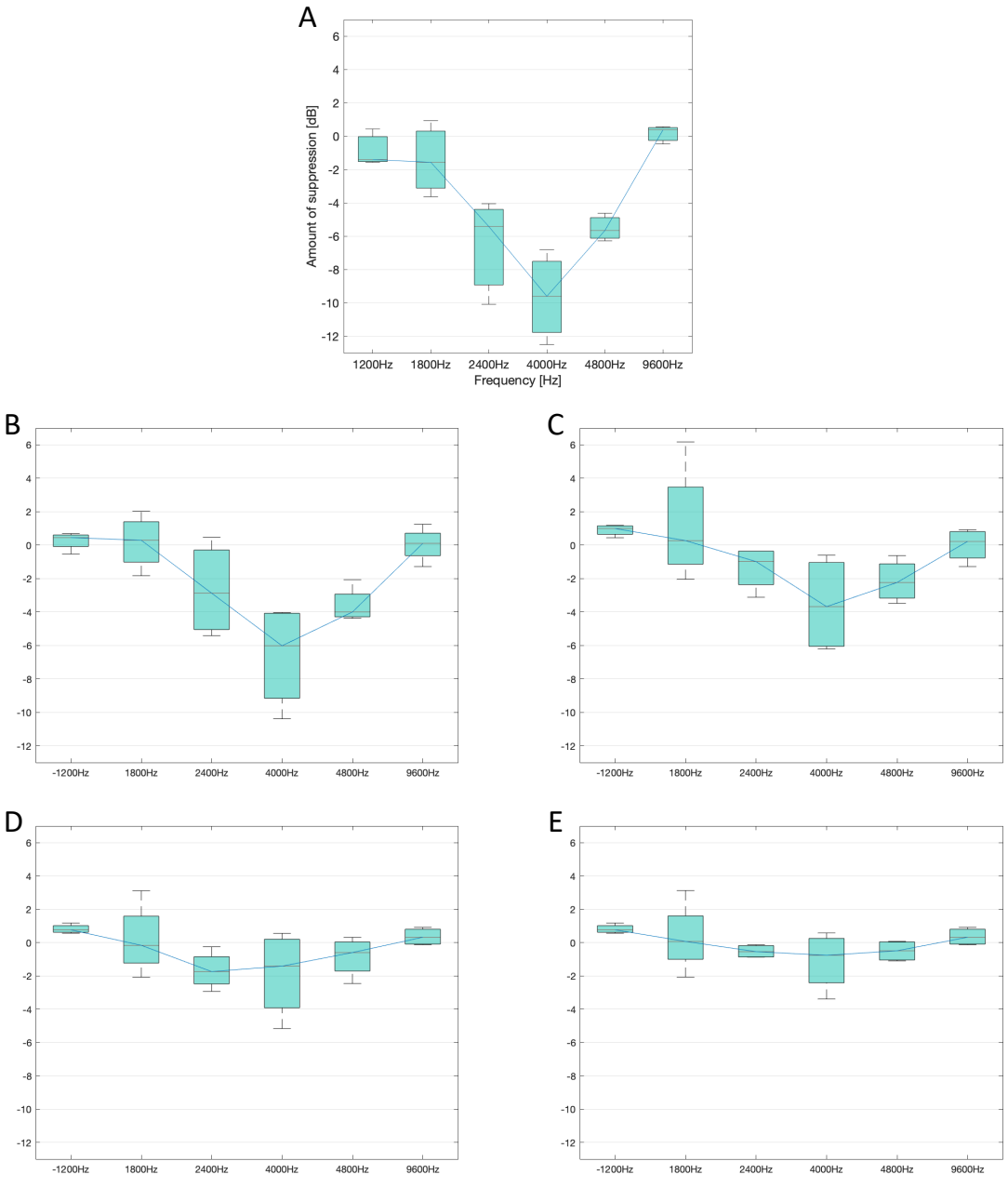

Fig. 1: CM recorded in male participants at the probe tone depending on the suppressor level and frequency: A: +6dB, B: +0dB, C: -6dB, D: -12dB, D: - 18dB

Female participants

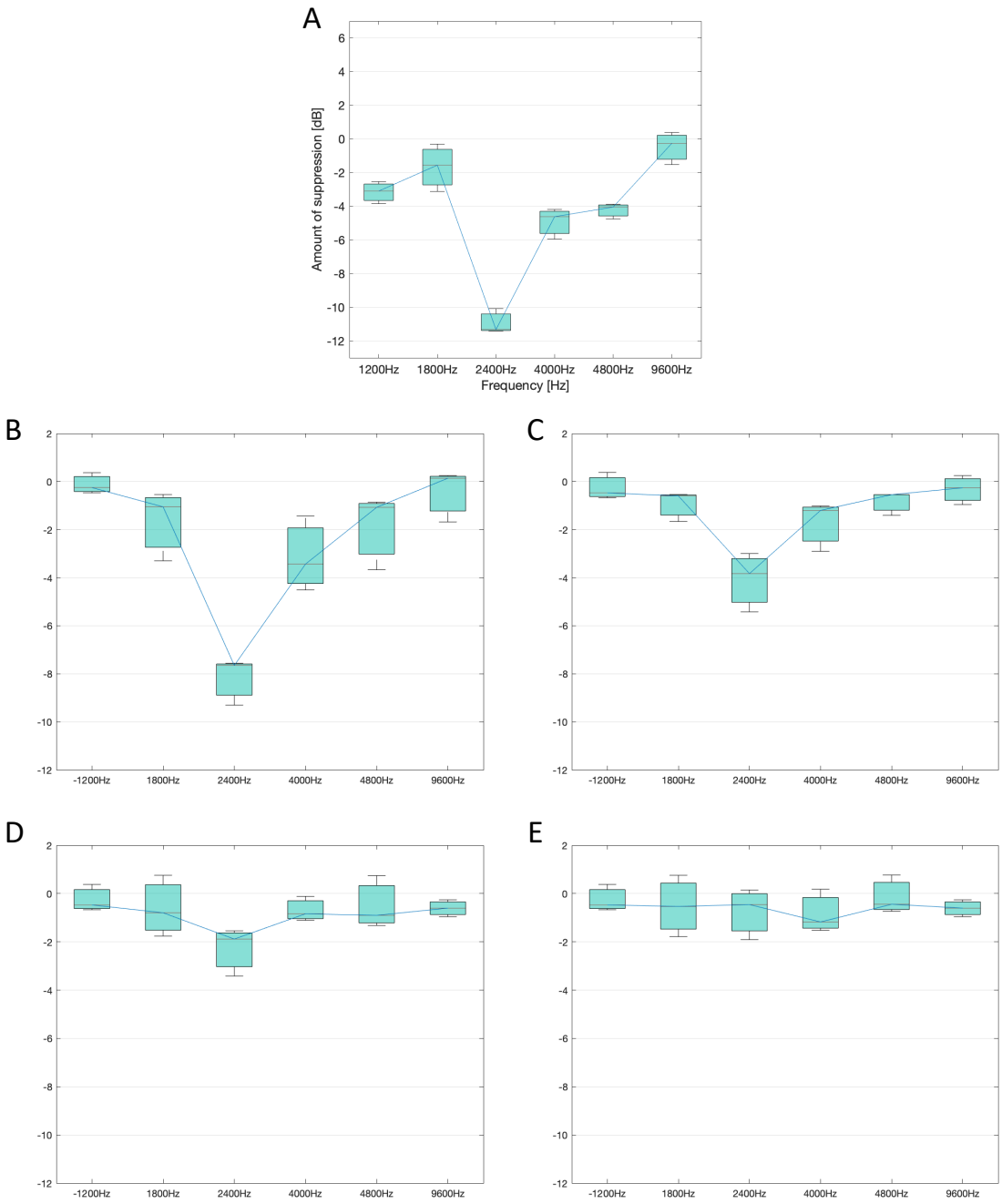

Fig. 2: CM recorded in female participants at the probe tone depending on the suppressor level and frequency: A: +6dB, B: +0dB, C: -6dB, D: -12dB, D: - 18dB

Appendix E: Pairwise comparison of the data from 2TS experiment

Numbered cases: 1 – 1.2kHz suppressor; 2 – 1.8kHz suppressor; 3 – 2.4kHz suppressor; 4 – 4kHz suppressor; 5 – 4.8kHz suppressor; 6 – 9.6kHz suppressor

Pairwise Comparisons

Measure: suppression

(I) suppressor	(J) suppressor	Mean Difference (I-J)	Std. Error	Sig.[b]	95% Confidence Interval for Difference[b]	
					Lower Bound	Upper Bound
1	2	-.462	.561	1.000	-3.097	2.172
	3	6.862*	.802	.002	3.096	10.628
	4	5.522	1.450	.133	-1.290	12.335
	5	3.367	.957	.188	-1.130	7.865
	6	-1.484	.606	.749	-4.333	1.365
2	1	.462	.561	1.000	-2.172	3.097
	3	7.325*	.998	.005	2.637	12.012
	4	5.985*	1.098	.024	.827	11.143
	5	3.830	.924	.091	-.510	8.170
	6	-1.022	.751	1.000	-4.548	2.504
3	1	-6.862*	.802	.002	-10.628	-3.096
	2	-7.325*	.998	.005	-12.012	-2.637
	4	-1.340	1.808	1.000	-9.832	7.152
	5	-3.495	1.320	.573	-9.697	2.708
	6	-8.346*	1.071	.004	-13.380	-3.313
4	1	-5.522	1.450	.133	-12.335	1.290
	2	-5.985*	1.098	.024	-11.143	-.827
	3	1.340	1.808	1.000	-7.152	9.832
	5	-2.155	.996	1.000	-6.833	2.523
	6	-7.007*	1.300	.025	-13.116	-.897
5	1	-3.367	.957	.188	-7.865	1.130
	2	-3.830	.924	.091	-8.170	.510
	3	3.495	1.320	.573	-2.708	9.697
	4	2.155	.996	1.000	-2.523	6.833
	6	-4.852*	.489	.001	-7.147	-2.557
6	1	1.484	.606	.749	-1.365	4.333
	2	1.022	.751	1.000	-2.504	4.548
	3	8.346*	1.071	.004	3.313	13.380
	4	7.007*	1.300	.025	.897	13.116
	5	4.852*	.489	.001	2.557	7.147

Based on estimated marginal means

*. The mean difference is significant at the .05 level.

b. Adjustment for multiple comparisons: Bonferroni.

REFERENCES

Alberti, P. W. (2001) 'The Anatomy and Physiology of the Ear and Hearing', *Occupational exposure to noise: evaluation, prevention and control*.

Allen, J. (1998) 'A review of active and passive basilar membrane cochlear mechanics.', *The Journal of the Acoustical Society of America*. Acoustical Society of AmericaASA, 99(4), p. 2582. doi: 10.1121/1.415105.

Antoli-Candela, F. J. and Kiang, N. Y. S. (1978) 'Unit activity underlying the N1 potential', in Nauton, R. F. and Fernandez, C. (eds) *Evoked electrical activity in the auditory nervous system*. London: Academic Press, pp. 165–189.

Ashmore, J. (2008) 'Cochlear Outer Hair Cell Motility'. doi: 10.1152/physrev.00044.2006.

Ayat, M. *et al.* (2015) 'Cochlear microphonic broad tuning curves', in, p. 030010. doi: 10.1063/1.4939325.

Ayat, M., Teal, Paul D. and McGuinness, M. (2014) 'An integrated electromechanical model for the cochlear microphonic', *Biocybernetics and Biomedical Engineering*. Korea Institute of Oriental Medicine, 34(4), pp. 206–219. doi: 10.1016/j.bbe.2014.06.001.

Ayat, M., Teal, P D and McGuinness, M. (2014) 'An integrated electromechanical model for the cochlear microphonic', *Biocybernetics and Biomedical Engineering*, 34(4), pp. 206–219. doi: http://dx.doi.org/10.1016/j.bbe.2014.06.001.

Barral, J. and Martin, P. (2012) 'Phantom tones and suppressive masking by active nonlinear oscillation of the hair-cell bundle', *Proceedings of the National Academy of Sciences*. National Academy of Sciences, 109(21), pp. E1344–E1351. doi: 10.1073/PNAS.1202426109.

Batra, R., Kuwada, S. and Maher, V. L. (1986) 'The frequency-following response to continuous tones in humans', *Hearing Research*. Hear Res, 21(2), pp. 167–177. doi: 10.1016/0378-5955(86)90037-7.

Berlin, C. I., Morlet, T. and Hood, L. J. (2003) 'Auditory neuropathy/dyssynchrony its diagnosis and management', *Pediatric Clinics of North America*. W.B. Saunders, pp. 331–340. doi: 10.1016/S0031-3955(03)00031-2.

Brown, M. C. *et al.* (1983) 'Cochlear inner hair cells: Effects of transient asphyxia on intracellular potentials', *Hearing Research*, 9, pp. 13–14.

Brownell, W. E. *et al.* (1985) 'Evoked mechanical responses of isolated cochlear outer hair cells.', *Science (New York, N.Y.)*, 227(4683), pp. 194–6.

Brugge, J. F. and Howard, M. A. (2002) 'Hearing', *Encyclopedia of the Human Brain*. Academic Press, pp. 429–448. doi: 10.1016/B0-12-227210-2/00159-X.

Celesia, G. G. (2013) *Disorders of Peripheral and Central Auditory Processing1: Disorders of Peripheral and Central Auditory Processing*. Elsevier Health Sciences.

Charaziak, K. K., Shera, C. A. and Siegel, J. H. (2017a) 'Using cochlear microphonic potentials to localize peripheral hearing loss', *Frontiers in Neuroscience*, 11(APR). doi: 10.3389/fnins.2017.00169.

Charaziak, K. K., Shera, C. A. and Siegel, J. H. (2017b) 'Using Cochlear Microphonic Potentials to Localize Peripheral Hearing Loss', *Frontiers in Neuroscience*. Frontiers Research Foundation, 11(APR), p. 169. doi: 10.3389/fnins.2017.00169.

Charaziak, K., Siegel, J. and Shera, C. (2018) 'Spectral Ripples in Round-Window Cochlear Microphonics: Evidence for Multiple Generation Mechanisms', *Journal of the Association for Research in Otolaryngology : JARO*. J Assoc Res Otolaryngol, 19(4), pp. 401–419. doi: 10.1007/S10162-018-0668-6.

Cheatham, M. A. and Dallos, P. (1982) 'Two-tone interactions in the cochlear microphonic', *Hearing Research*. Elsevier, 8(1), pp. 29–48. doi: 10.1016/0378-5955(82)90032-6.

Cheatham, M. A. and Dallos, P. (1992) 'Two-tone suppression in inner hair cell responses: Correlates of rate suppression in the auditory nerve', *Hearing Research*. Elsevier, 60(1), pp. 1–12. doi: 10.1016/0378-5955(92)90052-O.

Chen, F. *et al.* (2011) 'A differentially amplified motion in the ear for near-threshold sound detection', *Nature Neuroscience 2011 14:6*. Nature Publishing Group, 14(6), pp. 770–774. doi: 10.1038/nn.2827.

Chertoff, M. E., Earl, B. R. and Diaz, F. J. (2012) 'Analysis of the cochlear microphonic to a low-frequency tone embedded in filtered noise', *Citation: The Journal of the Acoustical Society of America*, 132, p. 3351. doi: 10.1121/1.4757746.

Chimento, T. C. and Schreiner, C. E. (1990) 'Selectively eliminating cochlear microphonic contamination from the frequency-following response', *Electroencephalography and Clinical Neurophysiology*. Electroencephalogr Clin Neurophysiol, 75(1–2), pp. 88–96. doi: 10.1016/0013-4694(90)90156-E.

Cooper, N. P. (1998) 'Two-tone suppression in cochlear mechanics', *The Journal of the Acoustical Society of America*. Acoustical Society of AmericaASA, 99(5), p. 3087. doi: 10.1121/1.414795.

Coraci, L. M. and Beynon, A. J. (2021) 'Use of an Extra-Tympanic Membrane Electrode to Record Cochlear Microphonics with Click, Tone Burst and Chirp Stimuli', *Audiology Research 2021, Vol. 11, Pages 89-99*. Multidisciplinary Digital Publishing Institute, 11(1), pp. 89–99. doi: 10.3390/AUDIOLRES11010010.

D Bushby, K. M. *et al.* (1992) *Centiles for adult head circumference*, *Archives ofDisease in Childhood*.

Dallos, P., Popper, A. N. and Fay, R. R. (1996) *The Cochlea*. New York, NY: Springer New York (Springer Handbook of Auditory Research). doi: 10.1007/978-1-4612-0757-3.

Dean, M. S. and Martin, F. N. (2000) 'Insert Earphone Depth and the Occlusion Effect', *American Journal of Audiology*, 9.

Dong, W. and Olson, E. S. (2013) 'Detection of Cochlear Amplification and Its Activation', *Biophysical Journal*. The Biophysical Society, 105(4), p. 1067. doi: 10.1016/J.BPJ.2013.06.049.

Easton, G. S. and McCulloch, R. E. (1990) 'A Multivariate Generalization of Quantile-Quantile Plots', *Journal of the American Statistical Association*. JSTOR, 85(410), p. 376. doi: 10.2307/2289773.

El-Badry, M. M. and McFadden, S. L. (2009) 'Evaluation of Inner Hair Cell and Nerve Fiber Loss as Sufficient Pathologies Underlying Auditory Neuropathy', *Hearing research*. NIH Public Access, 255(1–2), p. 84. doi: 10.1016/J.HEARES.2009.06.003.

Elliott, S. J., Ku, E. M. and Lineton, B. (2007) 'A state space model for cochlear mechanics.', *The Journal of the Acoustical Society of America*, 122(5), pp. 2759–2771. doi: 10.1121/1.2783125.

Encyclopedia Britannica (2016) 'Britannica Online Encyclopedia', *Encyclopædia Britannica*.

Fallah, E., Strimbu, C. E. and Olson, E. S. (2021) 'Nonlinearity of intracochlear motion and local cochlear microphonic: Comparison between guinea pig and gerbil', *Hearing Research*. Elsevier, 405, p. 108234. doi: 10.1016/J.HEARES.2021.108234.

Faris, C. (2011) 'Scott-Brown's Otorhinolaryngology, Head and Neck Surgery, 7th edn', *Annals of The Royal College of Surgeons of England*. Royal College of Surgeons of England, p. 559. doi: 10.1308/147870811X598605b.

Feirn, R. *et al.* (2013) 'Guidelines for the Assessment and Management of Auditory Neuropathy Spectrum Disorder in Young Infants NHSP Clinical Group', (August), pp. 344–354.

Ferraro, J. and Tibbils, R. (1999) 'SP/AP area ratio in the diagnosis of Ménière's disease', *American journal of audiology*. Am J Audiol, 8(1), pp. 21–28. doi: 10.1044/1059-0889(1999/001).

Fontenot, T. E., Giardina, C. K. and Fitzpatrick, D. C. (2017) 'A Model-Based Approach for Separating the Cochlear Microphonic from the Auditory Nerve Neurophonic in the Ongoing Response Using Electrocochleography', *Frontiers in Neuroscience*. Frontiers, 11(OCT), p. 592. doi: 10.3389/FNINS.2017.00592.

Forgues, M. *et al.* (2014) 'Distinguishing hair cell from neural potentials recorded at the round window', *Journal of neurophysiology*. J Neurophysiol, 111(3), pp. 580–593. doi: 10.1152/JN.00446.2013.

Fridberger, A. *et al.* (2004) 'Organ of Corti Potentials and the Motion of the Basilar Membrane', *Journal of Neuroscience*, 24(45).

Friedman, M. (1937) 'The Use of Ranks to Avoid the Assumption of Normality Implicit in the Analysis of Variance', *Journal of the American Statistical Association*, 32(200), pp. 675–701. doi: 10.1080/01621459.1937.10503522.

Gelfand, S. A. (2009) *Hearing: An Introduction to Psychological and Physiological Acoustics*, *Informa Healthcare*.

Gibbin, K. P., Mason, S. M. and Kent, S. E. (1983) 'Prolongation of the cochlear microphonic in man: Cochlear microphonic ringing', *Acta Oto-Laryngologica*. Informa Healthcare, 95(1–4), pp. 13–18. doi: 10.3109/00016488309130910.

Greenhouse, S. W. and Geisser, S. (1959) 'On methods in the analysis of profile data', *Psychometrika*. Springer-Verlag, 24(2), pp. 95–112. doi: 10.1007/BF02289823.

Greenwood, D. D. (1996) 'Comparing octaves, frequency ranges, and cochlear-map curvature across species.', *Hearing research*, 94(1–2), pp. 157–62.

Greger, R. and Windhorst, U. (2013) *Comprehensive Human Physiology: From Cellular Mechanisms to Integration*. Springer Science & Business Media.

Hakizimana, P. *et al.* (2012) 'Sound-induced length changes in outer hair cell stereocilia', *Nature Communications*, 3, p. 1094. doi: 10.1038/ncomms2100.

He, W. *et al.* (2012) 'The group delay and suppression pattern of the cochlear microphonic potential recorded at the round window.', *PloS one*. Public Library of Science, 7(3), p. e34356. doi: 10.1371/journal.pone.0034356.

Herdman, S. J. (2007) *Vestibular Rehabilitation*. F.A. Davis.

Hudspeth, A. (1982) 'Extracellular current flow and the site of transduction by vertebrate hair cells', *Journal of Neuroscience*. Society for Neuroscience, 2(1), pp. 1–10. doi: 10.1523/JNEUROSCI.02-01-00001.1982.

Hudspeth, A. J. *et al.* (2000) 'Putting ion channels to work: mechanoelectrical transduction, adaptation, and amplification by hair cells.', *Proceedings of the National Academy of Sciences of the United States of America*, 97(22), pp. 11765–72. doi: 10.1073/pnas.97.22.11765.

Hudspeth, A. J. (2014) 'Integrating the active process of hair cells with cochlear function', *Nature Reviews Neuroscience*. Nature Research, 15(9), pp. 600–614. doi: 10.1038/nrn3786.

Hutson, K. A. *et al.* (2021) 'Light sheet microscopy of the gerbil cochlea', *Journal of Comparative Neurology*, 529(4), pp. 757–785. doi: https://doi.org/10.1002/cne.24977.

Huynh, H. and Feldt, L. S. (1976) 'Estimation of the Box Correction for Degrees of Freedom from Sample Data in Randomized Block and Split-Plot Designs', *Journal of Educational Statistics*. JSTOR, 1(1), p. 69. doi: 10.2307/1164736.

Jahan, I. *et al.* (2013) 'Beyond generalized hair cells: Molecular cues for hair cell types', *Hearing research*. NIH Public Access, 297, p. 30. doi: 10.1016/J.HEARES.2012.11.008.

Jewett, D. L. and Williston, J. S. (1971) 'Auditory-evoked far fields averaged from the scalp of humans.', *Brain : a journal of neurology*, 94(4), pp. 681–96.

Kanis, L. J. and de Boer, E. (1993) 'Self-suppression in a locally active nonlinear model of the cochlea: a quasilinear approach.', *The Journal of the Acoustical Society of America*, 94(6), pp. 3199–206.

Kanis, L. J. and de Boer, E. (1994) 'Two-tone suppression in a locally active nonlinear model of the cochlea.', *The Journal of the Acoustical Society of America*, 96(4), pp. 2156–65.

Keifer, C. D. (2016) *Toledo Hearing Doctor*. Available at: http://www.toledohearingdoc.com/hearing/anatomy-and-physiology/ (Accessed: 3 March 2016).

Kleppner, D. and Kolenkow, R. J. (2010) *An Introduction to Mechanics*. Cambridge University Press.

Ku, E. M. (2008) *Modelling the human cochlea [Ph.D. thesis]*. University of Southampton.

Kumar, A. U. and Jayaram, M. (2005) 'Auditory processing in individuals with auditory neuropathy.', *Behavioral and brain functions : BBF*. BioMed Central, 1(1), p. 21. doi: 10.1186/1744-9081-1-21.

LePage, E. L. (2003) 'The mammalian cochlear map is optimally warped.', *The Journal of the Acoustical Society of America*, 114(2), pp. 896–906.

Li, H. *et al.* (2021) 'Three-dimensional tonotopic mapping of the human cochlea based on synchrotron radiation phase-contrast imaging', *Scientific Reports 2021 11:1*. Nature Publishing Group, 11(1), pp. 1–8. doi: 10.1038/s41598-021-83225-w.

Liberman, M. C. and Kiang, N. Y. (1984) 'Single-neuron labeling and chronic cochlear pathology. IV. Stereocilia damage and alterations in rate- and phase-level functions.', *Hearing research*. Elsevier, 16(1), pp. 75–90. doi: 10.1016/0378-5955(84)90026-1.

Lindsey, H. (2014) 'Making Sense of Auditory Neuropathy Spectrum Disorder', *Hearing Journal*, 67(6), pp. 8-9,12. doi: 10.1097/01.HJ.0000451359.32725.3f.

Liu, Y.-W. and Neely, S. T. (2010) 'Distortion product emissions from a cochlear model with nonlinear mechanoelectrical transduction in outer hair cells.', *The Journal of the Acoustical Society of America*, 127(4), pp. 2420–2432. doi: 10.1121/1.3337233.

Lyon, R. F. and Mead, C. A. (1998) 'Cochlear hydrodynamics demystified'. California Institute of Technology.

Manchaiah, V. K. C. *et al.* (2011) 'The genetic basis of auditory neuropathy spectrum disorder (ANSD)', *International Journal of Pediatric Otorhinolaryngology*, 75(2), pp. 151–158. doi: 10.1016/j.ijporl.2010.11.023.

Meaud, J. and Grosh, K. (2014) 'Effect of the attachment of the tectorial membrane on cochlear micromechanics and two-tone suppression.', *Biophysical journal*. The Biophysical Society, 106(6), pp. 1398–405. doi: 10.1016/j.bpj.2014.01.034.

Moheimani, R. and Fleming, A. (2006) *Piezoelectric Transducers for Vibration Control and Damping*, *Piezoelectric Transducers for Vibration Control and Damping*. Springer-Verlag. doi: 10.1007/1-84628-332-9.

Møller, A. (2006) *Hearing: Anatomy, Physiology, and Disorders of the Auditory System*. 2nd editio. Elsevier.

Møller, A. R. (1983) ‘On the origin of the compound action potentials (N1, N2) of the cochlea of the rat.’, *Experimental neurology*, 80(3), pp. 633–44.

Mountain, D. C. and Cody, A. R. (1999) ‘Multiple modes of inner hair cell stimulation’, *Hearing Research*. Elsevier, 132(1–2), pp. 1–14. doi: 10.1016/S0378-5955(99)00013-1.

Mountain, D. C. and Hubbard, A. E. (1993) ‘A piezoelectric model of outer hair cell function’, *The Journal of the Acoustical Society of America*, 95.

Neely, S. T. (1981) ‘Finite difference solution of a two-dimensional mathematical model of the cochlea.’, *The Journal of the Acoustical Society of America*, 69(5), pp. 1386–91.

Neely, S. T. and Kim, D. O. (1986) ‘A model for active elements in cochlear biomechanics’, *The Journal of the Acoustical Society of America*, 79(5), pp. 1472–80.

Nuttall, A., Dolan, D. and Avinash, G. (1991) ‘Laser Doppler velocimetry of basilar membrane vibration’, *Hearing research*. Hear Res, 51(2), pp. 203–213. doi: 10.1016/0378-5955(91)90037-A.

Özdamar, O. and Dallos, P. (1976) ‘Input–output functions of cochlear whole-nerve action potentials: Interpretation in terms of one population of neurons’, *The Journal of the Acoustical Society of America*. Acoustical Society of America, 59(1), p. 143. doi: 10.1121/1.380818.

Palmer, A. R. and Russell, I. J. (1986) ‘Phase-locking in the cochlear nerve of the guinea-pig and its relation to the receptor potential of inner hair-cells’, *Hearing Research*, 24(1), pp. 1–15. doi: 10.1016/0378-5955(86)90002-X.

Patuzzi, R., Yates, G. and Johnstone, B. (1989) ‘The origin of the low-frequency microphonic in the first cochlear turn of guinea-pig’, *Hearing Research*, 39(1–2), pp. 177–188. doi: 10.1016/0378-5955(89)90089-0.

Pickles, J. O. (1988) *An Introduction to the Physiology of Hearing*. 2nd editio. Academic Press.

Potrusil, T. *et al.* (2020) ‘Finite element analysis and three-dimensional reconstruction of tonotopically aligned human auditory fiber pathways: A computational environment for modeling electrical stimulation by a cochlear implant based on micro-CT’, *Hearing Research*. Elsevier B.V., 393, p. 108001. doi: 10.1016/j.heares.2020.108001.

Pujol, R. (2014) *Outer Hair Cells (OHCs): Overview*, *Journey into the world of Hearing, www.cochlea.eu*. Available at: http://www.cochlea.eu/en/hair-cells/outer-hair-cells-ohcs (Accessed: 4 February 2016).

Purves, D. *et al.* (2001) 'The Middle Ear'. Sinauer Associates.

Pushpalatha, Z. V. and Konadath, S. (2016) 'Auditory Brainstem Responses for Click and CE-chirp Stimuli in Individuals with and without Occupational Noise Exposure', *Noise & Health*. Wolters Kluwer -- Medknow Publications, 18(84), p. 260. doi: 10.4103/1463-1741.192477.

Ramamoorthy, S. *et al.* (2014) 'Filtering of Acoustic Signals within the Hearing Organ'. doi: 10.1523/JNEUROSCI.0722-14.2014.

Rance, G. (2005) 'Auditory neuropathy/dys-synchrony and its perceptual consequences.', *Trends in amplification*. SAGE Publications, 9(1), pp. 1–43. doi: 10.1177/108471380500900102.

Rance, G. and Chisari, D. (2016) 'Auditory neuropathy in a patient with hemochromatosis', *Journal of Otology*. Chinese PLA General Hospital, 11(4), p. 185. doi: 10.1016/J.JOTO.2016.10.002.

Rance, G. and Starr, A. (2015) 'Pathophysiological mechanisms and functional hearing consequences of auditory neuropathy', *Brain*, 138(11), pp. 3141–3158. doi: 10.1093/brain/awv270.

Rapin, I. and Gravel, J. (2003) '"Auditory neuropathy": Physiologic and pathologic evidence calls for more diagnostic specificity', *International Journal of Pediatric Otorhinolaryngology*. Elsevier Ireland Ltd, 67(7), pp. 707–728. doi: 10.1016/S0165-5876(03)00103-4.

Reichenbach, T. and Hudspeth, A. J. (2014) 'The physics of hearing: fluid mechanics and the active process of the inner ear.', *Reports on progress in physics. Physical Society (Great Britain)*. IOP Publishing, 77(7), p. 076601. doi: 10.1088/0034-4885/77/7/076601.

Ren, T., He, W. and Kemp, D. (2016) 'Reticular lamina and basilar membrane vibrations in living mouse cochleae', *Proceedings of the National Academy of Sciences of the United States of America*. National Academy of Sciences, 113(35), pp. 9910–9915. doi: 10.1073/pnas.1607428113.

Rhode, W. (2007) 'Mutual suppression in the 6 kHz region of sensitive chinchilla cochleae', *The Journal of the Acoustical Society of America*. J Acoust Soc Am, 121(5 Pt1), pp. 2805–2818. doi: 10.1121/1.2718398.

Ruggero, M. A. and Temchin, A. N. (2005) 'Unexceptional sharpness of frequency tuning in the human cochlea.', *Proceedings of the National Academy of Sciences of the United States of America*. National Academy of Sciences, 102(51), pp. 18614–9. doi: 10.1073/pnas.0509323102.

Russell, I. and Sellick, P. (1978) 'Intracellular studies of hair cells in the mammalian cochlea', *The Journal of physiology*. J Physiol, 284(1), pp. 261–290. doi: 10.1113/JPHYSIOL.1978.SP012540.

Ryan, A. (1976) ‘Hearing sensitivity of the mongolian gerbil, Meriones unguiculatis’, *Journal of the Acoustical Society of America*. Acoustical Society of AmericaASA, 59(5), pp. 1222–1226. doi: 10.1121/1.380961.

Santos-Sacchi, J. (1991) ‘Reversible inhibition of voltage-dependent outer hair cell motility and capacitance.’, *The Journal of neuroscience : the official journal of the Society for Neuroscience*, 11(10), pp. 3096–110.

Santos-Sacchi, J. and Dilger, J. . (1988) ‘Whole cell currents and mechanical responses of isolated outer hair cells’, *Hearing Research*, 35(2), pp. 143–150. doi: 10.1016/0378-5955(88)90113-X.

Sato, H., Sando, I. and Takahashi, H. (1991) ‘Sexual dimorphism and development of the human cochlea: Computer 3-d measurement’, *Acta Oto-Laryngologica*. Informa Healthcare, 111(6), pp. 1037–1040. doi: 10.3109/00016489109100753.

Shera, C. A. (2008) ‘Laser amplification with a twist: Traveling-wave propagation and gain functions from throughout the cochlea’, *The Journal of the Acoustical Society of America*. Acoustical Society of AmericaASA, 122(5), p. 2738. doi: 10.1121/1.2783205.

Simmons, J. L. and Beauchaine, K. L. (2000) ‘Auditory neuropathy: case study with hyperbilirubinemia.’, *Journal of the American Academy of Audiology*, 11(6), pp. 337–47.

Sininger, Y. and Starr, A. (2001) *Auditory Neuropathy: A New Perspective on Hearing Disorders*. Singular.

Starr, A. (1978) ‘Sensory Evoked Potentials in Clinical Disorders of the Nervous System’, *Annual Review of Neuroscience*. Annual Reviews 4139 El Camino Way, P.O. Box 10139, Palo Alto, CA 94303-0139, USA, 1(1), pp. 103–127. doi: 10.1146/annurev.ne.01.030178.000535.

Starr, A. and Achor, J. (1975) ‘Auditory brain stem responses in neurological disease.’, *Archives of neurology*, 32(11), pp. 761–8.

Steele, C. R. and Puria, S. (2005) ‘Force on inner hair cell cilia’, *International Journal of Solids and Structures*. Pergamon, 42(21–22), pp. 5887–5904. doi: 10.1016/J.IJSOLSTR.2005.03.056.

Strelioff, D. (1973) ‘A computer simulation of the generation and distribution of cochlear potentials’, *The Journal of the Acoustical Society of America*. Acoustical Society of America, 54(3), pp. 620–629. doi: 10.1121/1.1913642.

Tasaki, I. and Spyropoulos, C. S. (1959) 'Stria vascularis as source of endocochlear potential.', *Journal of neurophysiology*, 22(2), pp. 149–55.

Terence W. Picton (2010) *Human Auditory Evoked Potentials*. San Diego: Plural Publishing Inc.

Uus, K. and Bamford, J. (2006) 'Effectiveness of population-based newborn hearing screening in England: ages of interventions and profile of cases.', *Pediatrics*, 117(5), pp. e887--93. doi: 10.1542/peds.2005-1064.

Uus, K., Young, A. and Day, M. (2011) *Auditory Neuropathy Spectrum Disorder in Infants*. Manchester.

Vassiliou, A. *et al.* (2011) 'Meniere's disease: Still a mystery disease with difficult differential diagnosis', *Annals of Indian Academy of Neurology*. Wolters Kluwer -- Medknow Publications, 14(1), p. 12. doi: 10.4103/0972-2327.78043.

Versteegh, C. and van der Heijden, M. (2013) 'The spatial buildup of compression and suppression in the mammalian cochlea', *Journal of the Association for Research in Otolaryngology : JARO*. J Assoc Res Otolaryngol, 14(4), pp. 523–545. doi: 10.1007/S10162-013-0393-0.

Waddell, B. *et al.* (2013) 'SENSORY NEURONOPATHY; A CASE REPORT AND A REVIEW OF THE ROLE OF GANGLION NERVE BIOPSY IN DIAGNOSIS', *Journal of Neurology, Neurosurgery & Psychiatry*, 84(11), p. e2.127-e2. doi: 10.1136/jnnp-2013-306573.212.

Weiss, T., Mulroy, M. and Altmann, D. (1974) 'Intracellular responses to acoustic clicks in the inner ear of the alligator lizard', *The Journal of the Acoustical Society of America*. J Acoust Soc Am, 55(3), pp. 606–619. doi: 10.1121/1.1914571.

Withnell, R. H. (2001) 'Brief report: the cochlear microphonic as an indication of outer hair cell function.', *Ear and hearing*, 22(1), pp. 75–7.

Yost, W. A. (2007) *Fundamentals of Hearing. An Introduction*. Academic Press.

Young, A. and Ng, M. (2020) 'Ossiculoplasty', *Indian Journal of Otolaryngology*. StatPearls Publishing, 33(4), pp. 125–130.

Young, J. (2011) 'Modelling the cochlear origins of distortion product otoacoustic emissions', *Philosophy*.

Yule, C. J. (1873) 'The Mechanism of opening and closing the Eustachian Tube.', *Journal of anatomy and physiology*, 8(Pt 1), pp. 127-132.1.

Zeng, F. G. and Liu, S. (2006) 'Speech perception in individuals with auditory neuropathy', *Journal of Speech, Language, and Hearing Research*. J Speech Lang Hear Res, 49(2), pp. 367–380. doi: 10.1044/1092-4388(2006/029).

Zhang, M. (2012) 'Response Pattern Based on the Amplitude of Ear Canal Recorded Cochlear Microphonic Waveforms across Acoustic Frequencies in Normal Hearing Subjects', *Trends in Amplification*. SAGE PublicationsSage CA: Los Angeles, CA, 16(2), pp. 117–126. doi: 10.1177/1084713812448547.

Zhang, M. (2014) 'Effects of the intensity of masking noise on ear canal recorded low-frequency cochlear microphonic waveforms in normal hearing subjects', *Hearing Research*. Elsevier, 313, pp. 9–17. doi: 10.1016/j.heares.2014.04.004.